SWEDISH DEFENCE
RESEARCH AGENCY

Laser Based 3-D Imaging
New Capabilities for Optical Sensing

Technical overview and research problems

Ove Steinvall, Tomas Carlsson, Christina Grönwall

Håkan Larsson, Pierre Andersson and Lena Klasén

Laser Based 3-D Imaging
New Capabilities for Optical Sensing

Technical overview and research problems

Ove Steinvall, Tomas Carlsson, Christina Grönwall

Håkan Larsson, Pierre Andersson and Lena Klasén

Issuing organization	Report number, ISRN	Report type
FOI – Swedish Defence Research Agency	FOI-R--0856--SE	Technical report
Division of Sensor Technology	**Research area code**	
Box 1165	4. C4ISR / 5. Combat	
SE-581 11 Linköping	**Month year**	**Project no.**
SWEDEN	April 2003	E3036/E2025
	Customers code	
	5. Comissioned research	
	Sub area code	
	42. Surveillance Sensors	
	51. Weapons and Protection	
Author/s (editor/s)	**Project manager**	
Ove Steinvall	Lena Klasén/Svante Karlsson	
Tomas Carlsson	**Approved by**	
Christina Grönwall		
Håkan Larsson	**Sponsoring agency**	
Pierre Andersson		
Lena Klasén	**Scientifically and technically responsible**	
	Ove Steinvall	

Report title

Laser Based 3-D Imaging
New Capabilities for Optical Sensing

Abstract (not more than 200 words)

We are living in a three-dimensional world. The potential to image this world with cm resolution at full video rate and at both close and very long ranges will revolutionize many military and civilian applications. Many applications are found for example in robotics, rapid terrain visualization, augmented vision, reconnaissance and target recognition, weapon guidance including aim point selection and many others. The net-centric warfare will demand high resolution geo-data for a common description of the environment, for mission planning, for sensor management and sensor fusion, electronic warfare and communication and many others functions related to the network concept. One very important capability of 3 D imaging is to be able to see through dense camouflage and dense vegetation.

The ultimate solution for laser imaging might be a one-shot full 3D solution using a focal plane array with intensity and range (time) sensitive pixels. This report will discuss the technical status of 3 D focal plane arrays (3 D FPA) and other approaches and discuss applications for them, especially for long-range target identification and for terminal guidance. We describe the technology as found in open sources but also give examples of 3 D imaging and related activities at FOI. Hopefully we will convince the reader about the importance of this area. Some recommendations for further plans are given.

Keywords

Laser radar, Laser sensing, 3 D imaging, Target recognition, Target identification, Laser receivers, 3 D FPA, 3 D Focal plane arrays, Terminal guidance, 3 D processing

Further bibliographic information	Language English
ISSN 1650-1942	**Pages** 104 p.
	Price acc. to pricelist

Rapportens titel (i översättning)
Laserbaserad 3 D avbildning
En ny förmåga hos optiska sensorer

Sammanfattning (högst 200 ord)

Vi lever i en 3 dimensionell värld. Möjligheten att avbilda denna med cm upplösning och i full videotakt kommer att revolutionera många militära och civila tillämpningar. Många tillämpningar finns inom robotik, terrängvisualisering, förstärkt verklighet, spaning och måligenkänning, vapenstyrning inkluderande träff-punktsbestämning och många fler. Det framtida nätverksbaserade försvaret kommer att kräva högupplösta geo-data för gemensam lägesbild, för uppdragsplanering, sensorfusion och telekrig samt kommunikation. En mycket intressant förmåga för högupplöst 3 D avbildning utgör möjligheten att se genom tät kamouflering och tät vegetation.

Den ultimata lösningen för laseravbildning kan vara en lösning baserad på ett laserskott och full 3 D bild mha av en avstånds- och intensitetskännande fokalplanearray. Denna rapport diskuterar teknisk status hos 3 D fokalplanearrayer och liknande koncept samt deras tillämpningar, bl a för långräckviddig spaning och slutfasstyrning. Vi beskriver teknologi som återfinns i öppen litteratur, men ger även exempel på aktiviteter kring 3 D avbildning på FOI. Förhoppningsvis kan vi övertyga läsaren om områdets vikt och betydelse. Några rekommendationer för framtida planering ges.

Contents

Introduction

Laser systems have the capability of range-resolved imaging with high resolution. High range resolution (HRR) methods for target recognition have also become one of the key areas in automatic target recognition in the radar area. Laser detection can be based upon non-coherent (direct) detection, reducing the problem of target interference which is one of the main problems in the HRR recognition using microwave radar.

Laser systems can also employ coherent detection[1] giving a high shot noise limited sensitivity but having the drawback of severe speckle problems. However, several methods can be used to reduce the speckle problem, such as multiple frame integration and frequency diversity. Coherent laser radar can also give vibration information of the target suitable for target recognition.

The high range resolution can be used in several different schemes for target classification often described as 1D, 2D and 3D methods. Figure 1 illustrates the principles and type of data output.

1D   2D   3D
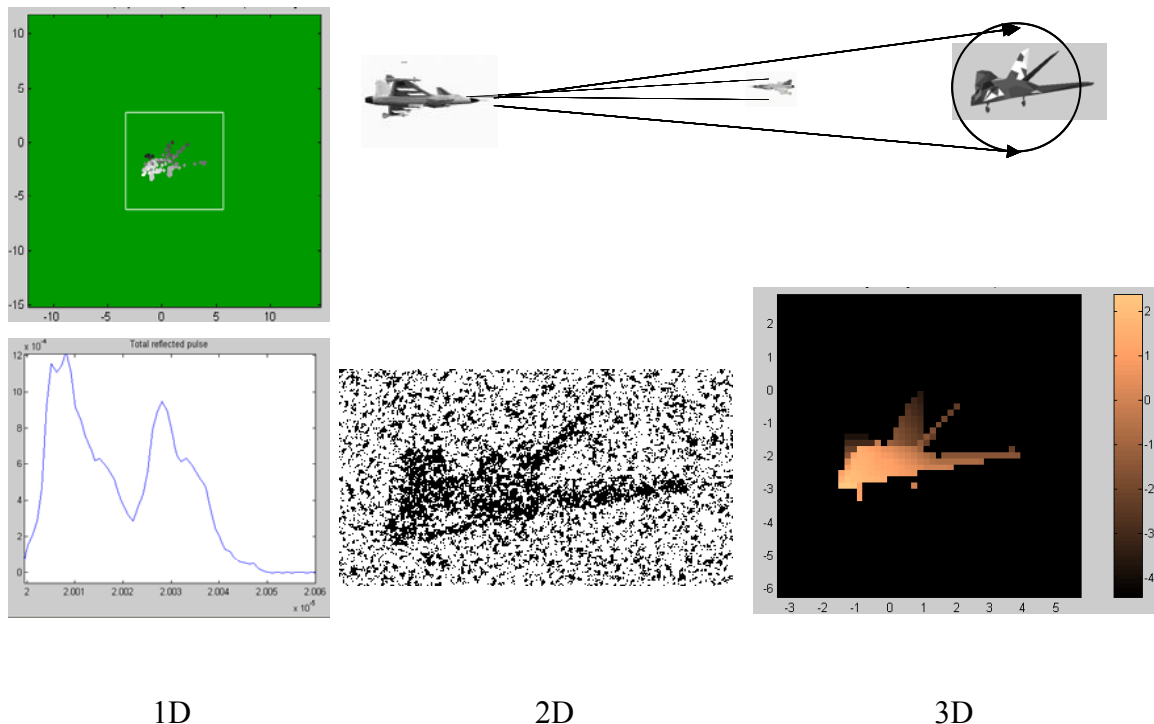
Figure 1. *Illustration of the principles for and data type of 1D (range profiling), 2D (Gated Viewing, burst illumination) and full 3D imaging.*

The 1 D, or high range resolution profile[2] (HRRP), technique has an advantage in its simplicity. In principle, it is a conventional laser range finder with a short (1-3 ns) pulse and high receiver bandwidth. The problem lies in the robustness of using single waveforms without knowing the exact aspect angle of the target with respect to the laser beam. Auxiliary data from a radar or IR track might help to estimate the target angle.

2 D imaging[3] by range gating or burst illumination, as the method also is called, relies on the the principle of time controlling a camera with respect to a pulsed illuminating

source. Powerful diode pumped lasers and camera tubes with higher spatial and time resolutions will make this technique an interesting complement to passive EO imaging. Future eye-safe laser systems, which not only perform ranging but also target classification and/or identification, will be of great interest. A 3 D "image" may be deduced from a series of time sliced 2 D images stacked along the range axis. This, however, needs multiple exposures of the target, which can be a disadvantage. The ultimate solution for laser imaging might be a one-shotfull 3D solution using a focal plane array with intensity and range (time) sensitive pixels. This report will discuss the technical status of 3 D focal plane arrays (3 D FPA) and try to discuss applications for them, especially in long-range target identification and for terminal guidance.

This report is restricted to land and air applications. We have also omitted the atmospheric lidar applications, although 3 D FPA:s are of very high relevance also for both atmospheric and underwater sensing. The report will start with a technical overview of laser systems for 3 D imaging and data collection mostly based on scanning systems. After that, a description of 3 D FPA technology will follow. Processing of 3 D data is briefly described with emphasis on some FOI-related activities. We will then give some system examples for 3 D laser sensing and estimate performance together with an exemplification of different capabilities of these kinds of systems. Finally we discuss active/passive EO sensing and the potential for new and extended system performance. We also comment on the new capabilities that new hardware will give, as well as point out some R&D issues for 3 D imaging.

Motivation for 3 D imaging

Below, we have listed some reasons why 3 D imaging, and especially that which relies on 3 D FPA will revolutionise future laser/EO system capabilities. We have also tried to evaluate the most relevant and beneficial application areas. The motives are:

• **3D (FPA) will enable integrated true active/passive imaging and multifunctional systems.**

• **3 D FPA:s will allow the same laser to perform several functions, from rangefinding to imaging and mapping.**

• **3 D means much improved automatic target recognition (ATR):** As a rule **of** thumb: 200 pixels per target at 15-20 cm range resolution and 40 cm cross range resolution for robust ID[4]. The ATR improvements are due to some of the following facts:

- Target range/size as processing variable
- Target signature dependence on the environment
  (Ladar uses size/shape versus lighting, contrast, DT, etc.)
- Less affected by known CM and signature variation/suppression
- Processing 3-D data substantially reduces false target rate and
  missed targets, compared to current ATR technology[5]

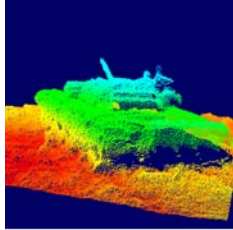• **High resolution (<10-20 cm) range imaging will also**:

-Allow robust template matching and target recognition plus fingerprinting
(using measured dimensions to the cm level)
- Allow determination of orientation– threat (fighting vehicles, …..)
- Allow recognition and detection of "hard" targets (see through smoke, fires, camouflage, 80-90 % vegetation coverage)…
– Facilitate UGV (UAV) navigation through terrain (close to the ground)
– Facilitate UGV (UAV) route planning
– Increase the capability of high resolution terrain mapping for general mission planning etc.
– Allow robust missile seeker/munitions targeting– target recognition-tracking-aim point selection with high countermeasure resistance

• **No scanner required for small FOV imaging, moderate scanning demands for systems with large area coverage rate.**

• **Short (ns) laser pulse per image, which implies covert operation and no blurring due to platform motion.**

The table below tries to indicate the most relevant applications for laser-based 3 D imaging. The priorities can of course be discussed and re-evaluated.

Table 1. *Summary of application relevance and pay-off for 3 D imaging.*

- **Surveillance-**
- **Target detection**
- **Long range target classification / identification**
- **Obstacle avoidance**
- **Navigation**
- **Terrain following**
- **Weapon guidance incl. precise terminal guidance (aimpoint selection)**
- **Intelligent proximity fuses**
- **Active countermeasure systems**
- **Rapid terrain visualisation**
- **Underwater sensing**
- **Remote sensing of B/C agents**
- **Free space optical communication**

🟥	Highest payoff 3 D FPA
🟩	High payoff
⬛	Moderate or small payoff

Present 3 D imaging techniques

Scanning vs. staring and hybrid systems

The majority of laser radar systems developed so far are based on mechanical scanning of the beam to cover a volume. The 3-D "image" is built up by successive scans where each "laser shot" will return intensity and multiple range values corresponding to different structures within the beam footprint. In many systems the full return waveform is captured for each laser shot and stored for further processing.

We assume a total solid angle Ω_{tot} to be scanned with a narrow beam of angular extent Ω_{beam}. Let T_{dwell} be the time that the beam dwells on any point in the angular field Ω_{tot} The total search time for one scan across Ω_{tot} will then be:

$$T_{totsc-st} = (\Omega_{tot} / \Omega_{beam)}) * T_{dwell} \qquad\qquad (1)$$

The dwell time T_{dwell} must at least be larger than twice the propagation time to the target. For example, for 10 km and 128*128 pixels it takes about one second (!) to scan one frame during those limitations. This should be compared with a potential frame rate just corresponding to the propagation time if a flood illuminated approach was taken. This frame rate will be limited by the readout speed from the array and/or laser pulse energy and average power considerations.

For hybrid solutions, a detector array of n×m pixels will reduce the total scan time by a factor of n×m. For systems where a large search field is needed it might be ideal to use an array to lower the demand on the scanner frequency.

We assume that the laser radar is covering a swath below the platform and the 3-D and reflection data obtained from the sensor can be used for terrain navigation together with the main purpose of remote sensing of the ground and the vegetation. Let us assume a fan beam with the long side perpendicular to the flight direction. The flight speed is V m/s and the altitude H m. Let us then assume that the pixel area size on the ground is d_{res}^2, and that we have N=n×m such pixels for every laser shot. The array can be assumed to stare or to scan across the flight direction.

Scanning is often done with large mirrors (5-20 cm) in front of the transmitter /receiver module. Programmable scanners[6] let the scan mode adaptively be adjusted to the proper task, e.g. to generate an optimal semicircular scan pattern for a "search" mode and increase ground resolution when hovering with a helicopter. There is a practical size limit for post telescope scanners. For a 10 cm aperture the scan frequency may be 20-30 Hz at the most for scanning ± 20°. One way to reduce the scanning speed demand is to use the large mirror for slow scanning/pointing and a more rapid galvanometer scanner for image plane scanning. Another obvious way is to use a detector array. The scan frequency f_{scan} of a linear scanner with small turning time is:

$$f_{scan} = \frac{V}{d_{res} \cdot N}$$
(2)

For $f_{scan-max}$= 20 Hz and d_{res}=0.25m for example the V<5*N m/s. A detector array with N>10 is needed to get reasonable velocities and area coverage rates for tactical UAV applications. The discussion above motivates detector arrays for both smaller and larger FOV systems due to time and scanner considerations.

Examples of state-of-the-art scanning laser radar systems

Single element systems

We will restrict ourselves to direct detection systems with imaging capabilities. During the past couple of years there has been an increasing interest in airborne remote sensing using Digital Elevation Models (DEM) for use in city planning, mobile phone networks, forestry, flood risk assessment, power cable monitoring etc. A number of methods can be applied to generate DEM's from the well-established aerial photography, interferometric radar and synthetic aperture radar (SAR). Airborne laser radar is another technology with great promise. Recently a number of airborne nadir scanning laser radars have been developed for both military and civilian applications[1,7, 8] . These often have range resolutions on the order of 10 cm but relatively moderate area coverage rates in the range 1000-10 000 m^2/s (3.6-36 km^2/h) when operating in a high resolution mode with 0.25-0.5 m spot distance.

The energy per pixel needed for typical receiver optics (10 cm diameter) is on the order of 10 μJ, but depends on altitude, target reflectivity etc. From that we can estimate the necessary average laser power for a given spot density (transverse resolution) and area coverage rate. We assume that the swath S=0.7*H, meaning a maximum nadir scanning angle of 20 degrees. A certain area coverage rate, say 100 km^2/h and a given altitude, for example H=300 m results in a platform velocity of 132 m/s (475 km/h) while an altitude of 1000 m results in a velocity of 40 m/s (144 km/h). From figure 2, right part[9], we get an average power of 1 W for Y=100 km^2/h and H=1000 m. Note that a coverage rate as high as 1000 km^2/h for d_{res}=0.25 m can be achieved with a laser power as low as 10 W at H=1000 m if one could realize such a system (V=396 m/s!). Note that the assumed sensitivities etc. of the receiver and the assumed reflection from the tree and ground (5%) might be optimistic. A "down scaling" by a total factor of 10 might be a safe way in designing a system. Even with this assumption we arrive at moderate average laser powers (< 10 W) for very capable systems.

For realistic airborne applications, for example using UAV:s, the laser power may not be the most critical factor but the scan rate and the difficulty to realize a high velocity scanner for 5-10 cm post-aperture scanning. Rotating scanners like polygon and rotating wedges will have the speed but will not have a very good efficiency in distributing the laser shots. On the other hand, a detector array may use simple mechanical scanners and will have a very even shot distribution on the ground, which is a clear advantage when processing the data.
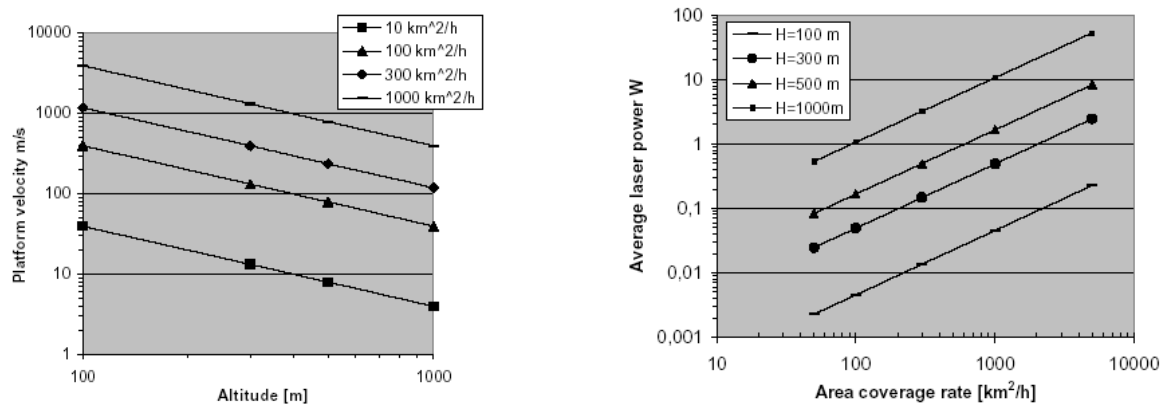
Figure 2: *Left: platform velocity vs. altitude for different area coverage rates. Right: average laser power vs. area coverage rates and different altitudes, H. A swath S=0.7*H is assumed together with the laser spot density of 4 m^{-1} (d$_{res}$=0.25m).*

There are about half a dozen commercial systems for airborne terrain and vegetation mapping like TopEye (Sweden), Airborne Laser Terrain Mapper (ALTM, Canada), TopoSys (Germany) and some others. For underwater applications[10] we have SHOALS (Canada), Hawk Eye (Sweden) and LADS (Australia) as examples of commercial systems for depth sounding. The pulse energy for depth sounding greatly exceeds that of land mapping why the rapid scanning need is not as critical as for the land case. Array detectors, however, offer a better transverse resolution, which is of interest for detecting small objects in the water (like mines).

The hardware for the Airborne Laser Terrain Mapper (ALTM) from Optech Canada is shown in figure 3 together with the specifications in table 1.

Figure 3: *Example of a commercial lidar for airborne terrain mapping, ALTM from Optech, Canada.*

The use of airborne laser terrain mappers is of high commercial and military interest. At FOI we are developing tools to handle laser data to form realistic synthetic environments for military planning, sensor and electronic warfare simulation. We combine these data with IR and aerial photography to form very realistic synthetic environments as can be seen from figure 4. A good deal of this data fusion process is automatic.

The laser radar is not the only sensor that can give 3 D information. For rapid terrain visualization lidar and ISAR are complementary concerning area coverage. In the US there is a program called RTV (Rapid Terrain Visualization) to establish techniques

Table 2. *Typical parameters for an airborne terrain mapper (ALTM, Optech)*

Parameter	Value
Laser	Nd:YAG, 1.047 μm
Laser pulse energy	20-200 μJ
Operating altitude	330-1000 m
Horizontal accuracy	Better than 1/2,000 x altitude
Laser PRF (max.)	50 kHz
Eye safe range	308 m
Scanner type	Oscillating mirror
Scanner angle	0 - ±20°
Scan frequency	30 Hz for ±20°, 50 Hz for ±10 °
Measurement density	Ex. 100 m swath and V_{flight}=50m/s gives about 10 measurement/m^2
Swath width	0-0.68*altitude
Single pulse accuracy	15 cm
Range accuracy	2-3 cm single shot
Weight sensor head	11.4 kg
Weight total sensor+rack	57 kg
Power:	35 Amps @ 28 VDC typical

Figure 4: *Synthetic scene in 3 D generated with the help of an airborne scanning laser radar (Top Eye) and data fusion with photography. Images FOI Dpt of Laser systems.*

and methods with a capability to rapidly produce the terrain data required to conduct contingency and crisis operations, see figure 5.

One interesting scanner used in the TopoSys system[11] is the fiber scanner. The principle is shown in Figure 5. An identical fiber line array is mounted in the focal plane of the receiving and transmitting lenses.
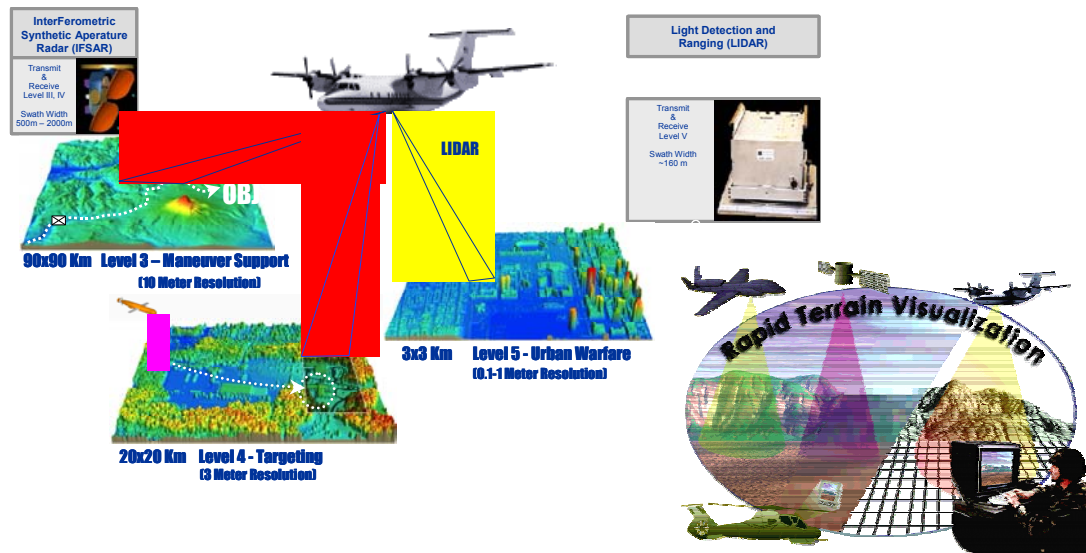
Figure 5: *ISAR and lidar are used as complementary tools in the US RTV (Rapid Terrain Visualization) program together with satellite imagery to form synthetic environments.*

By means of two rotating mirrors, each fiber in the transmitting and receiving path is scanned sequentially and synchronously. The mirrors relay the light either from the central fiber to a fiber of the fiber array mounted in a circle around the central fiber, or the other way around from the array to the central fiber. In this way, the light signal from the transmitting fiber is linked to the corresponding fiber in the receiving path. As, due to the small aperture of the fibers, only small moving mechanical parts are required, high scanning speeds up to 630 Hz can be achieved. This is not possible with conventional mirror scanners.

Figure 6: *Principle of the Toposys laser radar and example of urban mapping.* *www.toposys.com*

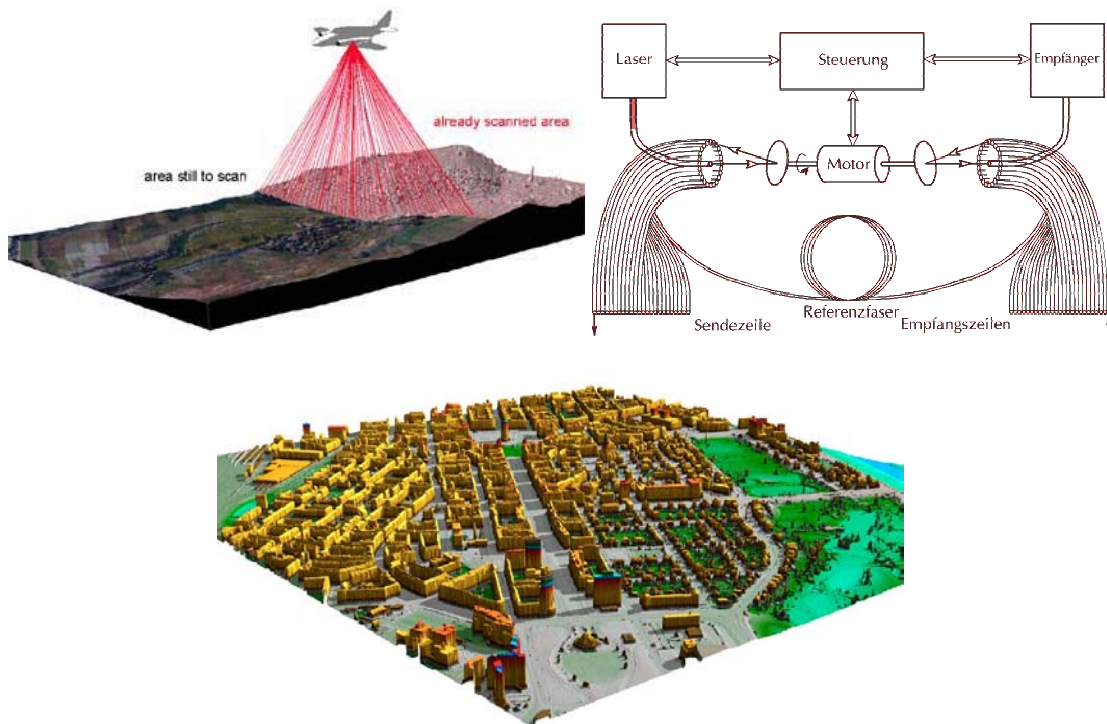Up to now, arrays of 128 fibers have been realized, and 256 or more will be possible in the near future. A laser pulse repetition frequency of up to 83 kHz is used at a wave-length of 1,55 µm. Due to this high repetition rate, very high density sampling can be obtained (typically 3-5 per m^2 from about 300 meters altitude).

There is a growing interest and use of land based laser radar 3D sensing for industrial use. Example of systems developed for this purpose are ILRIS 3 D (Optec Canada), RIEGL (Austria), Zoller and Fröhlich (Ge) and Cyrax (US). In the civilian field scanning 3 D laser radars are used for engineering, construction, and operations & maintenance activities in the manufacturing plant and civil/survey markets. They are also used for architectural, virtual reality, heritage preservation, forensic, and other applications. In the military field they are used for signature and 3D data collection to build accurate 3 D models, for example to be used for simulations in a synthetic landscape. At FOI we are using the ILRIS scanner at 1.5 µm and the RIEGL scanner at 0.9 µm for signature collection from military objects in their backgrounds.

Figure 7 shows the ILRIS 3 d scanner and figures 8 and 9 some examples of generated images at FOI and in the US showing the impact of the 11th of September terrorist action on the Pentagon building. Typical laser pulse rates of these systems are 1-50 kHz which limits the frame rate, especially for high resolution imaging. An image with 40° FOV and 1 mrad IFOV, for example, results in 0,46 Mpixels, which takes many seconds to scan, limiting the usefulness in dynamic scenes. Again a flash imaging using a full 3 D array detector will overcome this limitation.

Parameter	Data
Wavelength	1.5 µm
Max. range	350 m (4 % reflectance), 800 m (20% reflectance)
FOV	40° (±20°, programmable)
Divergence	0,2 mrad
Range resolution	1 cm
Angular resolution	Valbar 0.17 ; 0.34; 0.51; 0.68; 0.85; 1.02 mrad
Sampling frequency	2000 points/s
Size	30 x 30 x 20 cm^3
Weight	12 kg

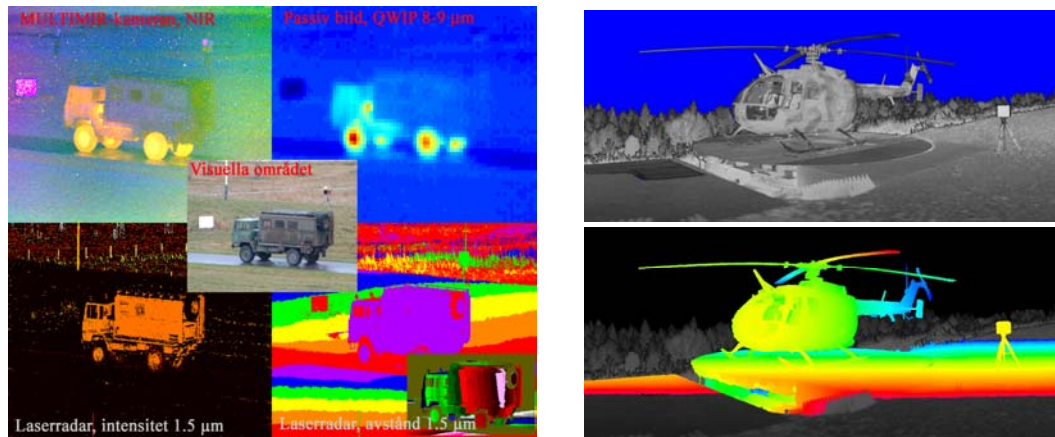**Figure 7:** *ILRIS 3 D laser scanner and key system parameters.*

Figure 8: *Left Passive IR, TV and laser radar intensity and range imagery of a truck. Right intensity and range image of a helicopter. Laser radar systems ILRIS 3 D for the left image and RIEGL for the right. Images FOI.*

Figure 9: *ILRIS 3 D images from the 11th of September terrorist action on the Pentagon building Images*

Examples of laser radars with linear arrays

Several systems using one dimensional detector arrays have been built. One important aspect not discussed so far is to use detector arrays to let the same laser and receiver optics perform several functions like 3D imaging (obstacle detection, target profiling, terrain mapping), designation and range finding. Thereby will the conflict of multifunctionality and the weight and volume constraint on platforms like UAV:s and helicopters be reduced. The US and Japanese joint program called CELRAP[12] addresses this problem. Detector arrays in both CMT (1*32 elements, avalanche photodiode) and InGaAs (128 element PIN diode) were tested.

Figure 10 shows an example of an image using a 128 element array. The image size is 100*128 pixels and took one second to grab. The low update rate again emphasizes the need for full 3 D focal plane imaging.

The LOCAAS Powered Low Cost Autonomous Attack System Advanced Technology Demonstrator program aims to demonstrate an affordable, miniature, autonomous, powered submunition. The submunition is said to provide the
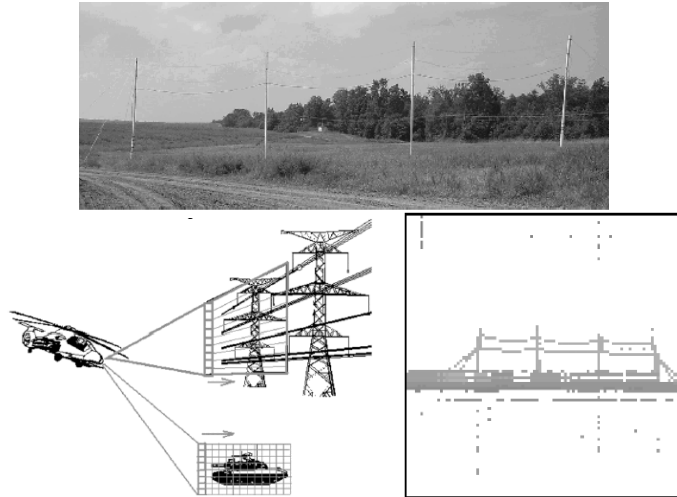
Figure 10: *Example of the use of linear arrays for obstacle detection and targeting. An image from a 128*1 element in the CELRAP system of wires and poles together with a photo of the target area.*

ability to search, detect, identify, track, and destroy mobile ground targets in different weather and terrain. LOCAAS has recently demonstrated full air vehicle flying qualities and guidance performance (2002). The LOCAAS was launched from a test aircraft flying at 200 knots at an altitude of 1,500 feet. After weapon release, the missile flew through a series of pre-determined waypoints, proving its ability to follow a mission-planned course.

LOCAAS[13] uses a low-cost laser radar sensor coupled with a multimode warhead and a maneuvering airframe to produce a high performance submunition. The warhead can be detonated as a long rod penetrator, an aero stable slug, or as fragments based on the hardness of the target. The laser radar allows target aim point and warhead selection to be made automatically. The powered LOCAAS uses a small turbojet engine, which is capable of powering the vehicle for up to 30 minutes. Powered LOCAAS has a 33 sq. nm search area. Figure 11 shows the geometry, and Figure 12 the UAV (missile) size and the compact laser radar seeker. This technology also incorporates multi-element receivers and a lot of real time signal processing for automatic target recognition. It is designed to be compatible with the F-16, F-22, Joint Strike Fighter, B-1, and B-2 aircraft. It can also be dispensed from a Multiple Launch Rocket System (MLRS) rocket or an Army Tactical Missile System missile.
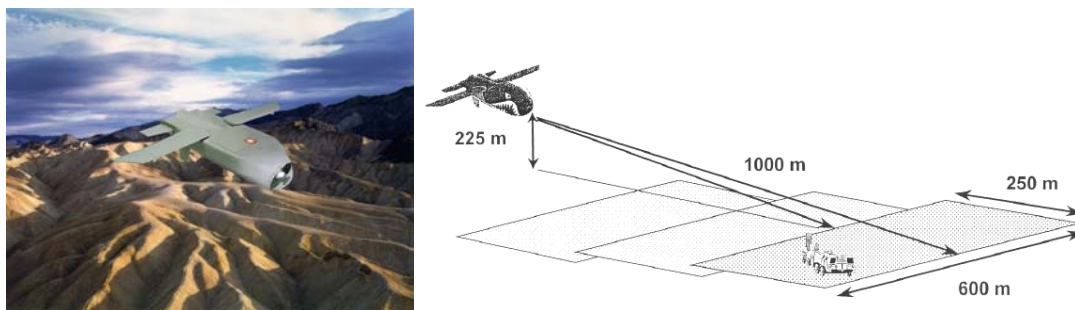

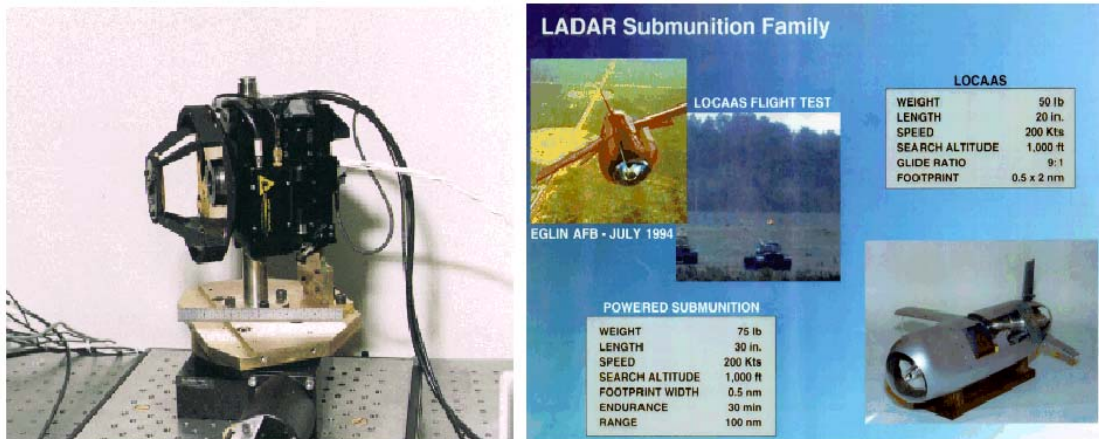**Figure 11:** *The LOCAAS search geometry.*

Figure 12: *The LOCAAS laser seeker head and some more information on the glide and powered versions studied in the program.*

Examples of parameters of interest are:

· Nd:YAG diode pumped laser, 6 W average power
· Area searched by one missile < 50 km^2.
· Spot density < 0.5 m
· Range accuracy < 0.15 m
· Altitude typically 225 m, searches a 250*600 m^2 surface at 1 km range in front of the missile in 2 seconds.

If we assume 0.025 m^2 per pixel (16 cm square) that gives 3 Mpixels per second a receiver detector array with, say, 25 detectors this will result in a pulse repetition frequency of about 120 kHz (corresponding to an ambiguity range around 1000 m).

Obstacle avoidance for helicopters

The obstacle warning system for Helicopters HELLAS[14] is available as an off-the-shelf system. It is developed by Dornier in Germany. The system generates a 3 D Ladar image based on a 1,5 µm Erbium-Fiber Laser. The system is specially designed to detect wires with a high detection probability of >99,5 % within one second. An analysis of helicopter accident data shows that 8% - 12% are caused by wire strikes (1). As accidents occur in good visibility at day or night and not only in poor visibility, the need for an active wire detection system is obvious.
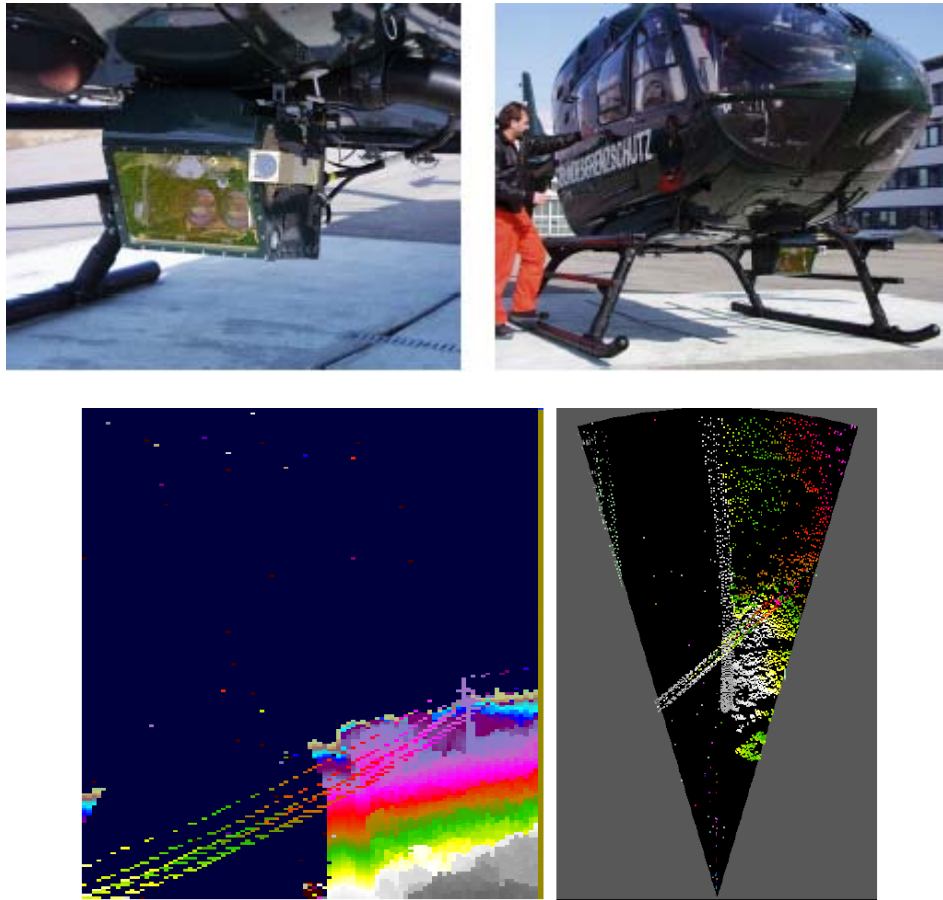
Figure 13: *Top: the HELLAS system installed in an EC135 German Border Police Helicopter. Below a typical range image obtained. Left: original sensor view. Right: a map projection of the same raw data. There is a river in the left half of the image and therefore there is no ground detection. From Schultz[14] et.al.*

The system has a fiber laser emitting at 1.54 μm at a prf approaching 40 kHz. The optical head is a biaxial system with fiber arrays for the transmitter and the receiver in the focal planes of the optics and an oscillating mirror for the horizontal scan axis. The fast scan in the horizontal direction is performed with the fiber-optics scanner. This scanner is a mechanical-optical multiplexer, which distributes the pulses of a single laser source to the fibres of the linear array (95 pixels) in the focal plane. The two scans create a "range image" with 200 lines and 95 columns at a frame rate of 2Hz. The 99.5% detection probability range exceeds 1 km for large objects and 500 m or 300 m for 10 mm wires in visibility conditions of 5 km or 1 km, respectively.

Figure 14: *Above: the scan geometry of the HELLAS sensor. Below: the principle of the fiber scanner os outlined. A scan efficiency (area fill factor) of 1:11 per single frame is obtained. From Schultz[14] et.al.*
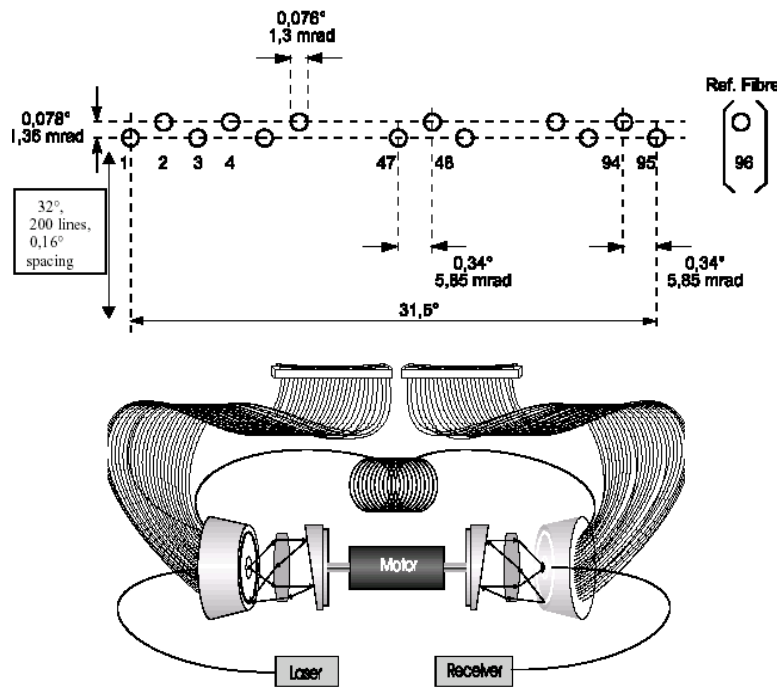
Autonomous systems

Robotics is a key enabling technology for future military operations. Small, lightweight and highly mobile robots will allow revolutionary operational concepts, for example to infiltrate behind enemy lines with minimal risk and to be able to act in hazardous environments containing mines and chemical/biological agents. All kinds of unmanned platforms will be of interest: UAV:s , UGV:s and AUV:s. Future UGV:s, for example, will be able to manoeuvre at speeds comparable to manned vehicles.

Future small UAV:s should be able to navigate in urban areas along the streets and make observations through windows, for example. The 3 D direct sensing and the 3 D data of the environment will be crucial for precision navigation, obstacle avoidance and intelligent route planning to provide cover. The 3 D sensor will of course also collect data and store these for updating existing terrain databases. The same 3 D sensor can also be used for targeting and, with a small addition, have the capability to communicate with the same or a collinear laser, enabling high bandwidth, secure transmission of data.
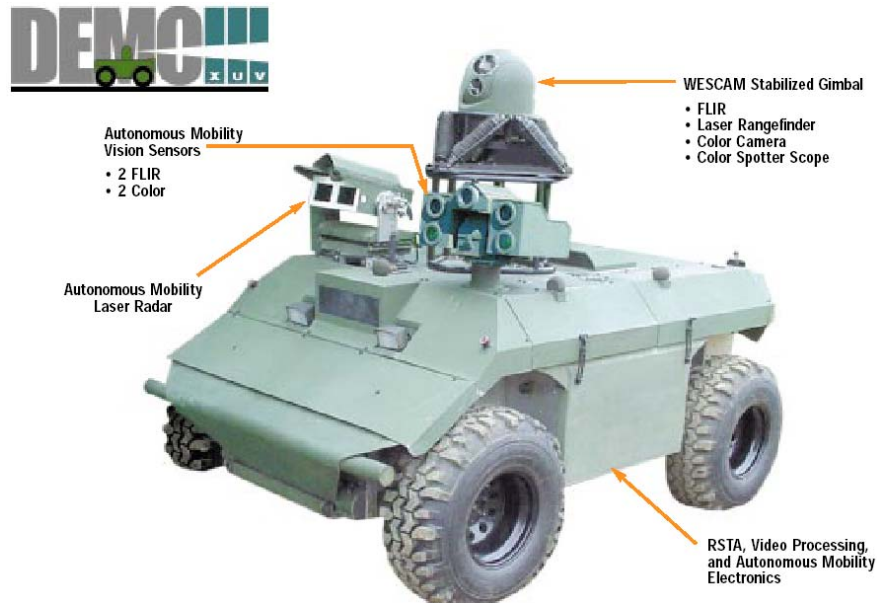
Figure 15: Experimental Unmanned Vehicle (XUV), US Army, see www.arl.army.mil/wmrd.

Autonomous day/night cross-country mobility requires the detection and negotiation or avoidance of various obstacles under a wide range of environmental conditions. In addition to fairly large obstacles, such as rocks protruding from the ground plane, consideration must be given to obstacles below the ground plane, such as streams and gullies. Other obstacles, such as trees and impenetrable vegetation, wires, and objects hidden by grass, must also be considered. The combination of passive IR and colour CCD sensors with laser radars or in the future sub mm (THz) radars will hopefully solve this difficult problem. One example of this is given by Rasmussen[15] who describes results on combining depth information from a laser range-finder with color and texture image cues to segment ill-structured dirt, gravel, and asphalt roads for input to an autonomous road following system (figure 16). Segmented images combined with laser range information and the vehicle's inertial navigation data were used to construct 3-D maps suitable for path planning.

Covert operation will also be important and this might impose emission limitations on the navigational part of the laser radar by emitting low power and adapting the emission to some high absorption part of the atmospheric spectrum.

Figure 16: *Left a test UGV for autonomous navigation. Fused laser range and CCD imagery. From Rasmussen[15].*

3D focal plane array technology

There are several concepts for scannerless laser radar (ladar) systems for smart munition, reconnaissance and other applications. We will briefly describe and compare them. The most effort will be put into describing the 3 D or "Flash imaging" FPA. The techniques that will be given an overview are:

1. FM/CW approach using a modulated laser and a "self mixing FPA"
2. Modulated gain tube and modulated laser
3. Streak camera tube
4. Flash imaging FPA
   a. With photodiodes (avalanche or unity gain diodes)
   b. FPA with an intensified tube for gain improvement

FM/CW chirped approach

US Army Research Labs (ARL) are working on the FM/CW ranging architecture[16,17,18] previously reported for coherent laser radars[19]. The following information is based on ref. 16 to 18. Figure 17 illustrates the principle.

The range image is obtained by directly amplitude modulating a near-IR diode laser transmitter with a radio frequency (rf) subcarrier that is linearly frequency modulated. The diode's output is collected and projected to form an illumination field in the downrange image area. The returned signal is focused onto an array of metalsemiconductor-metal (MSM) detectors where it is detected and mixed with a delayed replica of the laser modulation signal that modulates the responsivity of each detector. The output of each detector is an intermediate frequency (IF) signal (a product of the mixing process) whose frequency is proportional to the target range. This IF signal is continuously sampled over each period of the rf modulation. Following this, an N-channel signal processor based on field-programmable gate arrays calculates the discrete Fourier transform over the IF waveform in each pixel to establish the ranges to and the amplitudes of all the target pixels.

The current receiver approach is based on developing an FPA comprised of "self-mixing" detectors. In this design, the detector responsivity is varied with an applied local oscillator voltage to cause mixing with the modulated receiver light signal. Such a detector design requires consideration of more parameters than with conventional FPA detectors (i.e. responsivity, spectral response, dark current, and noise). With a "self-mixing" detector one must also consider achieving 1 GHz LO modulation and detection bandwidths, high conversion efficiency, 1-10 kHz IF bandwidths, high impedance LO drive loads, and low self-clutter signals (which will otherwise produce false targets). As an additional problem, the electromagnetic fields generated by the LO voltage must not upset operation of the read-out circuits. ARL has investigated a number of self-mixing detector candidates. The most promising self-mixing detector consists of a series of interdigitated metal fingers deposited on a substrate commonly referred to as a metal-semiconductor-metal (MSM) detector. A photograph of an ARL-fabricated MSM detector using a GaAs substrate is shown below. ARL has characterized a number of single pixel MSM detectors for the ARL ladar architecture, and has recently fabricated arrays of MSM detectors. In a recent paper[18],ARL

described a 1x32 pixel MSM array designed for use in the ARL ladar architecture. The detectors achieved a mixing efficiency of close to 40% with a voltage bias of less than 1.0 V_{rms} and appeared to be very uniform over the entire array. The detectors responded linearly with illumination levels, allowing easy mapping from measured signal to target reflectance. The electrical insulation between array elements was at least 40 dB.
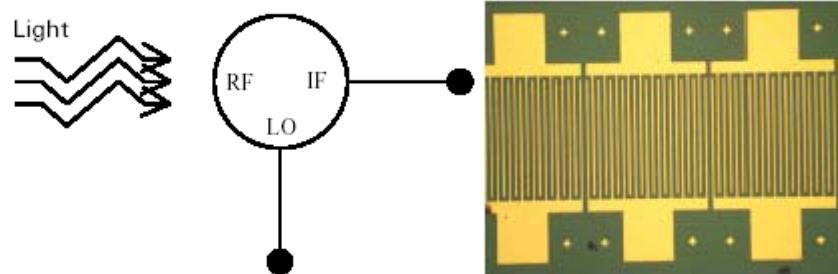

Figure 17: *Left the principle of the self mixing detector and right an example of 3 MSM elements in an array. From ARL, ref. 14.*

The signal processing load is based on range swath, range resolution, frame size and frame rate. For each pixel, and an assumed required range swath of 8 m with a range resolution of 0.25 m; the size of the signal processor FFT amounts to at least 64 points. The basic computational load for the smart munition system is then 320,000 64-point FFTs per second. For the reconnaissance system, the ladar is required to form a 32x32-pixel image over a range swath of 64 m. For a range resolution of .25 m, this requires the formation of 256 range gates, which in turn requires a 512 point FFT. The desired ladar frame is 10 Hz, thus the signal processor must execute 10,240 512-point FFTs per second. At this rate, the 32 channels require 224 µs to complete the processing. It is believed that FPGA:s can meet this demand.

The average power for a 5 km range capability is estimated to lie around 10 W. It is hard to find laser diodes in this range at the eye safe wavelength 1.55 µm, suitable for this long range target identification problem. However multi-watt lasers have been developed. It is easier in the submunition case to motivate and find suitable laser diodes at 0.8 µm.

Examples of advantages of this approach as we can judge are:

- Potentially cheap and compact design by using laser diodes as transmitters
- Flood light approach with potential for full 3 D image in a short time period corresponding to a chirped waveform
- Range resolution < 0.25 m and multiple ranges per pixel feasible.
- Multi-target capability within one pixel (maybe better than for pulse systems depending on range resolution)

Examples of disadvantages are:

- Complex method for range retrieval compared with the short pulse approach
- Non-trivial and partially unproven technology involved, such as high bandwidth chirp generation (200-800 MHz) and high power laser modulation, self mixing arrays using MSM detectors.
- Longer dwell times on target as compared to pulsed systems
- Potentially easier to counter electronically than short pulse systems due to longer dwell times per pixel.
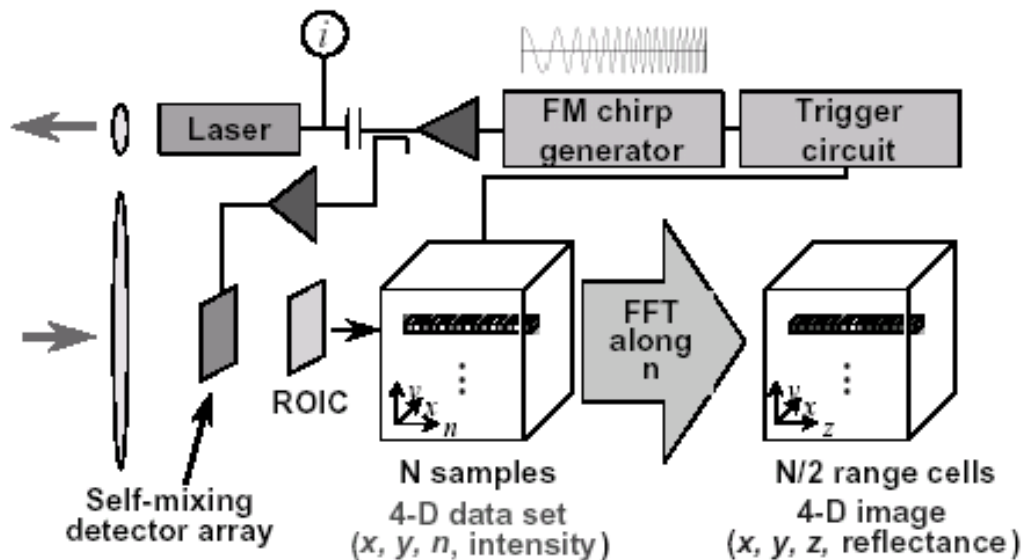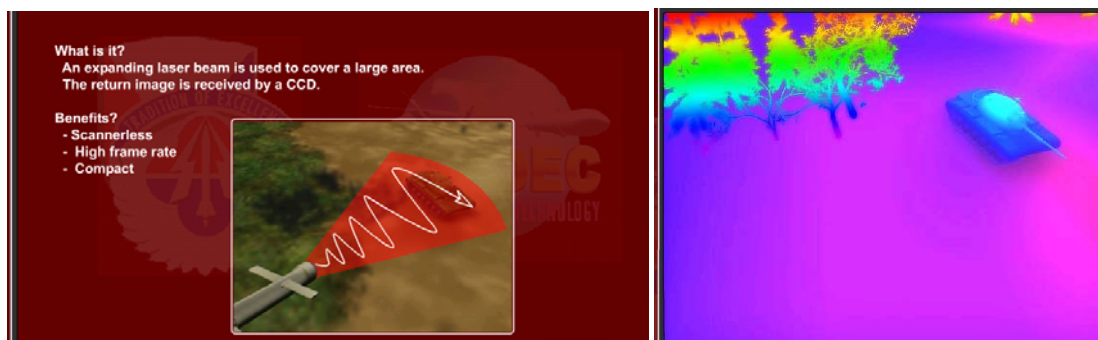- No absolute range

Figure 18: *Top images principles and range image , image from ARMDEC US Army research and development and engineering centre), Bottom image from US Army Res. Labs (ref. 13) shows the principle of the system.*

The block diagram of a 32x32-pixel imager appears in figure 19. In figure 20 there are some examples of ladar images from the ARL lab (ref.18).
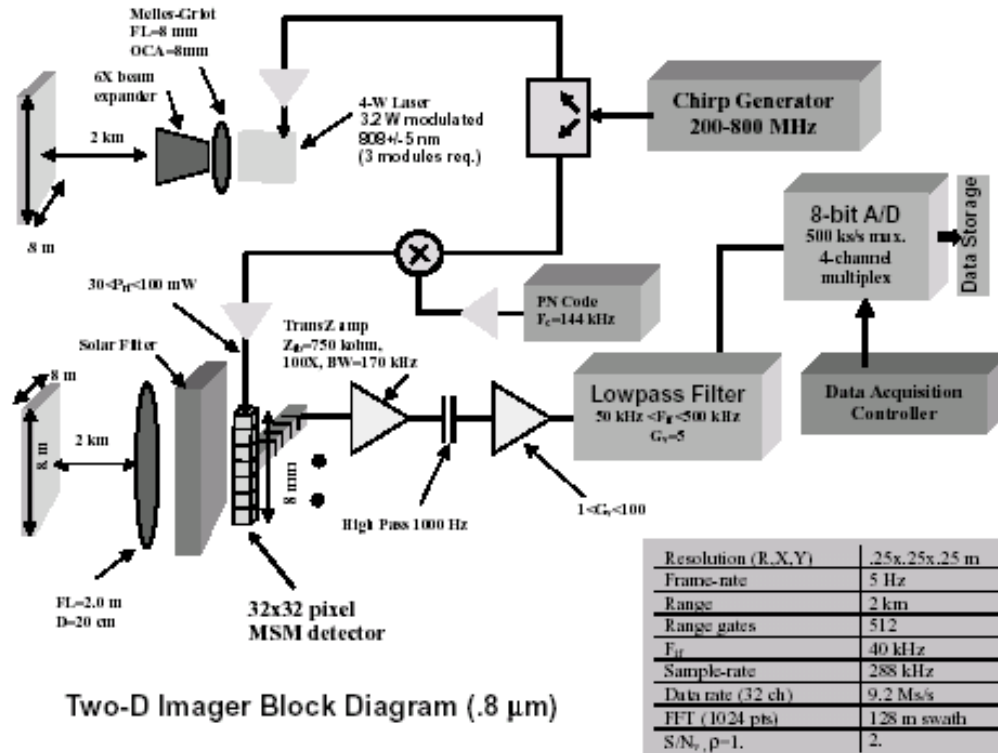
Figure 19: *Block diagram and anticipated performance for the 32*32 pixel imager. From ref. 17.*
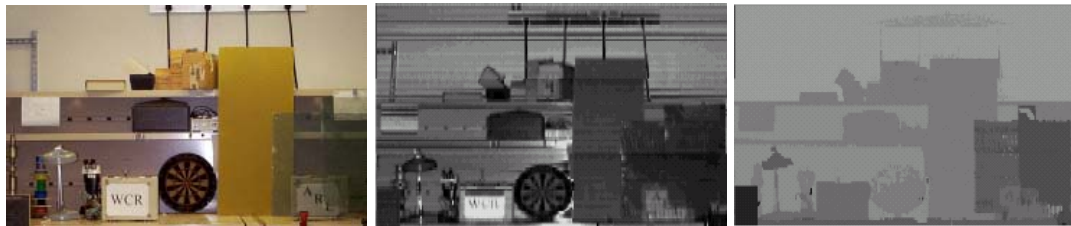
Figure 20: *Left a photo of a sections the ARL lab. Middle shows a ladar intensity image of the same scene and right the range inmagery. From ref. 18.*

Modulated gain tube and modulated laser

Sandia Laboratories has developed a very interesting scannerless laser radar[20]. The technique is to illuminate the scene with a modulated, diffuse source, and to measure the average reflected intensity with an imaging receiver incurring modulated gain. A sequence of intensity images is obtained at discrete steps in the relative modulation phase between the receiver and source. The range-processing algorithm deduces range based on the observed relationship between intensity and phase or frequency of modulation. Among the advantages with this approach we note that the data rate can be very high and that the final detection and read-out can be made with a conventional CCD FPA.

Using this technique, a commercial CCD camera plus an image intensifier can be used as a receiver in that range information is transformed into pixel intensity. The technique can thus lead to compact and inexpensive systems. To obtain range, the

gain of the intensifier is modulated at MHz rate and at least 3 snapshot images (usually 4-8) need to be evaluated. The range resolution ΔR has been shown to be best 15 cm at km ranges and sub-inch for short ranges (10's of meters). ΔR is obtained by the well known relation:

$$\Delta R = \frac{c\Delta\phi}{4\pi f} \qquad\qquad (3)$$

ϕ is the relative phase shift and f the modulation frequency for the intensifier gain. The technique has some drawbacks in that it needs multiple image registration (target/platform motion is of concern) and does not give absolute range, unless a number of modulation frequencies are used. To extend the operating interval while maintaining a given range resolution, a ladar sensor using dual modulation frequencies has been developed. The modulation frequency values can be scaled to meet the resolution and range interval requirements of different applications. Figure 21 shows an image example from the system.
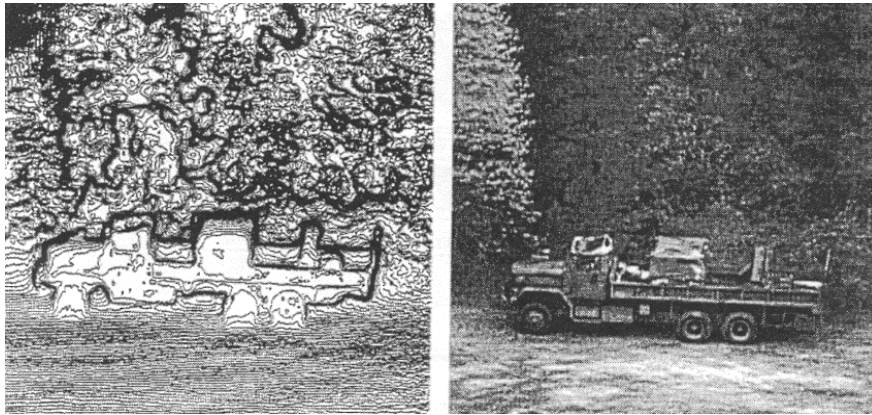
Figure 21: *Left a 1-foot iso-range contour image from the 256*256 pixel CCD. Right the corresponding photograph. From Sackos et al [21].*

One interesting idea is to use a diffuser in front of the illuminating laser to reduce speckle and uneven beam irradiance effects. Recent innovations developed in the laser radar include its compact size, small weight, sub-inch range resolution, absolute range over 150 feet, MHz range pixel rate, and eye safe laser illumination. A system recently developed for NASA[22] has been used on the Space Shuttle and can provide the range images of 640 by 480 pixels at 40-degree field of view, range resolution of 0.1 inches and a 7.5 Hz update rate. The modulation frequency was 140 MHz.

A conventional camera lens images the reflected laser light from the scene onto the cathode of an image intensifier tube. A 30 nm bandpass filter on the lens limits background light contribution. The intensifier optical gain is sinusoidally modulated by varying the micro-channel plate voltage within the tube at the laser modulation frequency. A gating function is applied to the cathode potential to eliminate return from outside the desired range interval as well as limiting the ambient light contribution. A fiber optic taper couples the intensified image on the phosphor output screen to a CCD detector. The CCD is read out by a conventional analogue video camera at 30 frames per second.

To demonstrate the absolute range stability and 0.1 inch range accuracy, Sandia conducted an experiment to detect small changes in the imaged scene. Figure 22 displays the laser range images taken of a perimeter fence from a 40 foot tower. After capturing a baseline range image, a person and vehicle traversed the scene in front of the fence. A second range image was acquired and subtracted from the baseline image. The difference image in Figure 22 indicates that the range accuracy and stability are sufficient to resolve the footprints and tire tracks. The time between the baseline and the second image was approximately 20 minutes.
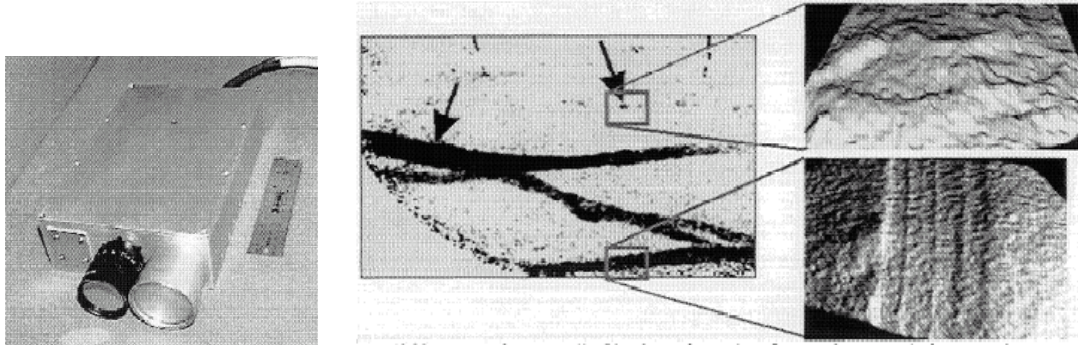

Figure 22: *Left one engineering version of Sandias scannnerless laser radar. Range difference image (middle) showing footprint from a shoe and tire tracks created between the baseline and second acquisition. Surface renderings (right) of the range image show the details of the impressions. From Smitpeter et.al.[20]*

In principle, this could be extended to short pulse laser exposures, thereby increasing the ranging capability and lowering the demand on pointing stability. To obtain a range image from a single pulse, we would need some way of parallel capture in multiple receivers, 3-4 to get good range resolution. However this makes the system complicated. As far as we know, the technology using pulsed laser has shown imagery up to 1.5 km[23].

One issue that does not seem to have been dealt with in the published work from Sandia is the influence of turbulence, target induced speckles, and platform motion on the range accuracy of the system. Some guide to system performance can be obtained by the relations[20]:

$$ I_n\left(t+\frac{R}{c}\right) = \left[A_0 + \sum_{i=1}^{\infty} A_i Cos\left(i2\pi f_0 \left(t-\frac{R}{c}\right) + \alpha_i \right) \right] * \left[B_0 + \sum_{j=1}^{\infty} B_j Cos\left(j2\pi f_0 \left(t+\frac{R}{c}\right) + \beta_j + j\theta_n \right) \right] \tag{4} $$

which gives the instantaneous pixel brightness of the nth image after receiver demodulation. The illumination at range R and time t, was transmitted at (t-R/c) and will be imaged at time (t+R/c), where c is the speed of light. The A and B coefficients in equation (2) include both sensor-dependent and scene-dependent parameters, such as background and reflectance. The fundamental modulation frequency is defined as f_0, and the relative phase between the transmitter and receiver waveforms is varied discretely, from image-frame to image-frame by the n term. The convention is to use the indices i and j to refer to harmonic order of the modulation-waveform component,

while n refers to the image number. The terms β_i and α_j are fixed components of transmitter and receiver timing at each harmonic.

The range can be calculated from:

$$R = c/4\pi f_0 \cdot \left[a\tan(\frac{I_3 - I_1}{I_4 - I_2}) + C \right] \qquad (5)$$

where I_n is the pixel intensity value for image nr I and f_0 is the modulation frequency. The range error for an AM modulated system is given by[24]:

$$\sigma_{R-AM} = \frac{c}{4\pi f_0 m\sqrt{SNR}} \qquad (6)$$

where m is the modulation index (proportional to A_1B_1) and SNR the signal to noise ratio. The range ambiguity is:

$$R_{amb} = \frac{c}{2f_0} \qquad (7)$$

Examples of advantages of this approach are as we can judge:

- Potentially cheap and compact design by using laser diodes as transmitters (the same as for the previous approach).
- Floodlight approach with full 3 D image for every 4-8 images.
- Very high range resolution (< 0.25 cm possible).
- Simple range processing.
- Range imagery at full video rate.
- Image intensifier tube plus conventional CCD for detection and read-out.

Examples of disadvantages are:

- Longer dwell times on target as compared to pulsed systems
- 4-8 images per range image means motion of laser and target can affect range accuracy and resolution.
- Potentially easier to counter electronically than short pulse systems.
- No absolute range unless several modulation frequencies are used.
- No multiple ranges per pixel feasible.
- Long range capability ?

Streak camera tube

Streak-tube imaging lidar (STIL)[25] is a new technique for obtaining high 3-D images from land and ocean. The principle is shown in Figure 23. A pulsed laser transmitter in conjunction with a time-resolved streak tube forms the basis of the system. The laser diverges to form a fan beam on the scene and the reflection is imaged onto the slit photo cathode of the streak tube. The fan beam moves in the flight direction.

27

Photoelectrons liberated from the photo cathode are accelerated, focused, and deflected in time using parallel-plate electrodes. A sweep voltage applied to steer the beam in time along an axis orthogonal to the fan beam allows a range-azimuth image to be formed on each laser pulse. This range-azimuth image is digitally recorded by conventional CCD technology. Synchronizing the PRF of the system with the forward speed of the platform means the in-track dimension is swept out in a push broom fashion.
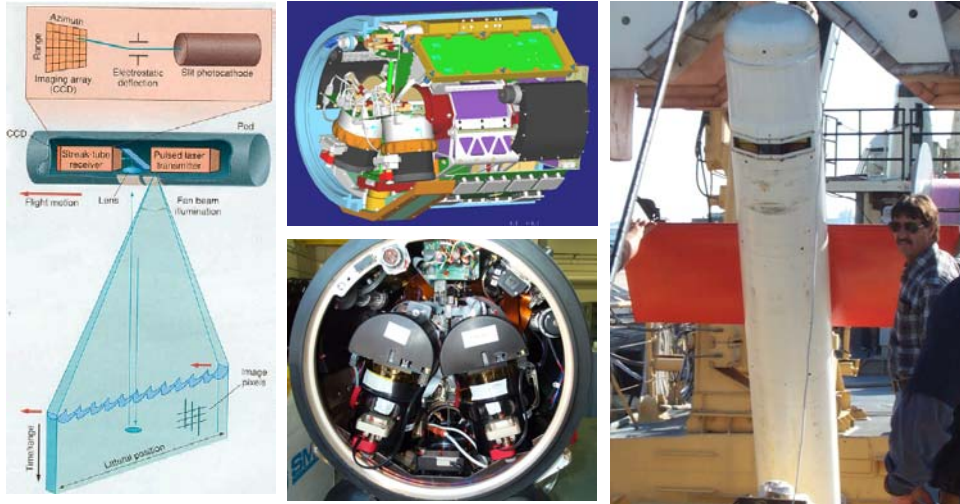
Figure 23: *Left the principle of the streak camera and middle and right show two streak camera tubes installed in an underwater vehicle for mine classification.*

Figure 24 demonstrates the range and contrast imaging capability, and also demonstrates the high resolution range information that the system can generate. Because the STIL system can collect multiple samples within the laser pulse length, the range resolution of the system is not governed by the sample period, but is given by:

$$\sigma_{range} = 0.6 \cdot \frac{c\tau}{SNR} \qquad (8)$$

where τ is the FWHM value of the laser pulse width.

An interesting extension of the streak camera can be made by using multiple slits, see Figure 25. In addition, the technique can also allow a significant number of applications to be explored, in which different spatial data is imaged onto the additional slits (e.g., different wavelengths or different polarization states).

Figure 24: *Above example of airborne 3 D imaging using a streak camera and below a scan across a vehicle from range within vehicle only, range image of the whole scene and reflectivity image of the whole scene. The range resolution on the vehicle images was 1 inch. From Gleckler[26]. The target is at close range (60 m) and the laser wavelength 532 nm.*
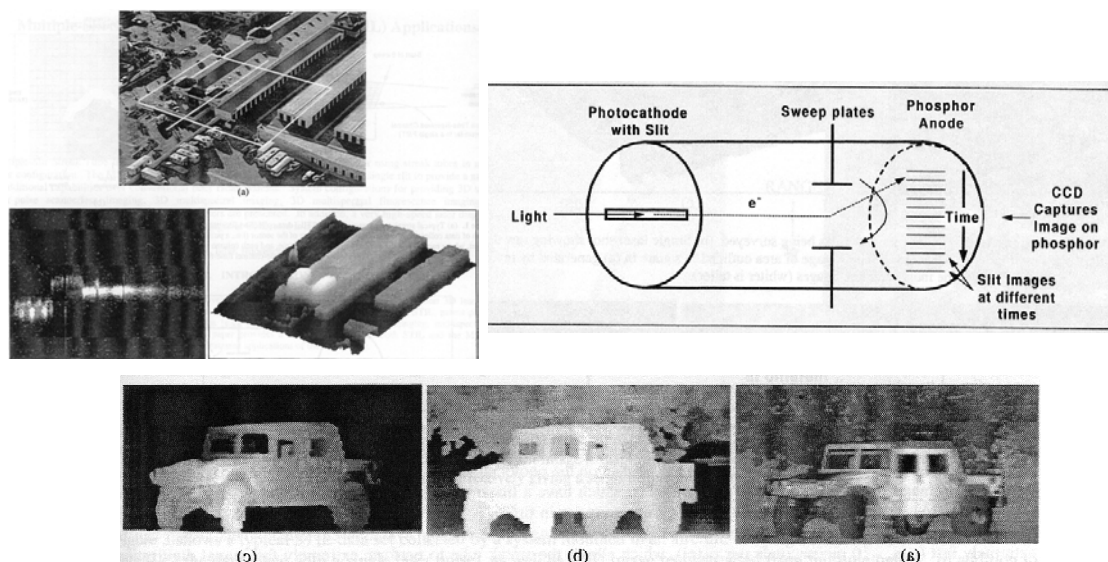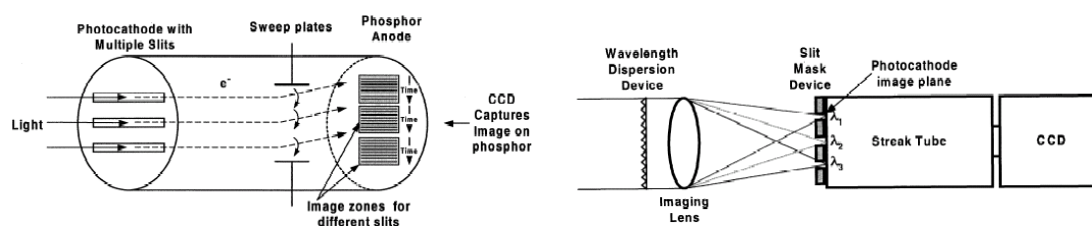

Figure 25: *Left, arrangement for the multiple slit streak camera system. Right, example of how to implement multispectral imaging for the multiple slit streak camera.*

For multi-spectral imaging and fluorescence imaging, the additional slits are used to capture different wavelengths. Figure 25 shows one hardware configuration used to perform the multi-slit spectroscopy function. The wavelength dispersion device (e.g., a diffraction grating) splits the wavelengths, while the Slit Mask Device (a spatial light modulator, for example) provides a programmable set of slits for selecting desired wavelengths. The transmitter can be a multi-wavelength source, with each of the transmitted wavelengths going to a different slit. Alternatively, it can be a single-wavelength transmitter, with one slit dedicated to the laser wavelength, and the other slits positioned at longer wavelengths in order to capture fluorescence phenomena. Each wavelength region will have a time and space resolved image. It is important to note that there are a number of trade-offs between the various dimensions of resolution, since the total number of pixels of the CCD is limited.

Figure 26 shows an example of an image showing reflection, fluorescence and range from a single laser exposure. The figure shows the results from a laboratory demonstration of a STIL fluorescence imager[27] operating at an excitation wavelength of 532nm and collecting three spectral bands: 532nm, 550-650nm, and 650-850nm. The scene consists of a green plastic trashcan with a house plant on top, located about

1 meter in front of a white wall containing three paper resolution panels with black bars. The bar targets have a 50% duty cycle and a period of 37mm. The resulting three spectral band images are colorized blue, red, and green, respectively. The 3-band composite displayed in RGB color enables the three spectral bands to be displayed simultaneously. Figure 26 shows the color image overlaid on top of a surface map to simultaneously display the spectral and range data. Three views of the 3D multispectral data are shown.
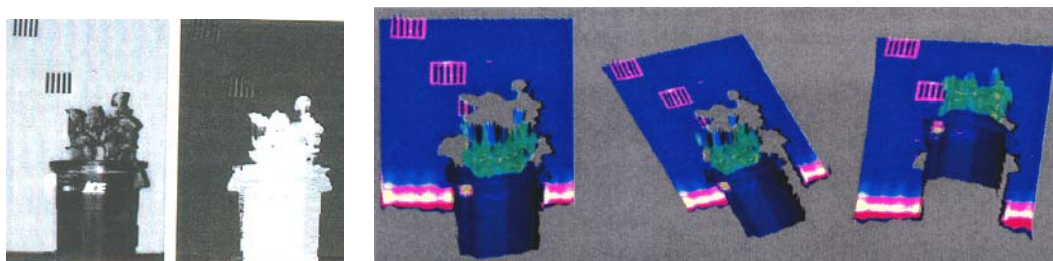

Figure 26: *Picture of a trashcan plus a houseplant seen with a SLIT camera in reflection, range and combined fluorescence and range. See text above for more details. From ref. 27.*

A 64x64-pixel lidar system that uses a streak tube to achieve range-resolved images was recently demonstrated. An array of glass fibers maps light from an area in the focal plane of an imaging lens to multiple rows of fibers on the streak tube's photocathode. Data processing yields 64x64-pixel contrast (intensity) and range images for each laser pulse. Range precision better than 2.5% of the range extent is exhibited for a wide variety of targets and terrains at image rates up to 100Hz. Field test imagery demonstrated the capability of the Flash lidar system for imaging vehicles hidden by a tree canopy as well as for imaging sub-surface mine-like targets in the ocean. Figure 27 shows an example of target under trees capability from an airborne system flying at 100 m altitude.

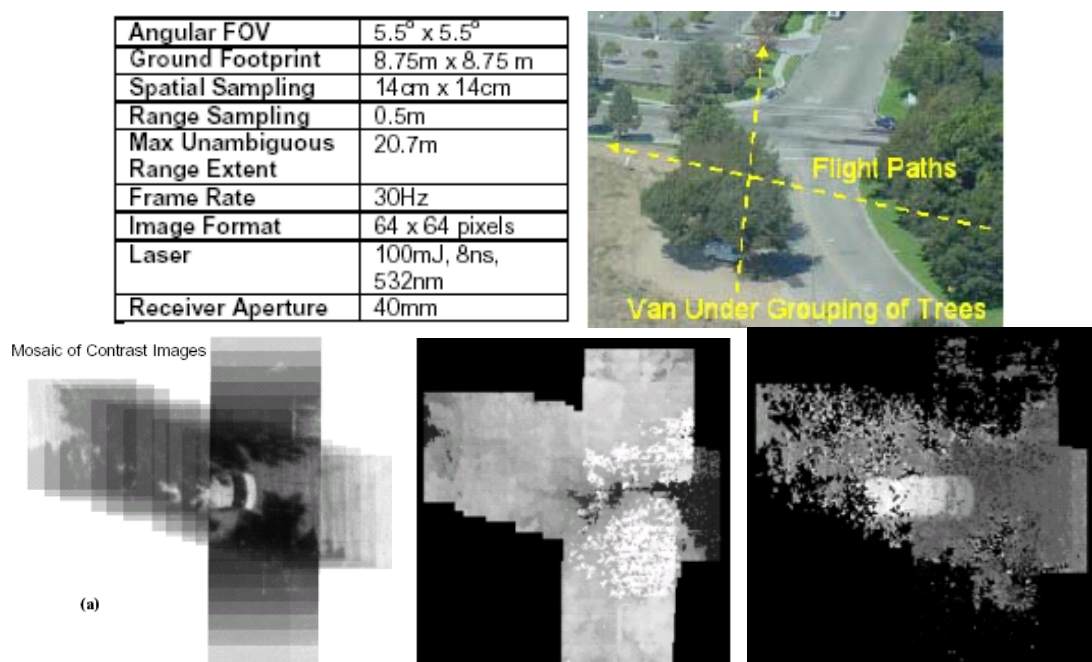|	
Angular FOV	5.5° x 5.5°
Ground Footprint	8.75m x 8.75 m
Spatial Sampling	14cm x 14cm
Range Sampling	0.5m
Max Unambiguous Range Extent	20.7m
Frame Rate	30Hz
Image Format	64 x 64 pixels
Laser	100mJ, 8ns, 532nm
Receiver Aperture	40mm

Figure 27: *Top the system parameters for an airborne experiment showing target under tree detection. Bottom: left the number of consecutive views which are used to form the final image, middle shows the*

first echo range image and left the last echo range image formed by combining multiple views. From Gelbart et.al [28].

Examples of advantages for the streak camera approach are:
- Versatility- a variety of laser radar configurations can be combined into several different measurements, such as 3D, multispectral, hyperspectral, multi-excitation hyperspectral, fluorescence-lifetime and polarization onto a single sensor taking data simultaneously.

- High range resolution (cm level)

- High time resolution (in principle ps) allows fluorescence lifetime to be added to observed parameters.

Examples of disadvantages are:

- Scanning or sensor movement in one direction is needed.
- Complex equipment using high voltage (kV)
- Not very compact
- Relatively high cost ?

Flash imaging FPA – technology status

The technology that seems to draw the largest attention in 3-D imaging for military applications right now is 3 D sensing focal plane arrays (FPA's).

A laser flood illuminates a target area with a relatively short (1-10 ns) pulse. The time of flight of the pulse is measured in a per pixel fashion. The position of the detecting pixel yields the angular position of the target element, and the time of flight yields the the range. With a single "shot", the complete 3 D image of a target is captured. An important feature to make this type of FPA a reality, is to have a Readout Integrated Circuit, ROIC, to capture information that determines the range of a return at each pixel Field of View, FOV. In this fashion, though all the 3-D information is captured in an instant, it can be read serially at a rate compatible with passive IR readout circuits.
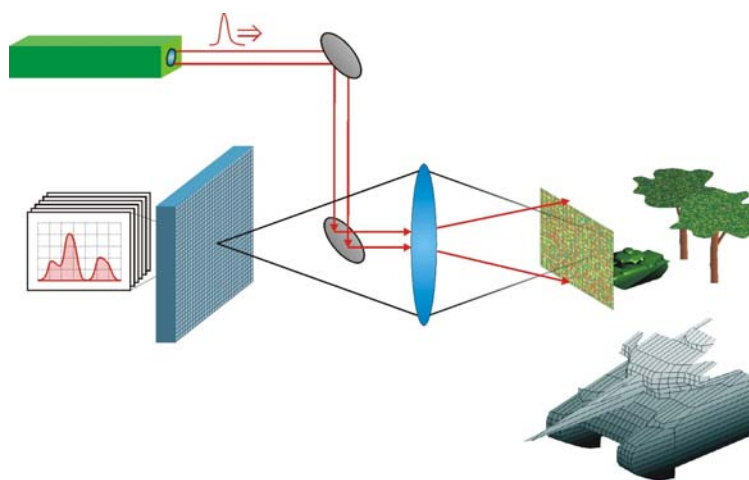

Figure 28: *The principle of the 3 D FPA flash laser imaging concept. Image idea after Raytheon[29].*

There are many problem areas associated with the development of a 3 D FPA detector. Some of these are

- Low noise important, only 100 photons per pixel may be available for long range imaging
- Large number of pixels wanted for shot capture , 128^2 or larger
- Uniformity of yield , time and sensitivity harder for large number of pixels
- High dynamic range (> 40 dB) to encompass target reflectivity and signal span due to range
- Time sampling 1 ns or better
- Small pixels for small IFOV (less than 10-50 m dep. on application)
- Small pixels limit cell size for read-out circuits
- Full waveform capture and return processing limited by electronic cell size.
- Electronic crosstalk between detectors in the array.

Many of these problem areas will be motivated in the text below. First a few comments on the noise, bandwidth, dynamics range and pixel size issues:

Noise

Assume that we want to observe a scene at range R=20 km with an average reflectivity ρ=10 % with a laser of energy Ep=100 mJ and that we are receiving the laser energy evenly distributed among the N_{pix} =128*128 pixels in a D=20 cm receiver. Assume a visibility of about 15 km which at 1.5 μm wavelength corresponds to roughly $T_{atm}{}^2$=10 dB in atmospheric double path loss. The number of photons per pixel is then easily calculated from:

$$N_{ph\_pix} = E_p \cdot \frac{\rho}{\pi} \cdot \frac{\pi D^2}{4R^2} \cdot \frac{1}{N_{pix}} \cdot \frac{1}{h\nu} \cdot T_{atm}^2 \qquad (9)$$

where hν is the photon energy =1.3 E-19 J at 1.5 μm. The number of photons per pixel according to the figures above is just 38! For a 1 J laser it would be 380 etc.
The low photon count means that we need low noise and sensitive detectors. Ten photons during 1 ns corresponds to 1.3 nW for 1.5 μm wavelength. Thus the NEP of each pixel should at least be less than 1 nW.

Bandwidth

Target depth structures on the order 15 cm need to be resolved. This means bandwidths on the order of 1 GHz.

Dynamic range

A laser radar return can in principle come from the near field (100 m) and from long ranges (10-20 km). Assuming a $1/R^2$ dependence (resolved target) this range effect can result in a need for dynamic range above 30 dB or more. The target reflectivity can also vary by a factor of 100 or more concerning ordinary surfaces and terrain. Including retroreflecting targets will add another 40 dB or so to the dynamic range if

we want to avoid sensor booming from these targets. A high dynamic range will probably lead to logarithmic amplification unless we want to accept a range of 40 dB in total, which might be handled without logamps.

We will briefly now review some of the developments in 3 D FPA:s. The US are leading this effort and have several different programs. In Europe, the effort has so far been limited to some activities connected to 2 D imaging pixilated arrays (UK) and linear arrays (Germany). There is, however, a growing interest among the European countries to increase investments in this area.

1/ Fibertek: 76 el IPF (Intevac) for BMDO

Fibertek Inc. is developing a 3D imaging laser radar under the sponsorship of the BMDO Discriminating Interceptor Technology Program (DITP)[30]. In this program, Fibertek is the prime contractor for a team including Fibertek, Schafer Corporation, the Electro-Optics Organization (EOO) and INTEVAC. The purpose of the interceptor ladar is to operate in conjunction with an IR focal plane array on an exo-atmospheric kill vehicle to provide increased probability of target recognition from a target complex containing a re-entry vehicle, replicas and other decoys.

The system will operate at exo-atmospheric ranges out to several hundred kilometers. At the longest ranges, targets are not fully resolved in angle, in which case the ladar utilizes range imaging and intensity modulation information to provide target discrimination. At ranges where targets are angularly resolved, the ladar uses shape and orientation information to provide additional target cueing. This combination of functional modes has been found to provide a discrimination capability that significantly enhances target selection capability over that of a seeker using a passive sensor alone.

The laser is of high interest for 3 D imaging as it gives a 1.3 ns pulse at 100 pps and with an energy exceeding 250 mJ. The laser transmitter is a diode-pumped slab oscillator-amplifier. All of the transmitter stages are conductively cooled Nd:YAG slabs.

The ladar uses a multipixel receiver with GHz digitization of the signal from each pixel. The receiver design utilizes an 8-bit A/D converter to digitize the detector anode signals. In the final system, a GHZ A/D channel configured as shown in the figure will follow each of the 76 anode pixels. This architecture relies heavily on COTS telecommunication chips that are advancing rapidly and thereby provide a growth path to even higher performance. The current generation of A/D provides 1000 MHz digitization rate and a record length of 8192 range bins. The higher resolution and longer record length allows significant simplification of the signal processing required to develop AARI ladar images. Upgraded chip sets with 1.5 GHz digitization rate are already available. Figure 29 shows a schematic sketch of the receiver.

The ladar detector is a multipixel Intensified Photodiode (IPD) manufactured by INTEVAC, shown in Figure 30. The tube incorporates a GaAsP photocathode in

order to produce over 25% Detected Quantum Efficiency at the laser wavelength of 532 nm. The tubes have an electron gain greater than 10,000 and are therefore capable of single photoelectron counting. In the imaging receiver each of the anode pixels is coupled through a low-noise preamplifier/filter into a digitizer channel. The individual preamplifier gains are adjustable in order to compensate for pixel-to-pixel differences in gain and sensitivity. Figure 30 also shows the 1 GHz digitizing board. Nineteen 4-channel boards will be used.
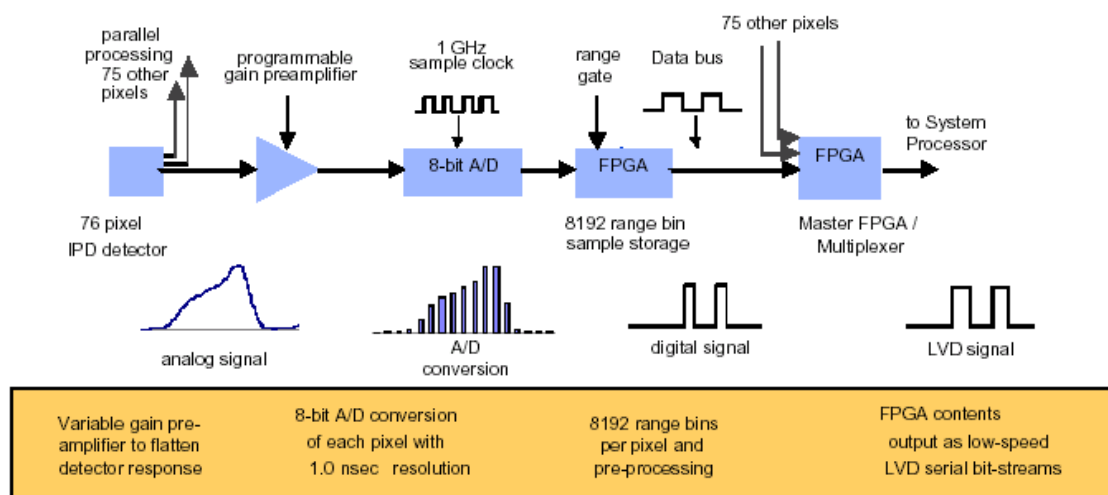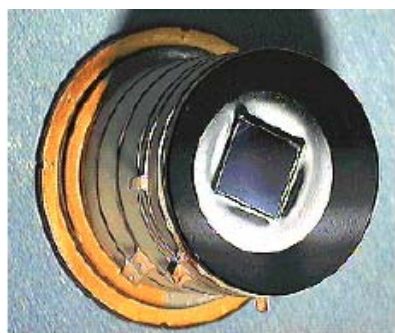

Figure 29: *Schematic diagram of the GHz multipixel receiver .From ref. 22.*

Figure 30: *Left: the Intevac 76 pixel detector based on an intensified tube. Right: a 1 GHz digitizing board. From ref. 30.*
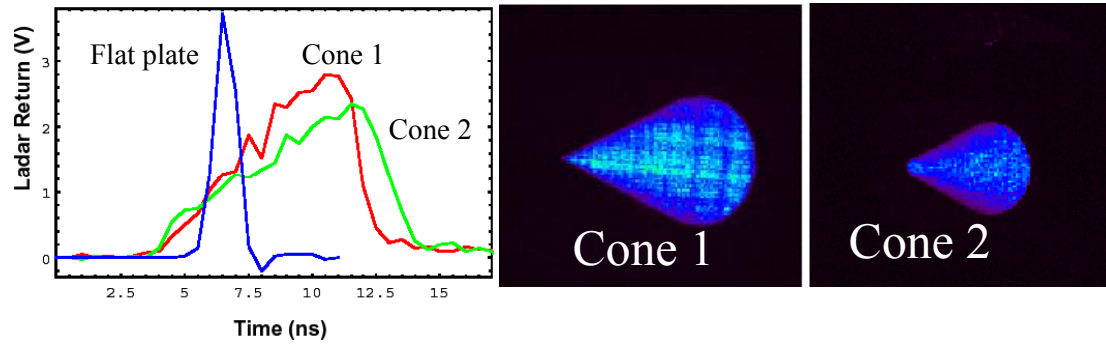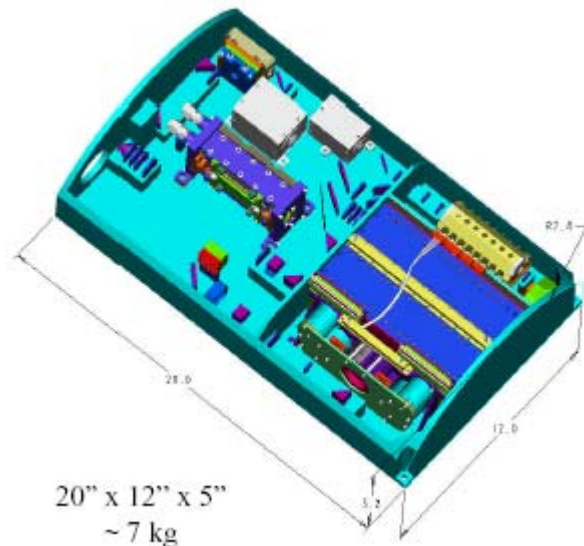
Figure 31: *Example of waveforms from different objects to be used for target discrimination.*

The 1-D performance is illustrated in Figure 31. The parameters for the final system are outlined in table 3. The parameters are impressive, especially the weight, bearing in mind the laser specifications.

Table 3. *Parameters for the BMDO laser system*

Parameter	Field Demonstration LADAR
Size	20 x 12 x 5
Mass	<10 kg
Range Resolution	15 cm (1 GHz)
Range Bins	8192
Intensity Levels	256
Pixels	76
Detector QE	5/30% (Hamamatsu/IPD)
Laser Energy/Pulse	250 mJ
Laser PRF	100 Hz
Laser Pulse Length	1.3 ns

Figure 32: *Left the final design for the 76 pixel imager, right the goal for the system parameters.*

2/ Eye safe laser radar, Advanced Scientific Concepts, WPAFB[31]

The low photon numbers for long ranges were discussed above. Like the Fibertek approach, the company Adv. Sci. Concepts is working for Wright Labs on 3 D FPA using a gain tube from Intevac as the front detector to have low noise gain. In this approach, the limiting SNR will be dictated by the photon statistics. The other way to achieve gain is to use avalanche photo diodes (APD's) - more of this approach later on. This gain tube is the type of eye-safe photocathodes developed for gated viewing. Figure 33 illustrates an electron bombarded (EB) image tube developed by Intevac.
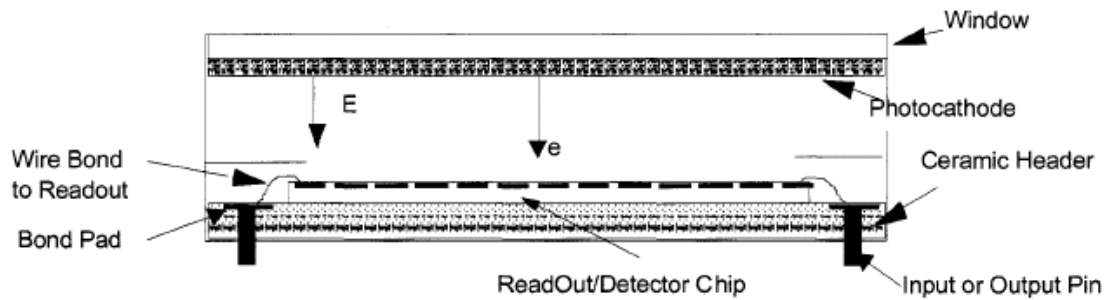
Figure 33: *The imaging laser radar sensor.*

The image tube sensor works as follows: photons pass through the window and interact with the photocathode producing a photoelectron. This electron is accelerated by the electric field E through a potential measured in kV and penetrates into the silicon of the ReadOut/Detector chip causing gain by impact ionization. Approximately one electron-hole pair is produced for each 3.6 eV for those photoelectrons which penetrate into the active silicon region. The noise factor is a very low 1.02. Another image tube configuration incorporates a microchannel plate (MCP) between the photocathode and the ReadOut/Detector chip. In this latter configuration the MCP amplifies the electron signal and the ReadOutDetector chip collects the electrons. The MCP has the advantage of higher gain, if that is necessary, but the disadvantage of higher noise factor.

Figure 34 shows the target objects used in 3-D image test. The objects are a cement bench, a bottle on the bench, a pair of laser goggles on the bench and a hat on the bench. The bench is in front of a large tree. The figure also shows a 2-D zoom of the objects and a 3-D image.

WFOV
Video image

Video zoom   32*32 el   32*32 el
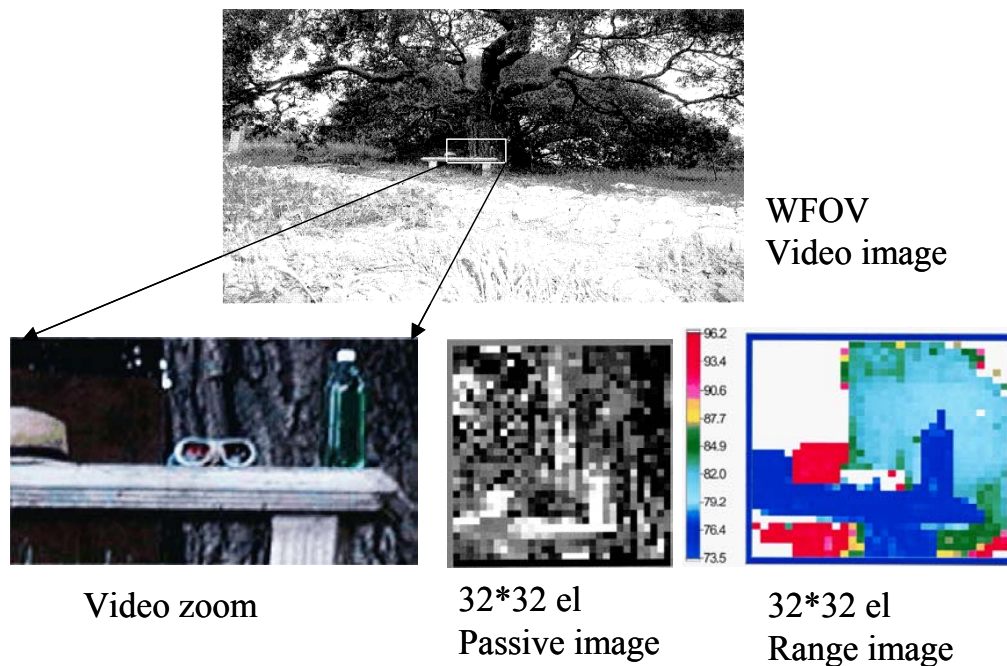   Passive image   Range image

Figure 34: *Video image of the scene and passive and active range imagery. The resolution is about 1 ft. The colour range scale is in feet. From ref. 23.*

A comparison of the passive 32*32 pixel image with the active 32*32 image shows the power of 3-D imaging: It is clear that the high contrast generated by the range differences of the objects and the background makes object identification much easier in the 3-D image.

The imagery shown in figure 34 was the first development. According to ref. 23, the technology used can be extrapolated to the many more and smaller pixels. In ref. 23, a unit cell design was tested that had 1.5 inch resolution at a range of 7 km, the equivalent of about 17.5 bits in dynamic range.

Table 4. *Development of 3D FPA imaging laser radars according to ref. 31*

	Old LR-FPA Design (1994-1996)	Currently Available
Unit Cell Size	400 um x 400 um	50 um x 50 um
Array Size	32 x 32	320 x 320
Laser Pulse	20 ns FWHM	2 ns FWHM

3/ Staring underwater laser radar (SULAR) 3-D Imaging [32]

For underwater imaging, the water backscatter is a limiting factor on contrast and resolution. Therefore, another approach for read-out is appropriate instead of capturing the first echo. The method applied by Stettner et.al is that of gated viewing by adding several range slices and sliding the range gate over the object of interest.

The device reported in ref. 32 potentially has the capability of sub-nanosecond integration times or, equivalently, better than 15 cm range resolution in air and better than 11 cm range resolution in water with modern CMOS technology. These chips have the capacity of better than 25 time slices. Similar experiments showed that 100×100 SULAR readout chips could be run with integration times shorter than 3 ns.
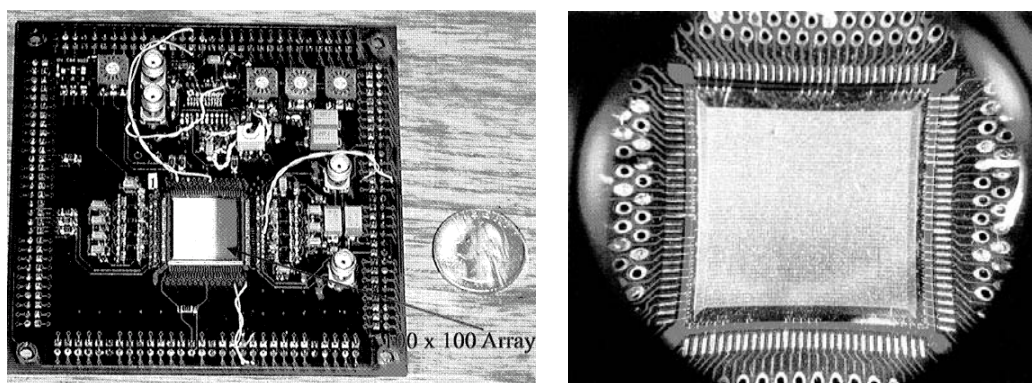

Figure 35: *A 100*100 SULAR array for underwater imaging. From ref. 32.*

The above described approaches all rely on having a gain tube as the front end to obtain low noise and high gain. We will now describe the approach of using avalanche photo diodes, run in conventional gain mode or in the so called Geiger mode.

4/ HgCdTe MWIR avalanche photodiodes for 3 D imaging[33,29].

The avalanche photodiodes made in silicon have been relatively unsuccessful in arrays much greater than about 10 x 10. One problem is gain non-uniformity. Apparently the slight detector to detector variation of material properties across the detector array causes the problem, as might be anticipated by the sensitive, exponential dependencies in the gain process. The silicon cut-off is just above 1 μm wavelength.

InGaAs has been proposed for 3 D imaging using both PIN and APD structures. It is however a common view that these detectors have higher noise than the HgCdTe diodes.

The HgCdTe detector offers the advantage of simultaneous detection of multiple wavelength photons emitted from an OPO source for enhanced range performance. The HgCdTe photodiodes can span a broad range of compositions corresponding to cut-off wavelengths from 1.3 to 11 μm. This offers the additional capability of tuning the spectral sensitivity to MWIR bands for enhanced operational capability during conditions of low visibility. This also has the potential to provide multi-spectral capability for enhanced discrimination of tree canopy, camouflage and the target. Further, innovative design concepts for the two-color HgCdTe detectors that will allow simultaneous active and passive sensing within the same single chip format are under investigation[34]. The passive mode could be an additional discriminant or provide wide field of view (WFOV) target acquisition and handoff, if needed.

The gain for a HgCdTe avalanche photodiode can be up to 100, with as low bias voltages as 6 V. The rise time can be as low as 0.35 ns. The shot noise current for an APD is given by:

$$I_S = \sqrt{2eIM^2F} \qquad (10)$$

where e is the electronic charge, M the gain , I the signal current and F the excess noise factor. This factor is used to quantify the noise due to statistical variation in the avalanche gain. It has recently been observed [35] that the F factor = 1 up to gains over 50 in contradiction with the old theory from McIntyre which predicts the F factor to be = 2 or more.

5/ Three-Dimensional Imaging Sensors Program at Lockheed Martin[36]

The detector in this program is a short wavelength infrared HgCdTe APD array based on DRS Infrared Technology's well established architecture of HDVIP® (High density, vertically integrated, photodiode). This device is a cylindrical n-on-p photodiode formed around a small via in the HgCdTe. The via serves as the interconnect conduit between the n-side of the photodiode and the input to the readout circuit.
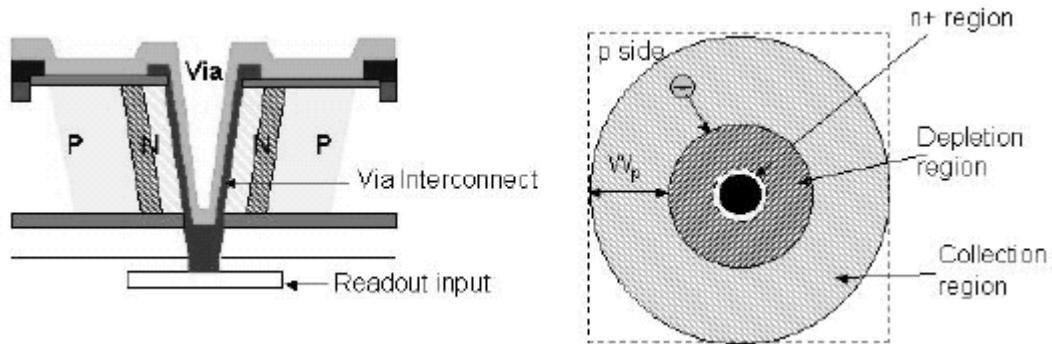
Figure 36: *Cross section and top view of the HDVIP diode used in avalanche mode .From ref. 36.*

The ROICs implement "on-chip" pixel level signal processing to generate 3-D imagery. The FPA will be scaled to a full-sized array (128x128) and a prototype system will be fabricated for validation and demonstration of the "Flash" LADAR concept.

At high biases extremely uniform APD gain behavior was observed over a range of temperatures from 180 K to 77 K. For example, APD gains higher than 100 were observed, in 40 µm pitch devices. The gains of test structures with the same diode diameter bar show remarkable uniformity, where at a nominal gain of 30, the variation in gain is + 6% at 5 V bias.

Two different ROIC's are discussed in the paper of ref. 36. One is an analog matched filter approach and the other a temporal sampling ROIC giving the full waveform. The analog matched filter readout integrated circuit (ROIC) approach seeks to replicate the traditional signal processing performed in single-detector LADAR systems. The design consists of a transimpedance amplifier (TIA) connected directly to the detector, implementing a matched filter function. The TIA feeds a peak detector, which finds and stores the peak detector signal value, as well as the time when it occurred. These stored values are then read out through a multiplexer. Figure 37 shows a conceptual drawing of this approach.
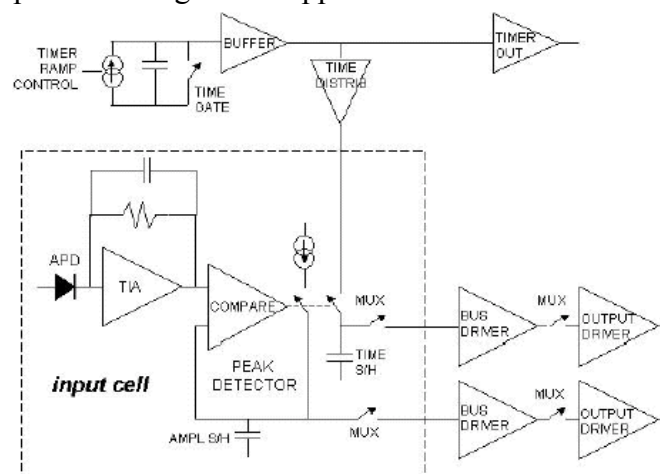

Figure 37: *The design of the peak detection unit cell in the ROIC. From ref. 36.*

The "waveform" ROIC described in ref. 28 provides over 50 samples, at high temporal resolution (as fast as 2 ns), for each pixel in a 128 x 128 array. The time-sliced waveform stored at each pixel will then be processed "off-chip" by a pulse

signal processor. The signal processor will implement a digital matched filter to discriminate target returns from extraneous signals, accurately resolve range, and provide intensity data. The matched filter is implemented by convolving a programmed template, designed to match the nominal pulse shape, with the data in steps of one data sample. Because many data samples are used at each step to generate the convolver's output, available signal-to-noise is used to best advantage. Since our approach stores the waveform of the return laser pulse, future growth to other signal processing algorithms is possible. This can give the system the ability to find targets that are partially concealed or camouflaged with nets, as illustrated in figure 38.
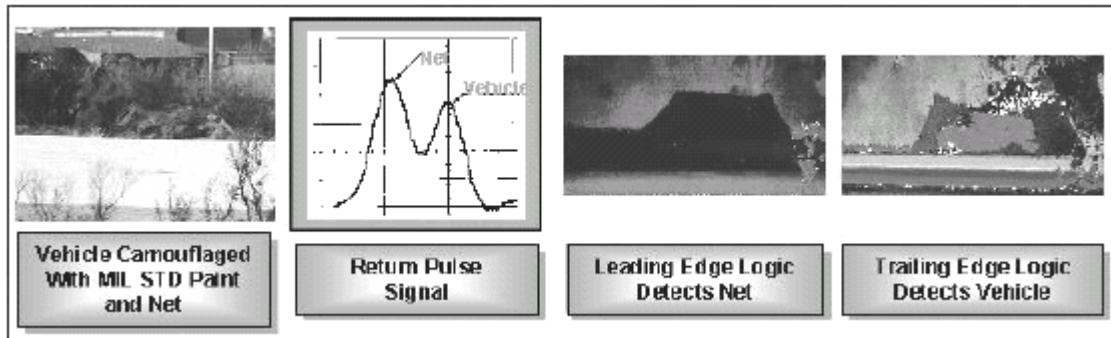
Figure 38: *Illustration of " see behind the net" using waveform processing. From ref. 36.*

The sample cell architecture is a standard "dump, ramp, sample" architecture. The operational sequencing is such that at some reference time, the charge well is reset to its zero signal level. After the reset function has occurred, the input multiplexing switches turn on in series to allow current from the detector to flow into the charge well, ramping the charge well voltage as the capacitor accumulates charge. After the detector sampling period is complete, the input multiplexing switches open and the charge level on the charge well is held until the output multiplexing operation reads out the signal level. The process then repeats after the frame start command is received. Since the time to create the image is short, there is no sample-and-hold in the unit cell. The readout of the data occurs after the integration is complete.
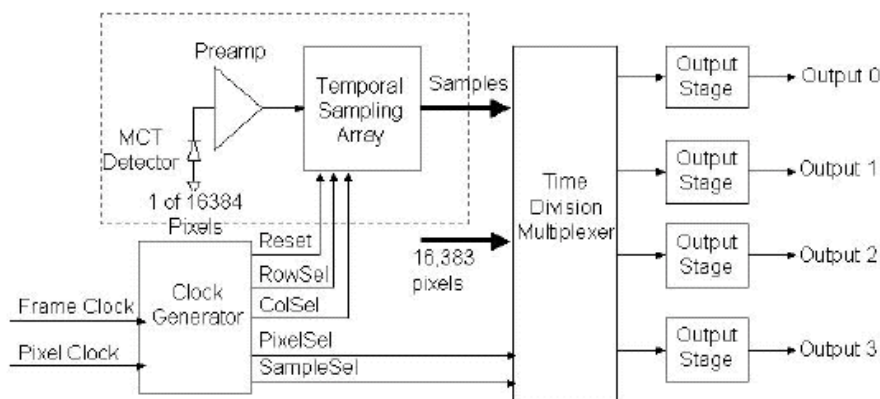
Figure 39: *The ROIC solution suggested for temporal sampling at 2 ns resolution and 50 samples. From ref. 36.*

6/ 3-D FLASH Ladar at Raytheon [37].

Raytheon's approach is to build on our existing base of high performance Mercury Cadmium Telluride, HgCdTe, detector diode technology to produce avalanche photo-diode (APD) arrays for 1.5 m operation. They plan to use a novel time-of-arrival approach and circuit concept to yield the highest amount of information in a flexible format. High speed silicon processes compatible with commercial foundries will be used to develop the ROIC. The ROIC and APD detector will be hybridized using the matured indium bump process and will be packaged in a compact housing for field demo. Figure 40 shows the detector and ROIC.

Figure 40: *Hybridized detector and ROIC array using Indium bumps. From ref. 37.*

The uniformity problem for detector NEP is illustrated in Figure 41.

Figure 41: *Illustrates the performance of an LPE array . The $7x7$ core has >94% of the APDs with NEP < 2nW at a gain of 13 with a 42MHz bandwidth. From ref 37.*

7/ Three-Dimensional Laser Radar with Geiger mode APD Array, MIT[38].

Lincoln Laboratory has an integrated program to develop technologies and address system issues relevant to 3-D laser radars. Technology development efforts include the development of silicon Geig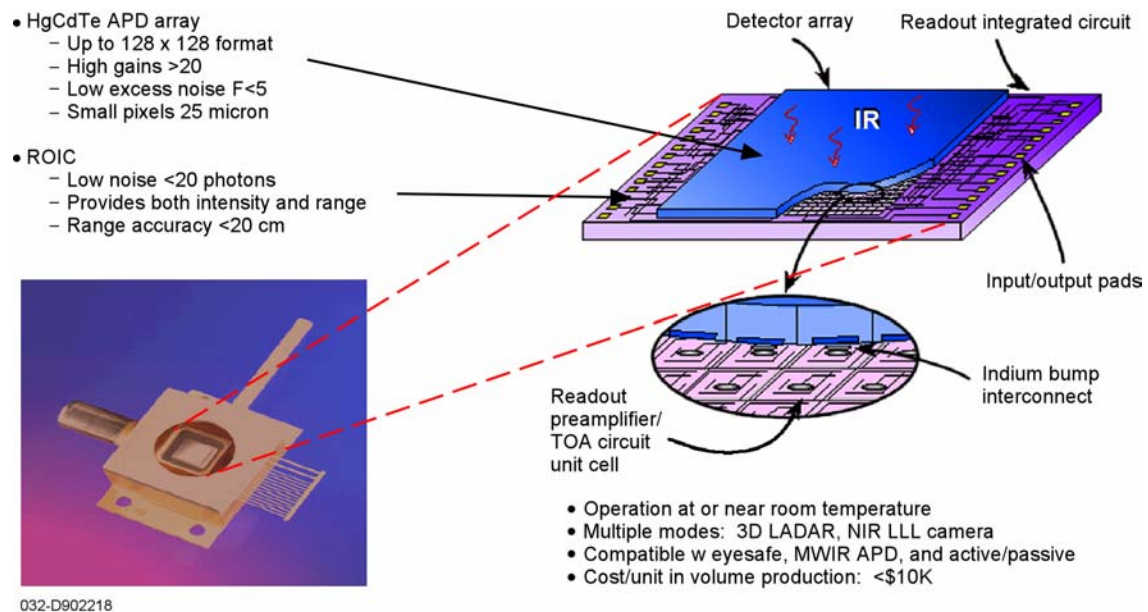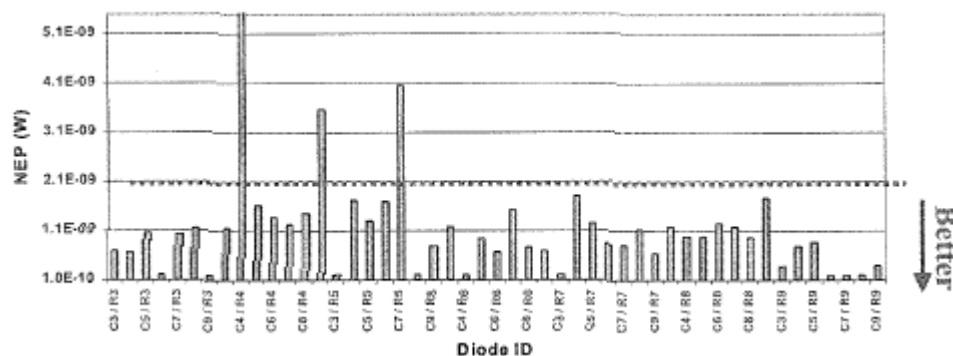er-mode APD arrays with associated timing circuitry, the development of InGaAs Geiger-mode APD arrays to expand the sensitivity of these devices to the short-wave IR, micro Nd:YAG laser development, and ladar prototype systems development. Figure 42 illustrates the circuit and operation.
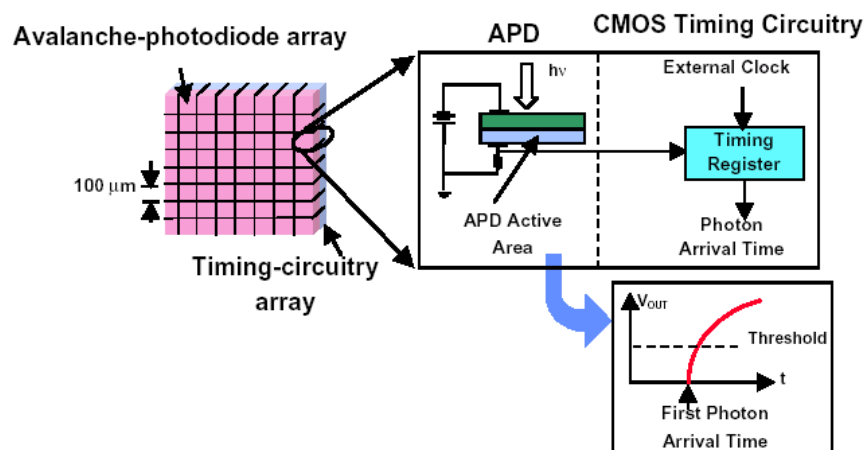
Figure 42: *Illustration of the circuit and operation of a detector working in the Geiger mode.*

Each hybrid pixel then contains a Geiger-mode APD and a timing circuit. The Geiger-mode APD can be thought of as a photodiode whose back bias voltage actually exceeds the level at which the detector will break down. When photoelectrons are generated at the device junction due to the absorption of one or more signal photons, they are accelerated in the electric field from the bias voltage. In the case of a "linear"-mode APD, the photoelectrons are accelerated enough to knock more electrons from the lattice and the total number of photoelectrons increases, resulting in gain. In a Geiger-mode device, the gain is so high that enough photoelectrons are generated to cause the device to breakdown and allow a large current to flow until any capacitance across the device is discharged.

The advantages to this mode of operation are several:

- High uniformity. The variations in the gain from pixel to pixel or as a function of operating parameters or just due to statistical variations become irrelevant, since the device is driven into saturation.

- High senitivity. Effectively, the device becomes sensitive to a single photon and the output is noiseless, except for fundamental shot noise.

- High subnanosecond time resolution.

Disadvantages:

- The saturation. More than one photoelectron being generated in the absorption region can be addressed by limiting the signal level to an average of less than a photoelectron per laser pulse and looking statistically at the number of detections per number of laser pulses. This represents the most sensitive form of optical measurement in which every photon is counted.
- No waveform and intensity (reflectivity) values.

The time counter generates a sequence of 2^{15}-1 psuedo-random numbers. Since the exact sequence is known, the random number can be decoded during readout with a simple lookup table to produce a count. Two effective bits of timing resolution are added by recording the clock state and a 90-degree phase-shifted version of the clock. Thus, 0.5-ns timing resolution can be achieved with a 500-MHz clock in a simple design.
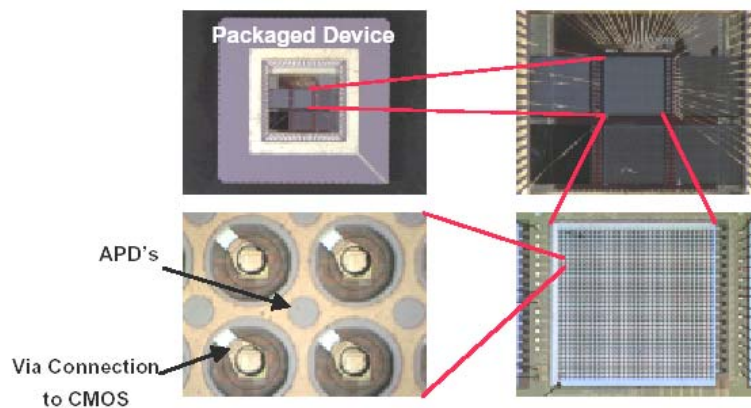
Figure 43: *A 32*32 pixel InGaAS array for 3-D imaging. Ref. 38.*

The material system being developed for this purpose is InGaAs. This material can be used for developing both 1 and 1.5 μm devices. The 1 micron devices are simpler and compatible with the well developed Nd:YAG laser. They can this be of high interest for short range applications (seeker etc.) where eye safety requirements are of less concern or can be met due to the high sensitivity of these detectors and high-PRF operation.

Developments of the μ−chip laser have been aimed at increasing the per-pulse energy output. Laser systems with outputs in excess of 250 μJ at 1 kHz PRF's have been developed, which continue to produce sub-nanosecond (380-ps) pulses. Figure 44 shows an example of microchip lasers at MIT.
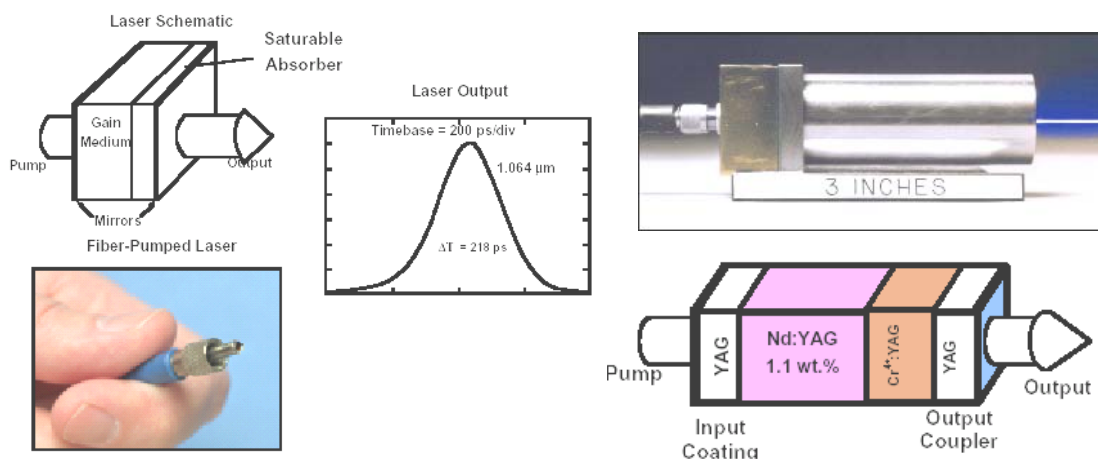
Figure 44: *Microchip laser development at MIT. Note the sub nanosecond pulse width. Right shows a high energy version. From ref. 38.*

An example of data collection is shown in Figure 45. Both the CCD and the APD sensors produced 128x128 images, which were matched in field of view, and the CCD camera could image a target that was actively illuminated. Comparison of a CCD image, in this case sunlight illuminated, with a 3-D image is shown in Figure 45. In this case the CCD image, which was collected as an average of 200 frames with 300 photoelectrons/pixel/frame, displays only one truck, but the truck behind the tree-line on the left is obscured. The corresponding 3-D image, using only an average of 0.3 photoelectrons /pixel over 200 frames, clearly shows the truck in the open and the truck behind the tree line when the data cloud is rotated in software and redisplayed. Again, the utility of photon-counting 3-D imaging is shown. Also shown is the usefulness of rotating 3-D images for the perception of targets in clutter. In the lowest image note how the low photon count CCD image from the low light level camera gives a hardly usable intensity picture, while the 3 D laser image, due to higher sensitivity and range information, is much easier to interpret.

Recently the MIT group[39] published a paper on a 4*4 avalanche photodiode array with photon counting capability and 3 cm range resolution. The reolution in the transversal directions was also 2-3 cm. With only 3 micoJ (3E-6 J !) they achieved very good imagery with only one pulse at 60 m range. This corresponds to ranges in the 10' s of km using a 1 J laser under good visibility.

Figure 46 shows image examples obtained during a sunny day.
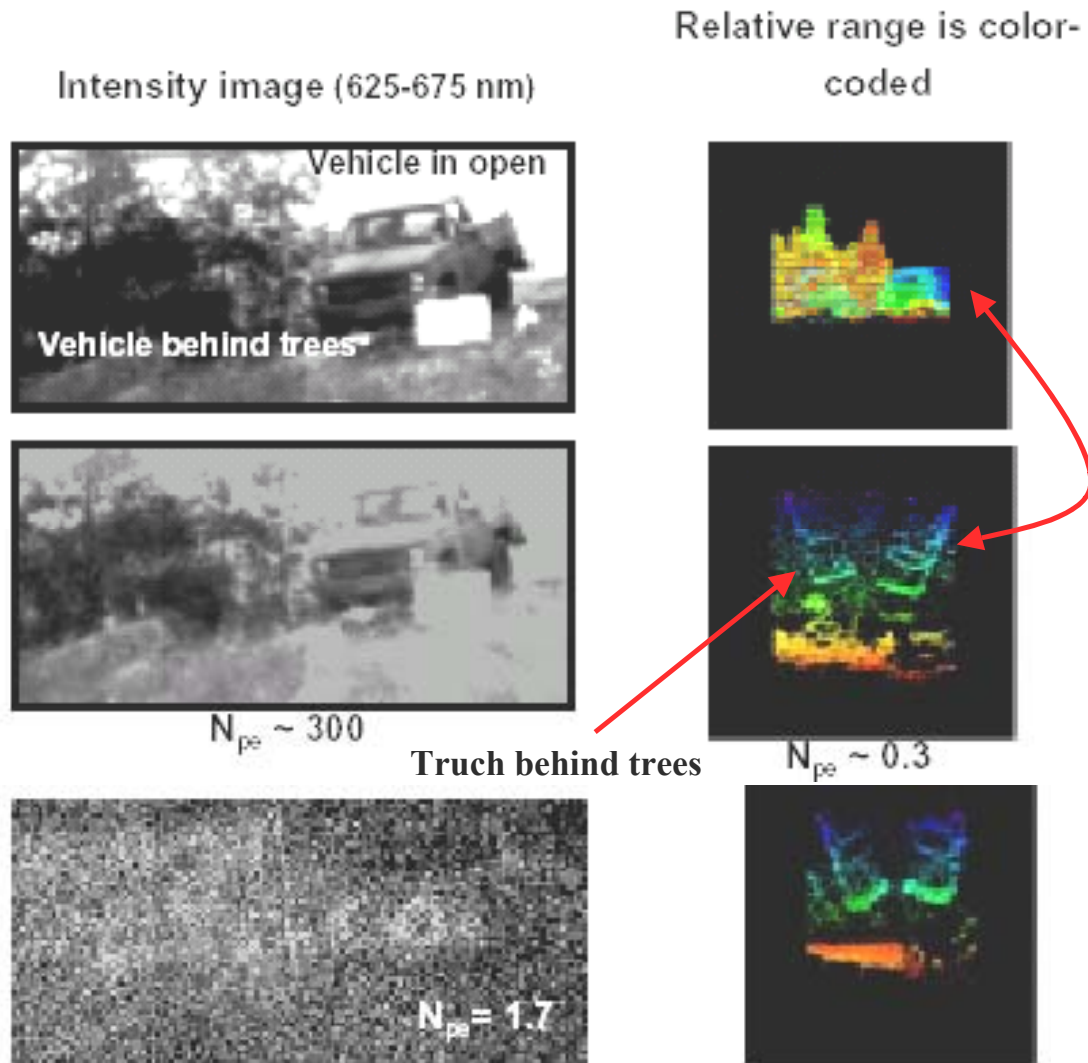
Figure 45: *1st and 2nd row: Comparison of intensity and 3-D images of a pair of trucks one behind a line of trees. Npe is the average number of photoelectrons for each image over 200 processed frames. 3rd row Comparison of laser intensity and 3-D images during darkness. From ref. 38.*
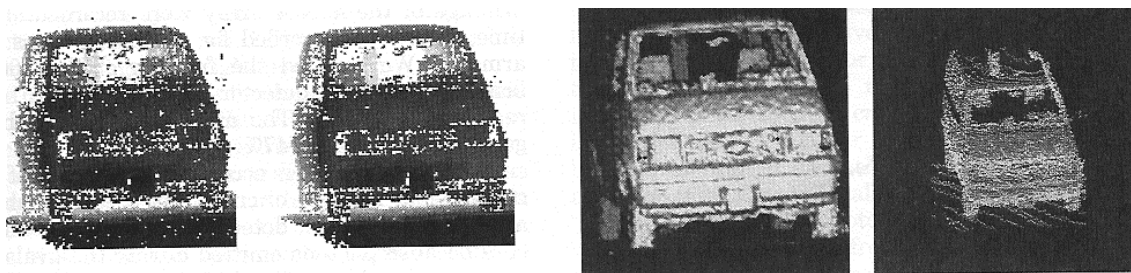
Figure 46: *Image of a Chevrolet Astro obtained by the MIT 3 D laser radar. From left to right: Single frame of target at 60 meter during a sunny day with only 3 microJ pulse energy, 3 frame average , next two rendered images from multiple frames. From ref. 39.*

8/ Adaptive LADAR Receiver for Multispectral Imaging, Rockwell[40]

The detector arrays are made of uncooled InGaAs PIN devices for imaging at 1.5 pm wavelength and cooled HgCdTe PIN devices for MWIR imaging at 3.8 pm wavelength. Rockwell is also investigating concepts using multicolor detector arrays for simultaneous imaging at multiple wavelengths (active-active and active-passive) that would provide additional spectral dimension capability for enhanced detection and identification of deep-hide targets. The system is suited for flash ladar imaging, for combat identification of ground targets from airborne platforms, flash-ladar imaging seekers, and autonomous robotic/automotive vehicle navigation and collision avoidance applications. Initially 64*64 arrays will be fabricated but the arrays are said to be scalable to 256x256 or higher depending on the system application.

The receiver camera will have adaptive gain and bandwidth controls to maximize SNR as a function of target range and signal conditions, and an integrated receiver echo processing unit with adjustable sampling rates to maximize the use of available receiver SNR and the characterize echo shape. Rockwell believes that the current state of the art in CMOS technology will allow sensitivities of approximately 30 electrons per pixel with timing resolution of <1 ns (<15cm depth resolution) in the future. The desired detector parameters are shown in the table below.

Table 5. *Desired detector parameters*

Characteristic	InGaAs	HgCdTe
Response Band	0.9-1.7μm	Band 1: 1.49/3.8μm Band 2: 1.52/3.6μm
Pixel Size	100x100 μm^2	100x100 μm^2
Array Size	64 x 64	64x64
Operating Temp	RT or 1-stage TE for InGaAs	195K using LN2 Dewar or TE cooled
Detector Qe	80%	70-80%
Non-uniformity	7%	7%
Cross talk	< 1%	< 1%
Dark Current	0.1 nA	0.25 nA
Detector Capacitance	30-50 fF	30-50 fF
Collection time	50 ps	150 ps

9/. 3D Time-of-flight distance measurement with custom solid-state image sensors in CMOS/CCD-technology [41].

In this dissertation by R. Lange , University of Siegen Germany, an imaging, i.e. non-scanning, TOF-camera is introduced, based on an array of demodulation pixels, where each pixel can measure both the background intensity and the individual arrival time of an RF-modulated (20 MHz) scene illumination with an accuracy of a few hundreds of picoseconds ($300 \cdot 10^{-12}$ s). The pixel's working concept is based on the CCD principle (Charge Coupled Device), allowing the transportation, storage and accumulation of optically generated charge carriers to defined local sites within the imaging device. This process is extremely fast and essentially loss-free.

The extracted pixel information is modulated into the active optical signal during the time of propagation of the light (or time of flight) through the observed scene. Each pixel works like an individual high-precision stopwatch, and since its realization is mainly based on CMOS technology this new technique will benefit from the ongoing technology developments in terms of improved time, and hence distance, resolution. Thanks to the use of CMOS, all commonly known CMOS APS (Active Pixel Sensor) features(Regions Of Interest addressing: ROI, AD conversion, etc.) can be implemented monolithically in the future. The pixels have been implemented in a 2 μm CMOS/CCD technology.

Lange has characterized several different pixel structures. The demodulation pixel with the best fill-factor and demodulation performance has been implemented (1) as a line sensor with 108 pixels and (2) as an image sensor with 64 x 25 pixels. Both devices have been integrated in separate range cameras working with modulated LED illumination and covering a distance range of 7.5 up to 15 meters. For non-cooperative diffusely reflecting targets these cameras achieve 7 centimeter accuracy. With the single exception of the demodulation pixel array itself, only standard electronic and optical components have been used in these range cameras. For a resolution of 5 centimeters, an optical power of 600 fW per pixel is sufficient, assuming an integration time of 50 ms (20 Hz frame rate of 3D images). This low optical power implies that only 0.06 electrons are generated per modulation period (Tmod=50 ns at 20 MHz modulation frequency). This is a surprising performance, because the above mentioned optical power implies that one electron is generated, statistically speaking, only every 13th modulation period. This means that single electrons are moved, distributed and added to the pixel with excellent reliability. The measured performance shows excellent fit to the theoretical resolution predictions

Lange claims that the work demonstrated (during 1999) was the first successful realization of an all-solid-state 3D TOF range-camera without moving parts that is based on a dedicated customized Photo ASIC. The measured performance was very close to the theoretical limits.

Lange was able to demonstrate robust, compact range cameras (2D and 3D) with excellent performance only limited in a very predictable manner by ubiquitous quantum noise of the employed light. According to the author, the ongoing miniaturization in microelectronics will lead to faster demodulation devices so that we can expect devices for demodulation frequencies beyond 100 MHz (sub cm resolution) in the future. Also, it will be possible to realize additional functionality such as on-chip A/D conversion, distance or phase calculation or even image processing tasks.

Table 6 gives a power budget example from Lange. A simple range scaling from the 50 degree FOV to 0,5 mrad corresponds to 13 km range if we neglect atmospheric losses. This indicates the usefulness of the technology for longer ranges. The ambiguity must, however, be taken into account.

Table 6. *Power budget calculations. From Lange (ref. 40)*

Boundary conditions		Calculation	
Optical power of 160 LEDs	900mW	Beam divergence at the target	7 m
Beam divergence	50°	Beam area at the target	38 m²
Target		Projected pixel size on the target	180 mm x 40 mm
Distance	7.5 m	Projected size of photogates in the target	36 mm x 40 mm
Reflectivity of target	0.7	Power on projected photogate area	34 μW
Objective (CS-mount)		Reflected power of projected pixel area	24 μW
Focal length	2.6 mm	Effective diameter of objective	2.6 mm
F/#	1.0	**Power on pixel in fW**	260
Transmission of lens:	0.7	Energy in pixel	6.5E-15 J
Transmission of filter:	0.5	Energy of 1 photon	3.16E-19 J
Sensor		Number of photons per pixel	20,600
Pixel size	14.5 μm x 12.5 μm	**Number of electrons per pixel**	13,400
Operating conditions		Sensitivity of output stage	3.6 μV/electr.
Integration time	25 ms	**Output voltage**	48 mV
Wavelength	630 nm		
Quantum efficiency	0.65	**Resulting distance accuracy**	< 9 cm
Conversion capacitance	40 fF		
Amplification of source follower	0.9		
Modulation frequency	20 MHz		
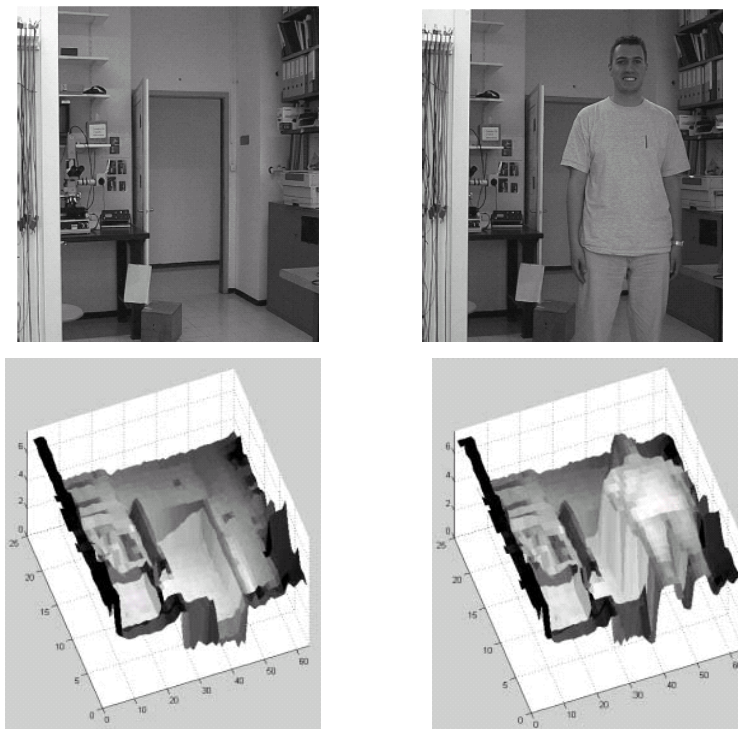
Figure 47: *Photo of a lab and the corresponding 3 D data from the CCD/laser sensor. From ref.40.*

Summary of described 3 D FPA approaches

In table 7 we have tried to sum up the various developments for 3 D FPA:s just described. Performance is either achieved or mentioned as program goals. All detectors are under development.

Table 7. *Summary of described 3 D FPA developments*

Parameter	Fibertek	ASC/ Wright	ASC/ SUL AR	Lockh Martin	Raytheon	MIT	Rock well	Univ of Siegen
Detector type	GaAsP IPD+ ROIC	EB, IPD+ ROIC	GaAsP IPD+ ROIC	HgCdTe, APD	HgCdTe, APD	InGaAs APD Geiger	InGaAs/ HgCdTe	Si CCD CMOS
Wavelength	532 nm	1500	532	1500	1500	1500/1060	1500/3800	0,4-1 μm
Array size	76	32*32	100*100	10*10 128*128	128*128	32*32 128*128	64*64	108 linear + 64*25
Pitch	? μm	50	100	25	?	100	100	13 μm
Bandwidth	GHz	GHz ?	?	?	?	GHz	40-200 MHz 400-500 MHz	20 MHz
Range resolution	15 cm	3-5 cm	20 cm (air)	<20 cm	<15 cm	3-5 cm	20 cm	4 cm
NEP/Noise	Single foton	?	nW	1 nW	<1 nW (20 photons)	Single phoelectrons	?	0.06 electrons during 50 ns
Dynamic range	8 bits	17.5 bits	?	?	?	?	?	?
Sampling time	1 ns	?	1-3 ns	?	?	0.5 ns	?	50 ns, phase meas.
Echo Processing	Pulse shape	No	No?	?	"super - resolution"	No	?	No

Processing of 3 D data

Single pixel processing

The capability for waveform processing from individual pixels is of value for several reasons:

- If the target, e.g. an approaching missile, is far away it may not cover more than one pixel. Thus, using the waveform is the only way to deduce the target shape and other characteristics.
- Structures of resolved targets will not always be revealed from simple peak finding algorithms. Surface slope and close structures can be deduced using different kinds of waveform processing.

Figure 48 shows an example of potential waveform processing to resolve a step in the target obtained from target geometry or for example a camouflage net in front of the target.
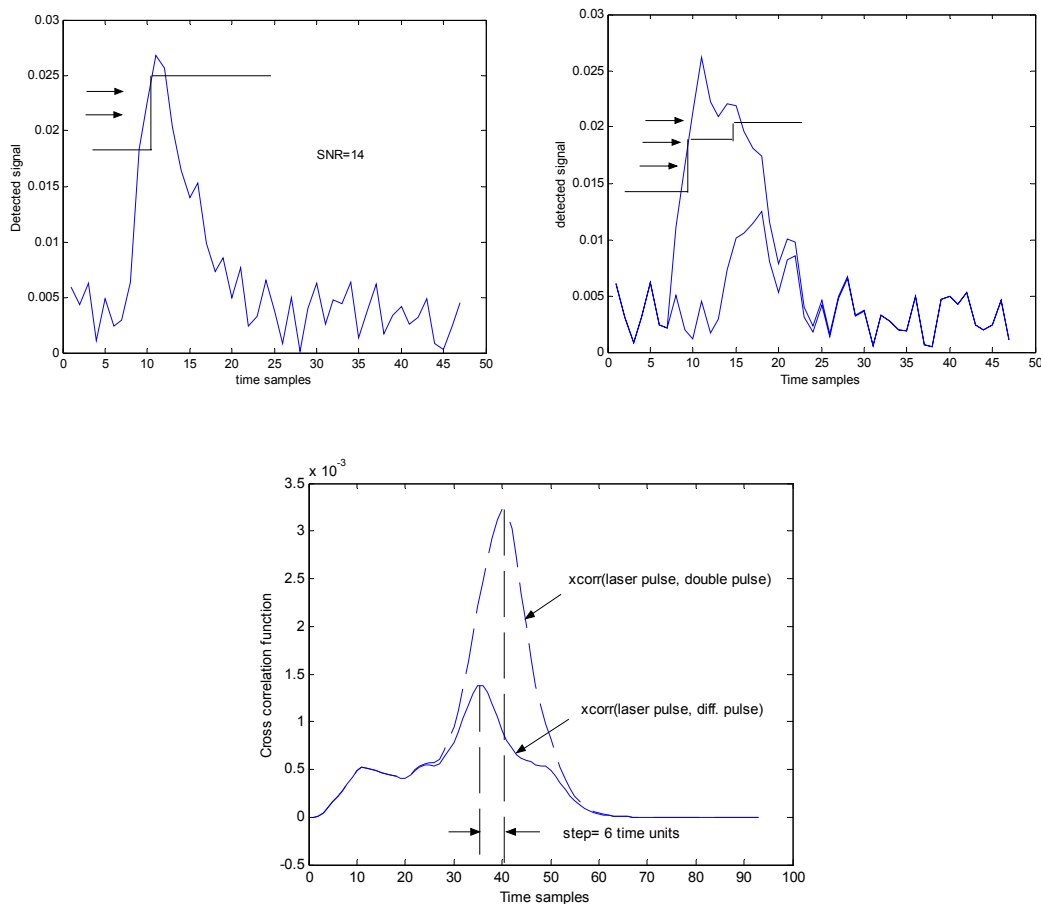
Figure 48: *Ex. of potential waveform processing to extract the second echo and the range step in a double pulse. Upper left shows a typical detected waveform from a single step and upper right the waveform from a double step. Below shows the cross correlation between the outgoing laser pulse and the single and difference echo pulses. The latter is obtained by finding the peak of the double pulse and subtracting the outgoing laser pulse shape normalised to the same peak value.*

Figure 49: *Example of waveform coupling to target shape.*

In Figure 49 we give an example of how target shape (beside target reflection) is coupled to that shape of the waveform. This is discussed in more detail in references[42,43]. Target recognition can be achieved by correlating with to a target library.

2D processing

A 3 D sensing FPA can provide both 2 D and 3 D data. By 2 D data we understand a range slice of the scene in which all pixels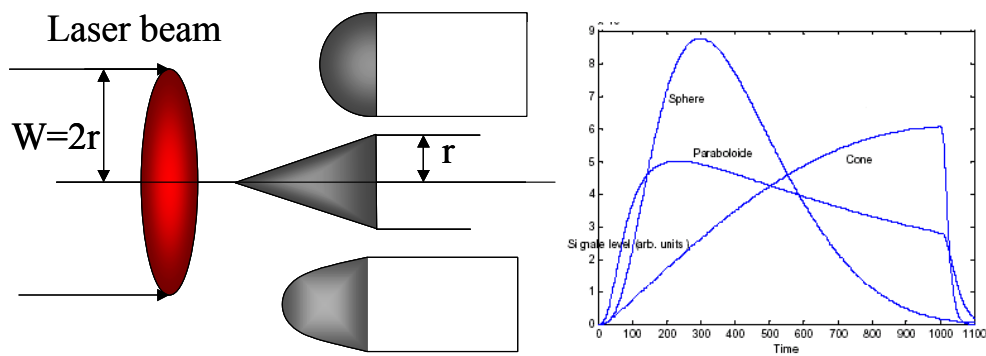 are given by intensity values corresponding to laser reflection. The 2 D laser image has the very important capability of segmenting a target from its background, provided that the gate width can be chosen short enough. The use of the silhouette and a short gate to get a true 3D resolved target are obvious extension to improve target recognition.

In a typical application a FLIR is locating a hot spot indicative of a potential target. The rangefinder/designator laser running up to 25 Hz can then be used to measure range to the target within 10-20 meters. A suitable gate, 50-100 ns corresponding to a range interval of 7.5-15 meters can be placed across the target, hopefully extracting it from the major part of the background. A further refinement, motivated for terrain concealed or camouflaged targets, would be to slide a shorter gate through the target and obtaining both the illuminated target and the silhouette or even a full 3 D reconstruction of the target. The price paid is multiple frame processing and a second long total illumination.

For sliding gates the problem of automatic frame selection for target recognition[44] can be based on contrast measures and on "hot spot" detection often characteristic of man made targets.

After segmenting the target from the background, the image quality may have to be improved due to degradation from atmospheric turbulence, target speckle and instrumental resolution limits and noise. The most straightforward and working technique for speckle removal (speckle is a multiplicative noise source) is multi-frame averaging. The adding of multiple frames requires motion compensation due to platform motion and atmosphere-induced image dancing[45]. See example in Figure 50.

Other techniques for image improvement include all the conventional image processing tools such as adaptive filtering, a method which can be described as local low-pass filtering with respect to lines and edges in the image. See Figure 51 for an example. Adaptive filtering can be extended to 3 D target data.
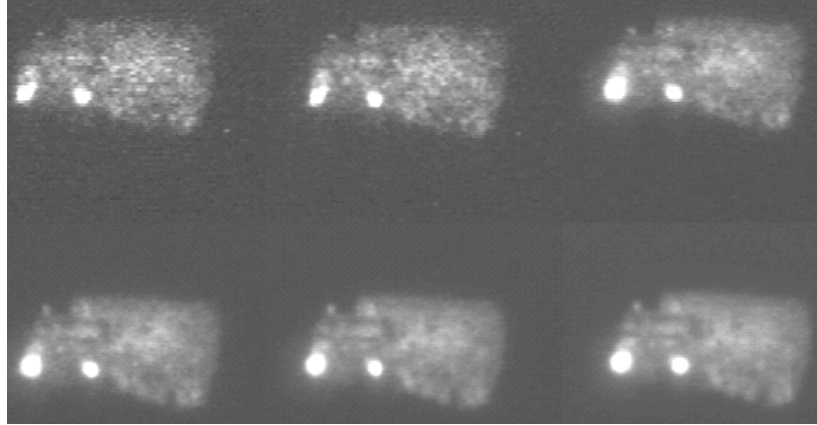

Figure 50: *A gated image of a military truck at a range of 10 km. From upper left to right: 1,2 and 5 averaged frames. Lower from left to right 10, 20 and 30 averaged frames. From ref. 43.*
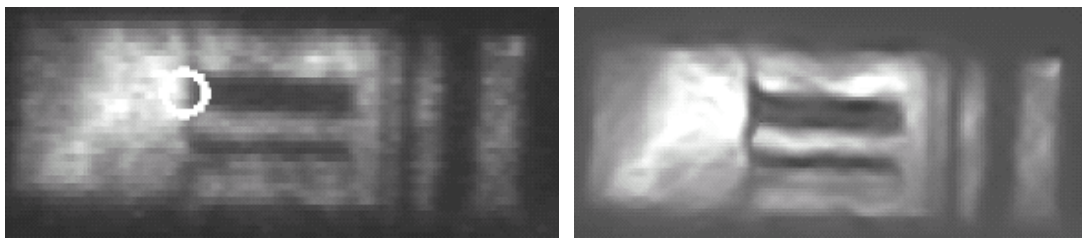

Figure 51: *Example of image improvement using adaptive filtering. In the circle of the left raw image the signal has a local vertical orientation, which is used for adaptive filtering in that region. The right figure shows the filtered output.*

The overall modulation transfer function, MTF, describes the resolution degradation of the image. The MTF describes the contrast loss vs spatial frequency. The spatial counterpart is the Fourier transform of the MTF, which is called the point spread function, PSF. The MTF is obtained from multiplication of the different resolution limiting factors:

$$ MTFtot = MTFoptics * MTFdet * MTFturb * MTFaerosol * MTFtarget(speckle). \quad \textbf{(11)} $$

Expressions for the different terms can be obtained from textbooks in optics[46, 47].

If the MTF can be estimated, substantial image improvement may be obtained by deblurring using different techniques. In the MATLAB® image processing toolbox several techniques are given, using Wiener, regularized and the so called Lucy – Richardson algorithms. The first two are using the least square solutions and an assumed PSF. In the absence of noise, the Wiener filter is the ideal inverse filter. In

Figure 52 we have applied a Wiener filter to blur and deblur an image of 277*122 pixels with a gaussian 5*5 pixel PSF.

The regularized filter implements a constrained least square solution where the constraint might be smoothness etc. The Lucy-Richardson algorithm uses maximum likelihood to find the inverse under the assumption of Poisson statistics (photon noise limited imaging).

The inversion methods need estimate of the PSF (or the inverse MTF). Looking at the above expression for the MTF, the aerosol MTF is of minor importance unless the optical density (OD) is >1. The target MTF can be estimated assuming a diffuse target, the turbulence MTF is the most important one and the hardest to estimate directly from measurements in a tactical scenario, although it is not impossible. Imaging stright structures like poles, buildings and bridges etc. might be uses to deduce the MTF. Model approaches relying on geometry and turbulence variation with altitude might also be a possible approach.

The processing methods for 2 D imaging will of course depend on whether the aim is operator interpretation or ATR (Automated Target recognition). In the first case the image should of course have enough quality to be easily recognized by an operator. Multiframe averaging, speckle reduction and deblurring are important tools for this application. Automated frame selection and combination of different gates are also of value for shorter and sliding gates.

For ATR additional features such as absolute size and template matching will be needed. Correlation against a target library might be of interest since range gated images are well segmented. Optical correlation might be an interesting alternative to electronic correlation. To reduce the template search space an estimate of target aspect angle will be of great value. Short gate widths will be needed for this.
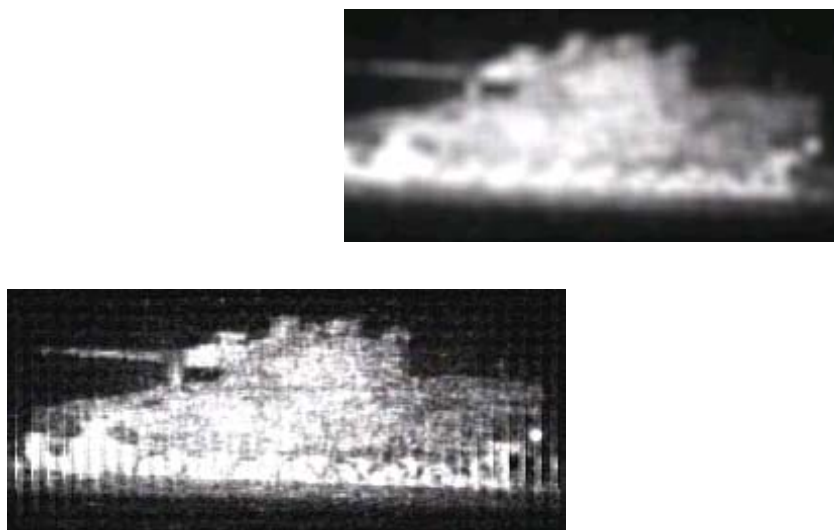

Figure 52: *Upper left, a close-up image showing target speckle but no atmospheric blurring. Upper right is a simulated blurred image, which mimics the effect of atmospheric turbulence. Below, we see the deblurred image, fairly similar to the original. The upper image has 277*122 pixels and the PSF is gaussian with 5*5 pixels.*

3 D from Gated Viewing Image Sequences

In Figure 53, we see three gated images portraying a terrain vehicle, taken from an image sequence acquired from a distance of 7.2 km with a gated viewing system developed at FOI. The figure illustrates that the "sliding" gate first starts to envelop the target from the front, at one point contains the target and finally leaves the target completely, giving a background image showing the silhouette of the target. This background image is used as an aid in selecting the area of interest for further processing. The bottom part of the target is occluded by the foreground. The gate width was 40 ns, corresponding to 6 m. In the image sequence, the gate was displaced in steps of 10 ns, corresponding to 1.5 m. The particular image sequence shown was acquired with the gate stepped manually, but the gated viewing system developed by FOI now has the capability of automatically sliding the gate over the target in steps down to 1 ns (15 cm).

Figure 53: *Gated viewing images of a terrain vehicle target at a distance of 7.2 km. Left: The front of the target is inside the gate. Centre: The entire target is inside the gate. Right: The gate is behind the target. The bottom part of the target is occluded by the foreground. Images FOI.*

The image sequence can be used for constructing an image containing 3-D information in each pixel. The range image in Figure 54 was constructed by applying an individual intensity threshold to each pixel and noting in which image in the sequence it exceeded this value. The intensity of each pixel was first low-pass filtered in the range domain in order to reduce noise.
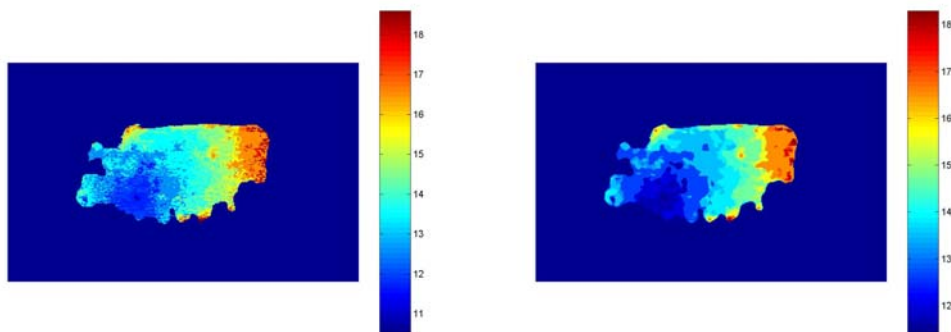
Figure 54: *Left: Range-resolved image of the target, where the pixel values represent range. The range scale is in meters. The absolute range values are arbitrary. Note that the glass of the windshield cannot be seen, because a laser of visible wavelength (532 nm) was used for illumination. Right: Median filtered version of the left image.*

By re-sampling the range-resolved image of Figure 53, we obtain the target object shown in Figure 55. The target object is a range-resolved image of 0.2 m/pixel cross-range resolution. At FOI, the processing of gated viewing data into this type of 3 D

object has been implemented[48] together with an adapted version of the model-based target recognition method described by Zheng et.al [48]. Some details of this method are covered in the next section. Note that the cross-range resolution of the target object of Figure 55 is twice of that of the laser radar images used by Zheng et.al.

Figure 55: *A range-resolved target object, which can be used for automatic target recognition. The cross-range (lateral) resolution is 0.2 m/pixel.*

3D processing

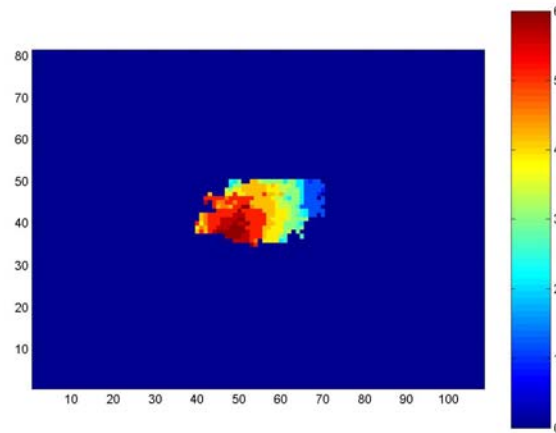3 D data for target recognition has the advantage over 2 D that both the boundary and the target internal structure can be used for processing, probably at the cost of more extensive computing.

Several methods have been proposed for 3 D laser radar data processing. Zheng[49] reviews some of these. The surface fitting approach to object recognition has been used extensively. The method relies on fitting different parts of the target with surface primitives from planar, cylindrical, and conic surfaces[50, 51,52] and even more complex surfaces such as superquadrics[53]. These methods have the advantage of relatively limited computational complexity but are sensitive to range errors, especially for higher order surfaces. The approach also has the drawback that it needs relatively high angular (cross range) resolution, not always the case for long range laser radars. Other authors[54] have used extracted edges which are then compared to a target model library. Shapiro[55, 56] et.al. have used detection theory, assuming a planar background and a known target shape, to calculate a likelihood ratio.

Target recognition from 3D laser radar data is challenging for several reasons. The range errors are due to noise and depend on the target geometry, target reflection and the range detection algorithm (peak finding, leading edge etc.). The target may also be occluded and embedded in terrain clutter, which may eliminate part of the target close to the ground etc. State of the art for pixel dimensions (25-50 μm) will reduce the angular (cross-range) resolution to maybe 0.25-0.5 meters at the range of interest (10 km +). The recognition task becomes more challenging when the number of candidates is large (because of many potential target types, position uncertainty, target orientation, and target articulation) and when the targets resemble each other.

The intuitive way of automated target recognition of 3 D targets is perhaps a model-based approach using template matching. CAD models of targets are used to generate a number of templates as a function of aspect. Zheng et. al [57] uses this to develop an automatic target recognition (ATR) system. The different steps in the processing are described by prescreening, surface fitting, boundary fitting and match evaluation.
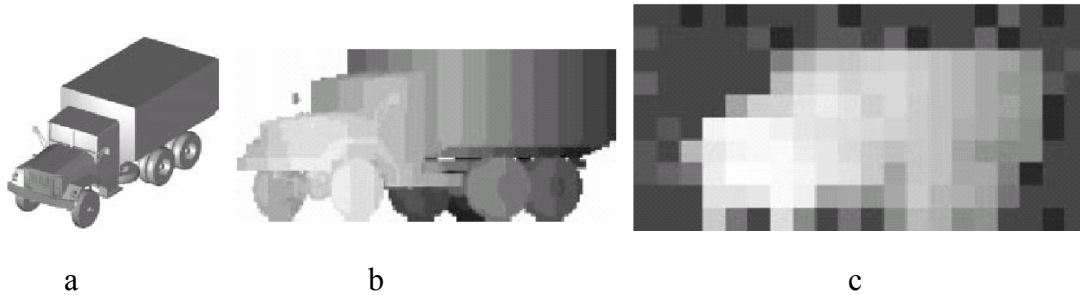

a   b   c

Figure 56: *Illustration of ladar image simulation. (a) Rendering of a vehicle CAD model, (b) range template at (315 , 0) and 0.1 m/pixel, and synthesized laser radar image at resolution of 0.4 m/pixel. From Zheng et. al[58].*

The prescreening described by Zheng involves extracting reliable (e.g., shift invariant) features from the data and comparing them to the corresponding feature sets predicted from CAD target models. If the extracted features are similar to the predicted features from a template, then that template remains in the candidate list. The features used by Zheng are 1-D projections of the laser radar imagery along the vertical, horizontal, and range axes.

Figure 57 shows average range curves for seven targets at 45 degrees azimuth (projections are along the horizontal axis). The curves for the same target are quite similar. The 1-D projections of different targets are quite different, providing good discrimination for prescreening. Any 3-D translation of a target will result in a shift of the 1-D curves that will not affect the matching scores.

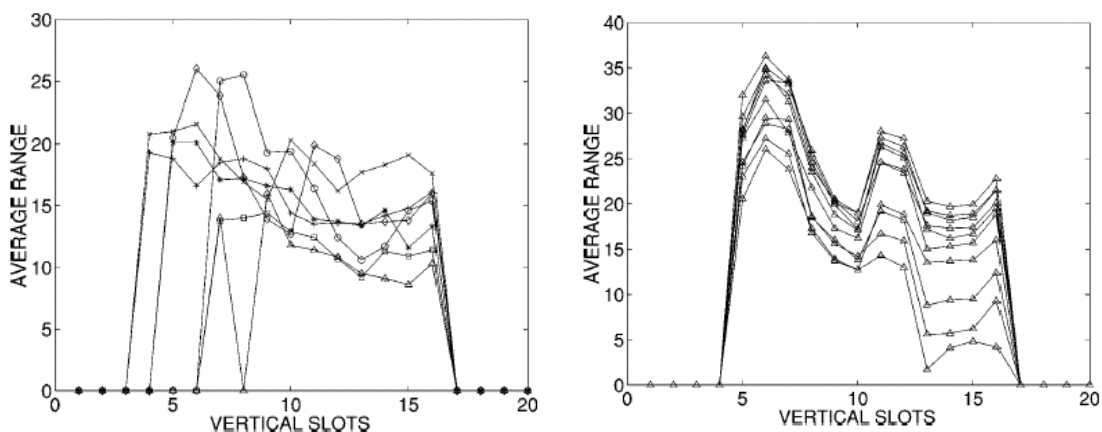**Figure 57**: *Left shows plots of average range for seven targets at 45 degrees azimuth and right plots of average range for fighting vehicle M1 from 0 to 45 degrees at 5 degrees increment. From Zheng et. al[59].*

The surface fitting is used to match the surface of the templates to the laser radar data. Zheng et.al. proposes to use the ratio of the total number of the fitted pixels and total

number of valid ladar pixel over the target for scoring the shape match. This metric is said to be better than mean square metrics, due to the relatively large number of outliers often present in ladar data. Outliers may be due to partial occlusion (short range pixels) and "noise" pixels due to sporadic detection in noise.

The boundary fitting detects a discontinuity in range values is likely to exist along the boundary of the target. Boundary fitting is used to determine if a consistent discontinuity exists for each hypothesized template. The bottom of targets are excluded from the boundary fitting because there should be no range discontinuity between the ground and targets, and partial occlusion of the bottom of the target occurs frequently. The same metric as for surface fitting is proposed by Zheng et.al.

The matching relies on both boundary and surface fitting. Incorrect small templates tend to have internal match scores but not to be supported by a boundary consistency check. On the other hand, boundary fitting alone tends to have good scores on cluttered background areas. To conclude, Zheng et.al. have used a projection-based prescreener, designed to filter out more than 80% of the candidate templates. An M of N pixel matching scheme was used for internal shape matching, while a silhouette fitting scheme is used for boundary matching. The model based system was trained on synthetic data and tested on a set of 276 real ladar images of military vehicles at various orientations and ranges. The system achieves above 90% accuracy in recognition of 0.4m crossrange resolution ladar images.

Wellfare et.al.[60] describe a set of detection, segmentation, and vehicle identification algorithms, which have been demonstrated on real and synthetic seeker data and have been targeted for the architecture and resources available on a tactically realistic processor for the LOCAAS program. In the LOCAAS scenario, a system level requirement for detection is to achieve 98% detection under nominal conditions. The LOCAAS scenario defines imaging at a 1 km range to target , a missile speed of 100 meters per second and an altitude of 300 meters. Inertial navigation (INS) data is used by the detection algorithm to transform each ladar pixel to a location in an earth-fixed Cartesian coordinate system.

Once a candidate target location has been identified, a set of pixels corresponding to the physical object at that location must be isolated from the background. The system level requirement for this segmentation is 90 %. The segmentation algorithm includes a screening mechanism to reject segmented objects which do not meet the usual criteria for targets such as trees and pieces of ground plane. The system level requirements are for less than 0.002 false alarms per square degree searched to be declared as targets by the classifier, with less than 0.2 false alarms per searched square degree to be output from the segmentation screening algorithm. Wellfare et.al. use the term "identification" to denote associating sensed vehicles with labels that are unique to that vehicle's external shape. Figure 58 outlines the main steps in the detection/segmentation algorithm process.

The classification algorithm design was based on the simple concept of matching unidentified segmented objects against a set of templates, each of which corresponds to a specific target identification that are unique to that vehicle's external shape Identification is obviously important when selecting priority targets to attack or friendly vehicles to avoid, but incorrect identifications can adversely affect aim point selection accuracy. This occurs because militarily effective aim points may be

located at very different offsets from the vehicle centroid for different target classes. These combined effects, when compared to operational effectiveness goals, led to the establishment of an initial goal of 85% probability of correct identification, with a horizontal-plane aim point circular error probable (CEP) of 0.5 meters, and a vertical error probable (VEP) of 1.0 meters. Since the objects and templates which are to be matched are three-dimensional, only very similar orientations of object and template can be properly compared. In order to avoid the storage and execution time penalties of exercising a matching algorithm against a large number of stored tem-plates to cover all possible angles, it proved to be more efficient to measure the orient-tion and then generate simple projections of the desired templates at the proper orientation for use in matching. Figure 59 summarizes the main steps in the processing.
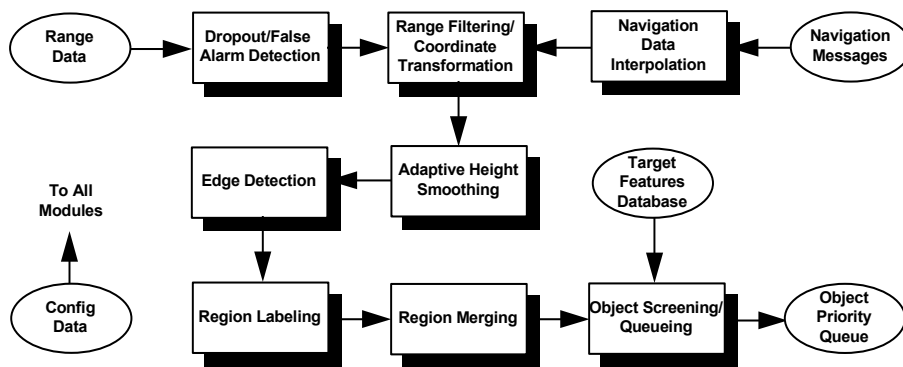

Figure 58: *The scheme for the detection/segmentation algorithm described by Wellfare et.al.*
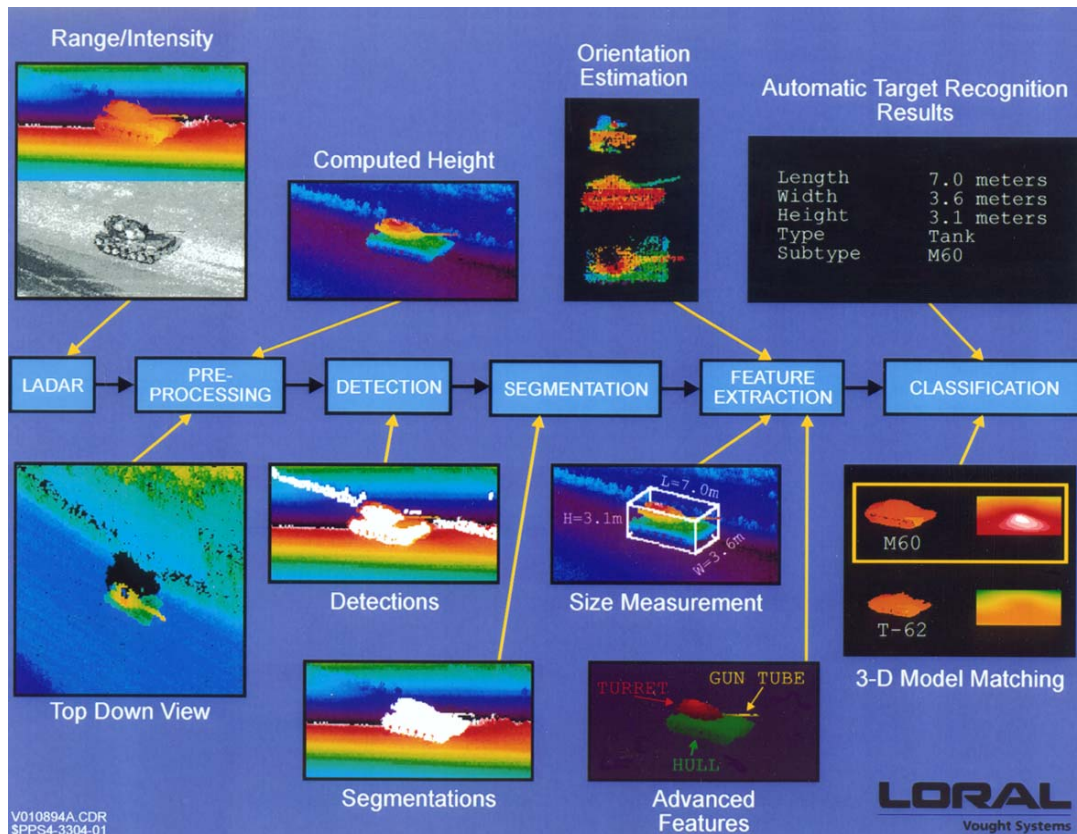
Figure 59: *The main steps in the automatic target recognition system described by Wellfare et.al.*

Due to the strict accuracy requirements for aim point selection and the small differences in target shape that must be used for identification, it is essential to perform the 3-D correlation over very small distance increments. According to Wellfare et. al. such small increments make extensions of standard one-dimensional correlation to three dimensions completely impractical for tactical applications. The chosen approach by Wellfare et.al. has centered on pyramidal algorithms which reduce the computational complexity of 3-D correlation to levels that are within an order of magnitude of those practical in today's tactical systems.
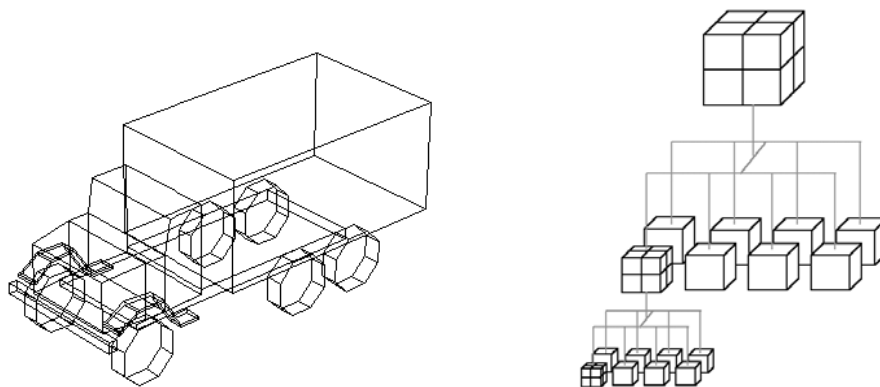
Figure 60: *Left, a wire frame target model and right shows an oct-tree used to make a processing efficient 3 D correlation. From Wellfare et.al.*

The target is modelled by a collection of polygons producing a wireframe representation, similar to that shown in Figure 60. The Pyramid Correlation module compares two lists of three-dimensional pixel locations for shape matching. Both segmented object and reference model pixel lists are entered into separate multi-resolution data

structures. A sparse oct-tree data structure is used to achieve efficient execution. The oct-tree represents a cubic volume in a pyramidal or tree form with the entire volume acting as the tip of the pyramid or root node of the tree. Each of the octants resulting from cutting the volume in half along each spatial dimension then acts as the next level of nodes. Any node can be subdivided until the desired local subdivision size is reached. An example oct-tree, which has been subdivided once at each of its levels is depicted in Figure 60. An example showing several correlation matches between segmented object and the corresponding projected reference pixels is shown in Figure 61. The correlation algorithm determines the offset between pixel sets in an iterative fashion over a fixed number of levels, updating the offset at each level using local comparisons within oct-tree cubes of progressively smaller dimension. The correlation match quality for each match level is a monotonic but non-linear measure of how well the numbers of object and reference pixels agree (on a proportional basis) within all occupied oct-tree cubes at the current and lower correlation levels.

The match quality can only reach the maximum when the 3-D spatial distribution of pixels is identical, and due to the smaller sizes of the oct-tree cubes, can only decrease as progressively higher resolution levels are explored. A minimum match quality input is provided which will terminate correlation matching as soon as it is apparent that the minimum requirement cannot be met with the current match.
The algorithms by Wellfare et.el. described above have been tested with good performance. Details are found in ref. 59.

The DARPA program Jigsaw [61] aims to develop compact laser radars for use with small UAV:s to identify targets hidden in forests or urban clutter. The idea is to combine multiple views of high resolution 3 D images to render an object suitable for operator identification. Figure 62 shows the ideas behind JIGSAW. Figure 63 gives example of how targets in vegetation can be revealed by a simple change of viewpoint.

Figure 64 shows an example of the use of an algorithm developed at FOI for ground extraction can be used for vegetation removal[62].
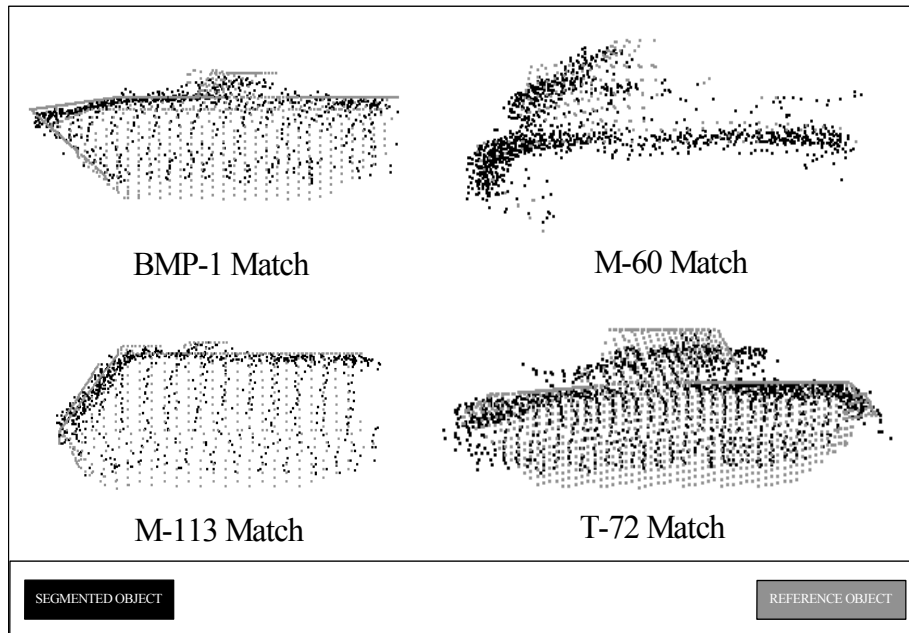
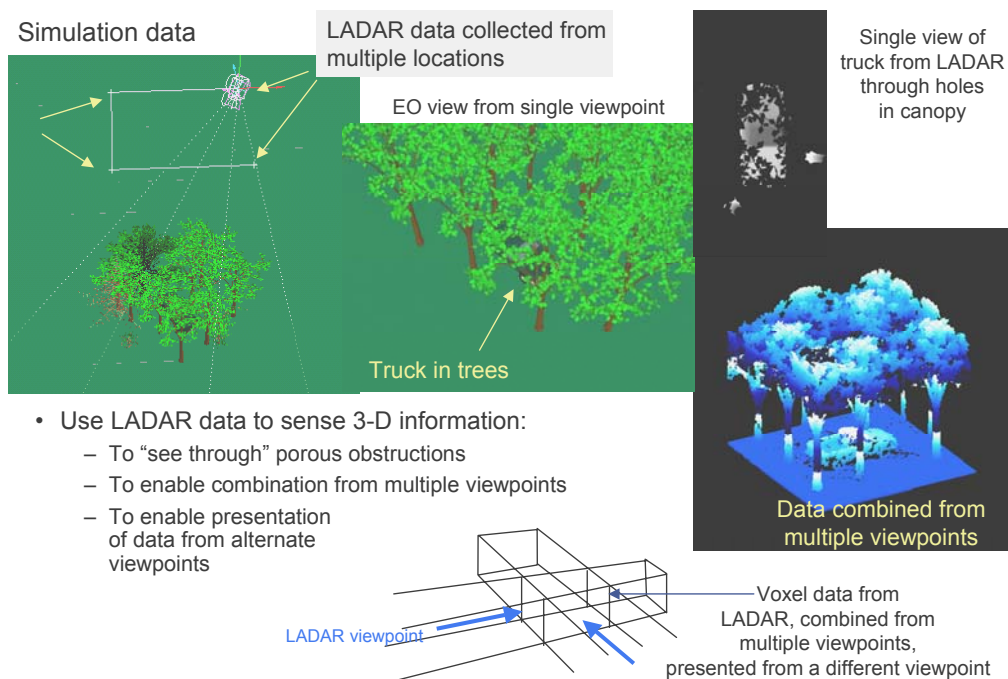**Figure 61:** *Example correlation match results. From Wellfare et.al.*

Figure 62: *The Darpa program for 3D laser radar called JIGSAW. From Darpa web site.*
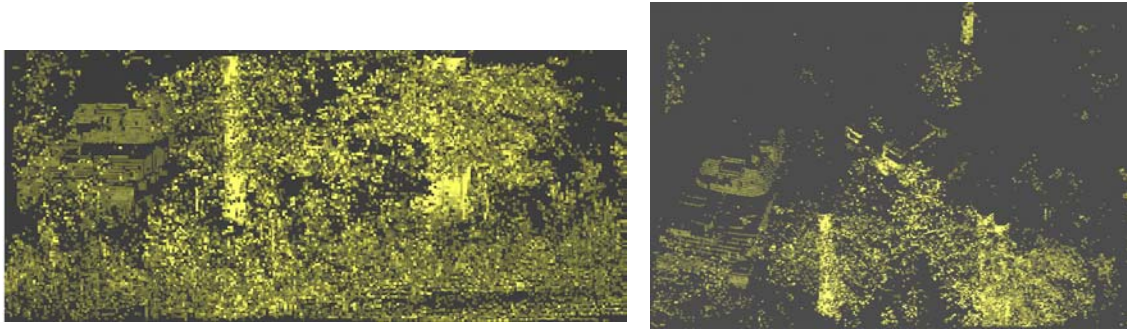
Figure 63: *Left a horizontal 3 D laser radar image of targets in vegetation. Right picture shows the same data viewed from another direction revealing the targets (tank and a HMVW). Source Darpa.*
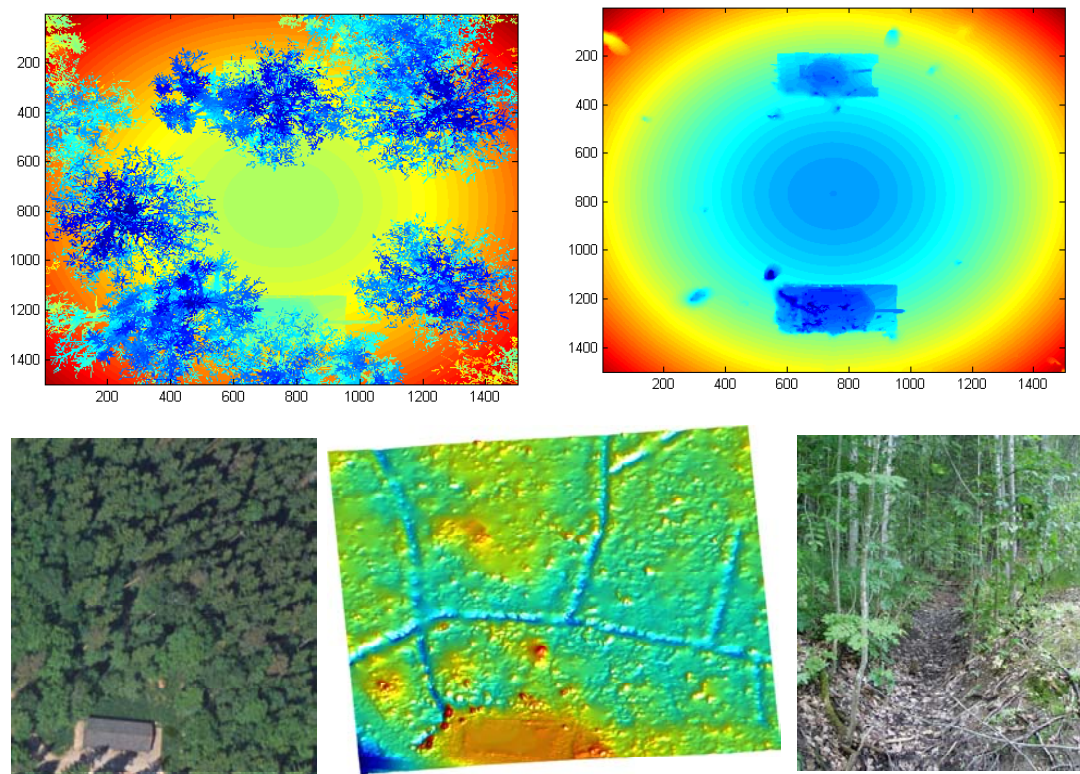
Figure 64: *Above: Left shows a color-coded range image with tanks in a forest. Right shows how algorithms developed at FOI can remove vegetation and display the targets. The images are based on simulated data. Below, aerial photography, 3 D ground extracted from laser radar data and close up view of ground showing ditches. This illustrates how the same type of 3 D filtering can be used for accurate ground extraction. This is almost impossible from a passive color CCD image. Images FOI.*

It is interesting to investigate how easy it is to see through vegetation by dense sampling with a 3 D laser radar. One impression of the capability to see through vegetation can be obtained by using a scanning laser radar looking at static scenes. Figure 65 show that even a single scan can be used to reveal a hidden target behind rather dense vegetation (80-90% coverage).

Scilling et.al[63] describes how mutiple returns can be used to obtain images through camouflage. They use a 1.2 ns laser pulse to obtain cm resolution.
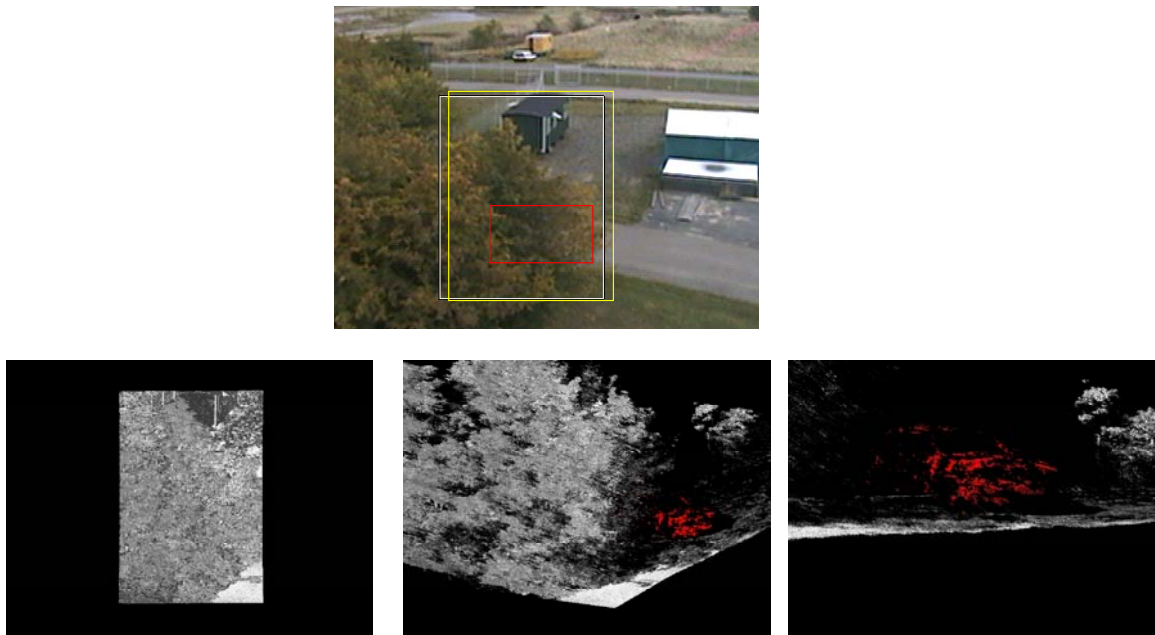
Figure 65. *Single view scan using a 1.5 micrometer laser radar (ILRIS 3 D Optech Inc.) through dense vegetation (pictute above – large rectangle). Below left to right: single view laser scan looked on from different angular perspectives. Target (car) is in red. Images FOI.*
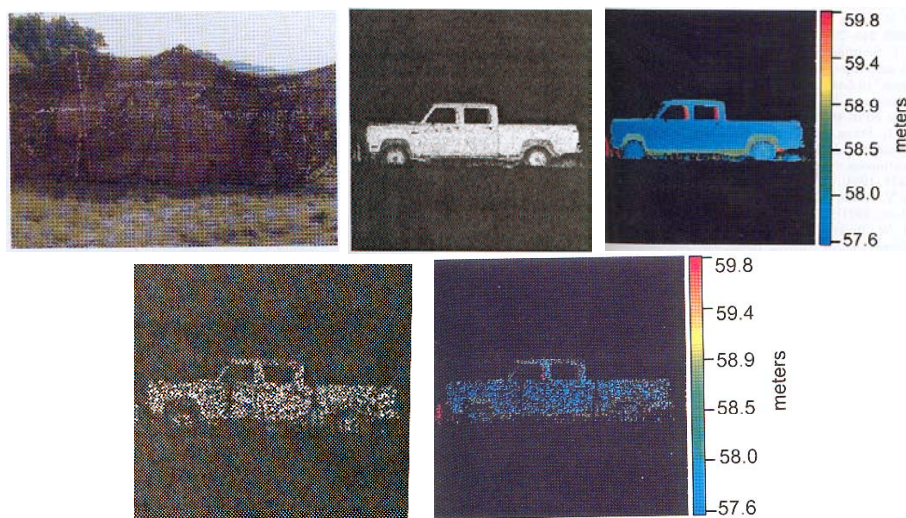
Figure 66. *Upper left shows a van behind a double camouflage net, upper and right middle the show intensity and range images of the truck without camouflage. Below shows intensity and range images with the camouflage net on the truck. About 30 % of the 3 cm transversely separated laser shots reached the truck. Range resolution about 3.5 cm. From Scilling et.al.[63]*

Target segmentation work at FOI

At FOI there is an ongoing work on target segmentation. In target segmentation geometric features of the target are extracted from 3D laser radar data. The goal with this method is to do a coarse recognition of the target, to determine its class (tank, truck, personal car etc.). This coarse estimate can be used for three different purposes. First, in many military applications it may be enough to know the objects class. It is more important to receive the estimate fast than having a large level of detail. The rectangle estimation process has shown to be rather fast, see Carlsson[64] (now Grönwall). The second purpose is in a recognition procedure where the unknown target will be matched with different object models from a database. If we have a coarse estimate of the object it will be possible to prune the number of hypothesis, and decrease the number of objects that the target will be matched with. Thirdly, these estimates can be used as initial settings for iterative search methods, for example methods proposed by Klasén[65] that will study the target in detail to determine its type (e.g., tank T72 or T80). If good initial values can be given, the computational burden in an iterative process can be decreased dramatically. Figure 67 is an example of simultaneous images from an airborne CCD camera and a scanning single detector laser radar used in evaluation of algorithms.
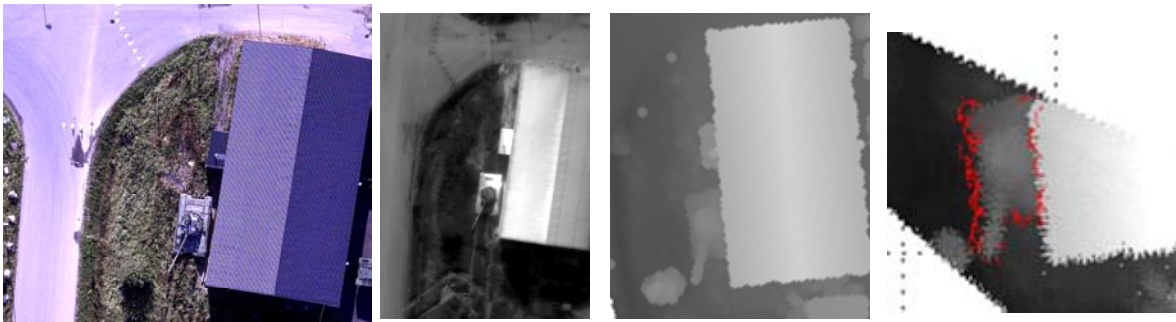
Figure 67: *Illustration of an urban scene with a tank (T 72) close to a building. Middle shows intensity and range imagery from a scanning laser radar and right the segmented tank. Images FOI.*

When the target is detected it is first studied in top view and the main axis and orientation are calculated using a method proposed by Carlsson[64]. In the proposed method, called minimum rectangle estimation, the convex hull of the samples on the target is calculated. Then the rectangle that with minimum area contains the convex hull is calculated. The resulting rectangle is the estimate of the main axis, orientation, length and width of the object. The rectangle calculation is then repeated along the main and secondary axis of the object. By this we retrieve estimates of the orientation in 3D, length, width and maximum size of the target. An example of data and rectangle estimation is shown in figure 68.

When the rectangles are estimated, they can be used for finding parts of the target. In this segmentation process we first study the target in top view, see figure 69. As we know the scanning direction, only the first and last sample on the target in each scan line is included in this calculation. First we calculate the squared distance from each sample to the nearest side of the rectangle. Samples that have "too large" distances in a certain criteria are marked as possible segmentation points. For each segmentation point the data set is separated into two parts and the rectangle calculation is repeated for each part, see figure 70. When a (sub-)data set cannot be further separated the

segmentation process is finished in this view, see figure 71. This segmentation idea can be described as we are trying to minimize the "empty parts" in a rectangle, so that all parts of the rectangle will contain samples. Further, it can also be formulated as a search for concavities on the target, see for example Svensson[66].
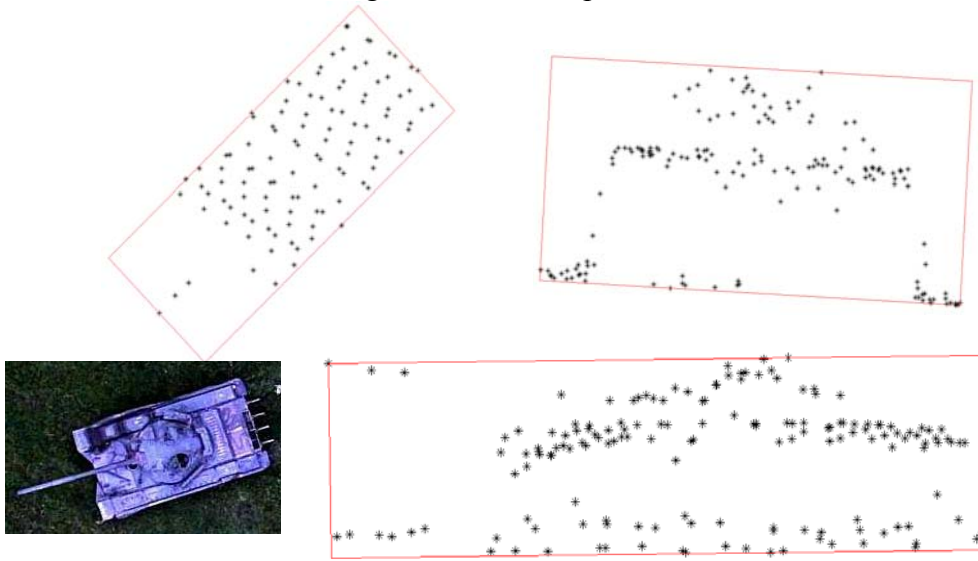
Figure 68*: Samples on a detected target (a T72), from a 3D scanning laser radar. Top, left: top view, top right: back view, bottom, left: visual image, bottom, right: side view. Rectangle estimates are marked. In the back and side views the ground points nearest the target are included.*
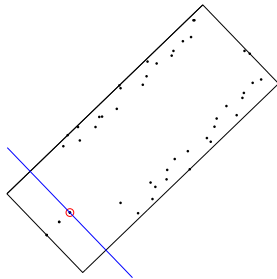
Figure 69: *Target segmenting in top view. Left: A sample that is too far away from all sides of rectangle is marked, this is a possible segmentation point. The line is perpendicular to the main axis of the target. Right: final segmentation.*
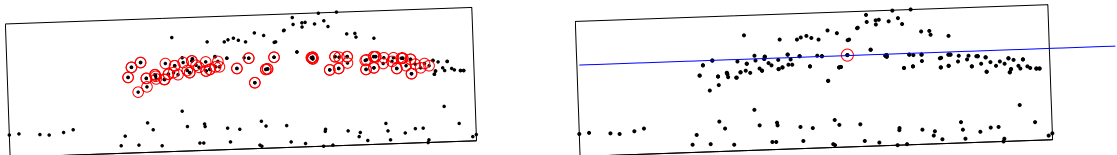
Figure 70: *Target segmenting of the main body in side view. Left: Data points that are too far away from all sides of rectangle are marked. The line is in this case parallel to the main axis of the target. Right: final segmentation.*
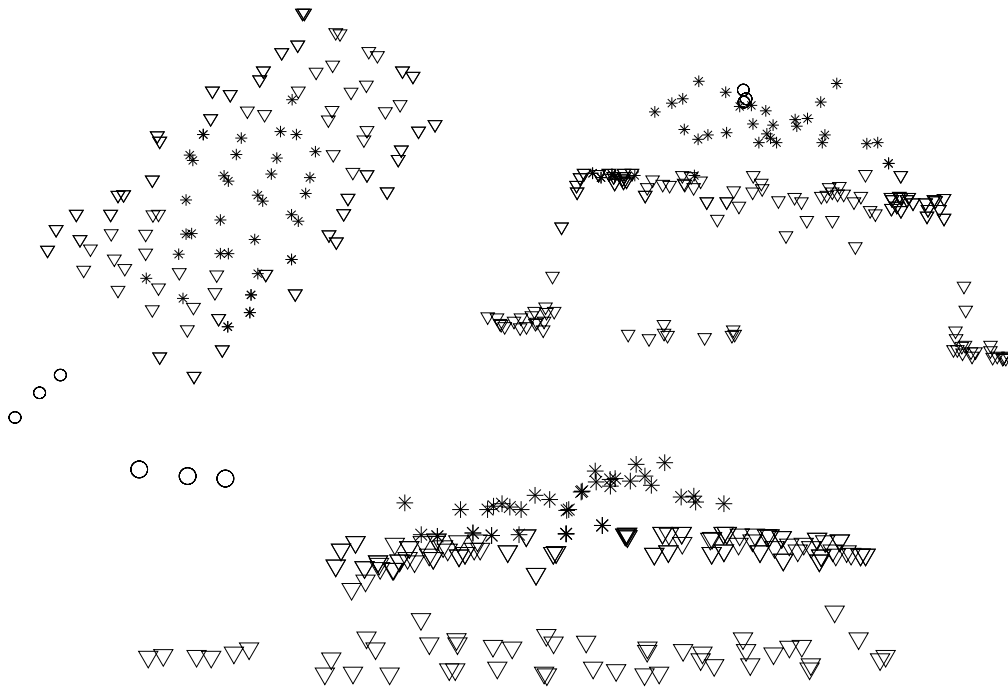
Figure 71: *Final segmentation of the target. The main parts (body, turret and barrel) have been identified.*

Modelling and simulation of laser radars and their data

Laser radar modeling[67,68] has been developed at FOI mainly for performance prediction dealing with system parameters, SNR etc.

Many of these theories have been useful to simulate and evaluate parts of a complex laser radar system, but complete system modeling has not been possible. For target recognition purposes, the FPA, in which both the spatial and temporal information was gathered, looked ideal. Already in the early stages, the interest of 3-D FPA was high, but since the technology was not currently available outside the development laboratories and not very well developed the answer was simulation. This required some way to simulate the pulse response from a ladar system. After that conclusion, the interest and need for 3-D laser radar simulation has resulted in a project performed at FOI, to implement a complete 3-D laser radar system simulation. The first version of the model, see Carlsson et al[69] was compiled a couple of years ago and has since then been adjusted to fulfill added requirements. The purposes of the simulation are motivated for at least two reasons. The first is to test a future system configuration and its performance at the design stage. The second is to test a current system to know its performance and validate the model.

The first idea of simulation covered two cases of standard systems. First, a staring ladar system, consisting of one laser source covering the whole target with the beam. In this case the receiver had to be an FPA. The second case is a scanning laser source with a remarkably smaller spot size. The receiver can in this case contain only one single detector element.

The general outline of the simulation model
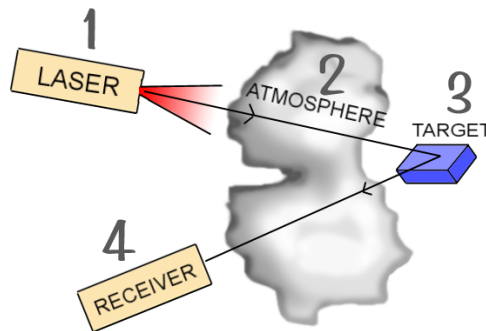
Figure 72: *The division into sub problems during the simulation.*

The simulation is (inspired from Der et al[70]) divided into four sub-problems according to Figure 72. To simulate the reflected waveform from a laser radar system, the problem has been divided into several sub-problems, where each sub-problem contains a lot of parameters controlling the simulation. The abstraction level of the simulation lies on a comfortable level. Too complicated models would require parameters not understandable by a normal user and too simple models would not simulate enough conditions and therefore not produce correct results.

Discretization

Since many of these sub-problems contain too advanced analytic mathematical expressions, especially when combined, the choice has been made to make the calculations discrete, both in the temporal (time) dimension as well as in the spatial dimension. This brings up the question of resolution. Which level of resolution generates the most time-efficient results compared to the correctness of the result? The answer to that question will definitely be a question of the date for the simulation since increased computer power makes the simulation quicker and quicker, and therefore gives the possibility to increase the resolution in the simulation. A reasonable resolution are in the spatial domain about 0.1 mrad, and in the temporal domain 0.1-1 ns.

Example of results

To give a sense of understanding of the result from this kind of ladar system, this simulation tool is an important part of the learning process. In this section, we will present a series of simulations from this tool[71] while one parameter at a time is changed. The aspects presented in this paper are different target geometries, effects of different reflection properties, atmospheric attenuation effects, different kinds of detection algorithms and for the case of scanning 3-D laser radar, different sizes of the scanning array.

Different target geometries.

The first simulation presented here is a reflection against a step illuminated and seen from some different angles, as the left part of Figure 73. The resulting waveforms are presented to the right in Figure 73, where the angle is the elevation as seen to the left.
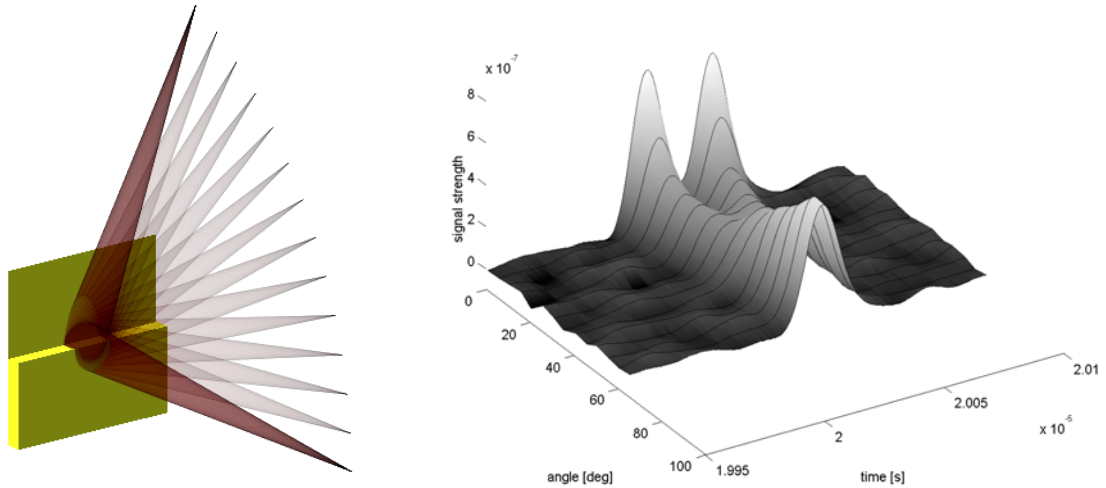
Figure 73: *The geometric step illuminated from different points of view.*

Notice the fact that while the elevation angle is small the reflection gives a double pulse response.

Reflection properties

The reflection properties are described by the bi-directional reflection distribution function (BRDF). Two different reflection conditions have been modeled and they are rendered in Figure 74, describing a helicopter, where the left image has a large specular part in the reflection while the right image only has a diffuse part of the reflection. The images describe the peak power in the reflected waveform. The parameters for the BRDF calculations used in the simulations in Figure 74 were, corresponding to assignments by Steinvall[72] for the left image A=1, B=0.25, m=1 and s=0.1, and for the right simulation A=0, B=0.5, m=1 and s is arbitrary.
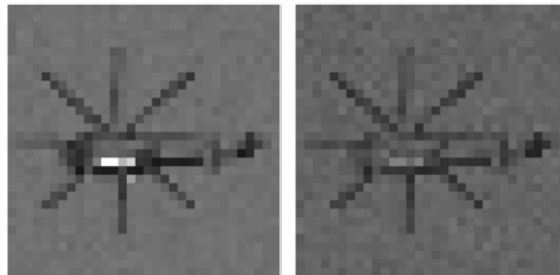
Figure 74: *Two different settings of the reflection. To the left the specular reflection is strong and to the right the reflection is pure diffuse.*

Atmospheric attenuation

At long distances to the target, the signal would be attenuated due to the atmosphere and fade into noise. In Figure 75, for instance, the target is placed at a distance of 10 km and instead, the visibility is changed (from left to right 6, 8, 10 respectively 15 km). It is obvious that the signal is much more easy to detect when the visibility increases. The parameters used in the simulations below are constant (except for the visibility) where for example the laser pulse energy E_p=1 mJ, the pulse width $T_{1/2}$=5 ns, the wavelength λ=1060 nm and the number of pixels in the scanning array were 32 times 32. The noise-equivalent-power (NEP, the standard deviation for the noise) stayed at a constant level of about 15 nW, while the peak power from the laser radar reflected at the target changed from 10 nW for 6 km visibility to 550 nW for 15 km
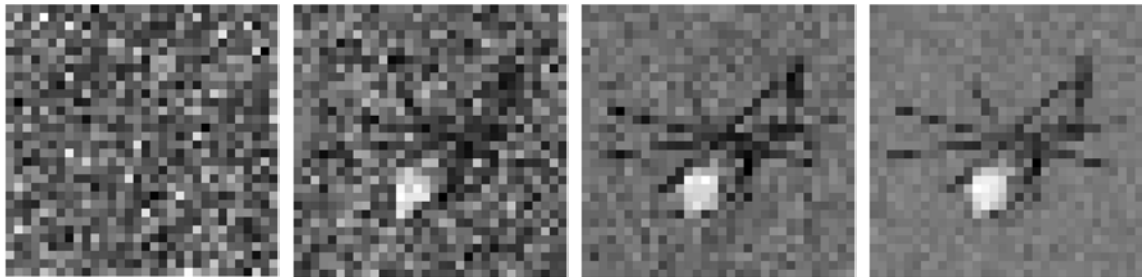
visibility.

Figure 75: *Example of maximum pulse response when the visibility is changed from 6 to 15 km.*

Simulation of top view measuring laser radar

From the general single spot simulation many other types of simulations can be performed. One example is described by Figure 76 and

Figure 77 below, which uses the original simulation model for a single pulse, but adds a detection algorithm to measure the distance to the target. The scan pattern is simply set to copy the simulated system. In the current example the scan pattern simulates a forward flying sensor scanning from side to side looking down at the ground.
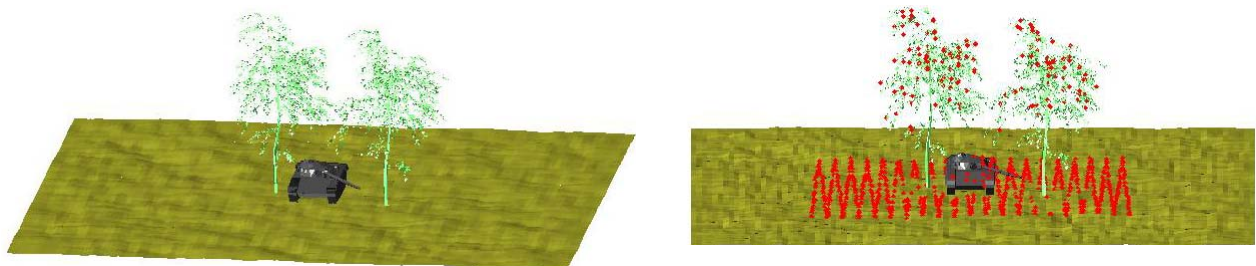
Figure 76: *The environment scanned with the top view scanning ladar. The red spots represent the detected ground positions.*
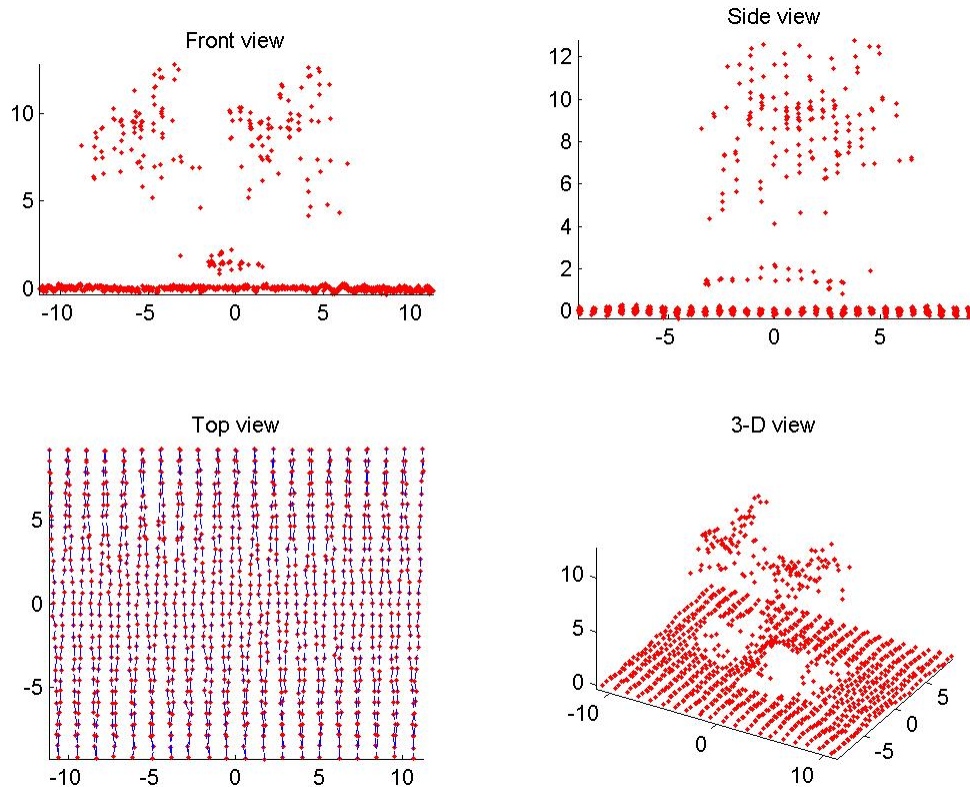
Figure 77: *The detected spots seen in different views. In the top row, the tank (T72) can be seen below the trees. The scale is in meters.*

Current work

The simulation field is now heading for extended simulations, as for example simulation of coherent ladar systems and gated viewing systems. The latter case is the easiest of the two and will be ready in the early 2003. The main differences are the noise algorithms and the system parameter settings.

The coherent ladar system simulation model requires more research and study and is currently postponed.

Ex. of modeling of laser radar systems performance

The laser radar simulation model described above can also be used for evaluation of target recognition algorithms. In this on-going work we study the properties of data from a general scanning laser radar system. By analyzing data from the system, we will recognize objects on ground. In the measurement system it is possible to add several design parameters, which makes it possible to test an estimation scheme under different types of system design. The measurement system model includes laser characteristics, object geometry, reflection, speckles, atmospheric attenuation, turbulence and a direct detection receiver. Thus, the data generation is based on sound calculations of physical properties. Data is analyzed by a general, parametric method. There are measurement errors present and thus, the parameter estimation is based on a measurement error model. The parameter estimation accuracy is limited by the Cramer-Rao lower bound.

Our goal with this work is to connect the design parameters of a measurement system with a parametric description of an object. This gives us a tool for evaluation of the effects of the system's design parameters on the result of the recognition algorithm. A first approach is reported by Grönwall[73,74] et.al.

Data dimensions

The collected data contains four dimensions; the position in north-south and east-west coordinates, (x,y), the altitude, z, and the intensity in the returning pulse, I. The scanning usually is performed in another direction than (x,y). Let us call the direction of the scanning ξ and the flight direction of the helicopter η. Thus, the data collection is performed in the coordinate system (ξ,η), see Figure 3. For moderate speeds ξ can be considered perpendicular to η.

Measurement error model

Let us define a regressor:

$$\varphi = (\xi,\eta,z)^T,$$ (12)

which contains data used for the size and orientation estimation. The regressor φ is a function of the measurement system:

$$\varphi = f(r,\alpha_{scan},\alpha_{pitch}),$$ (13)

where r is the slant range distance measured by the laser range finder in a certain scan angle, α_{scan}, and pitch angle, α_{pitch}. α_{scan} is considered parallel with ξ and α_{pitch} is considered parallel with η. Implicitly, φ is also a function of the object's shape, atmosphere, receiver, detector properties etc. Gauss approximation formula gives that the covariance of φ, $Cov(\varphi)$, can be approximated using a first order Taylor expansion by

$$R = Cov(\varphi) = f'Cov((r,\alpha_{scan},\alpha_{pitch})^T)f' + O(\|f''\|),$$ (14)

where f' and f'' are the first and second order derivative in r, α_{scan} and α_{pitch}, respectively, and O is the ordo operator.

Let us derive a model for one scan over a slope (i.e., a tilted plane) in the (ξ, z) dimension. As only one scan is studied, the η axis is constant and can be ignored. Note that the regressor now is redefined to $\varphi = f(r,\alpha_{scan})$. In each sample m we retrieve

$$\begin{pmatrix} \xi_m \\ z_m \end{pmatrix} = \begin{pmatrix} \xi^0 \\ z^0 \end{pmatrix} + \begin{pmatrix} e_\xi \\ e_z \end{pmatrix}$$ (15)

71

or

$$\varphi_m = \varphi^0 + e_\varphi, \qquad (16)$$

where φ_m m is the measured coordinate, φ^0 is the unobservable, true coordinate and e_φ is the noise in (ξ, z), respectively. Note that we have error in both coordinates and thus, we have a measurement error (ME) regression problem. For the estimation of a slope we use the following equation for a straight line

$$\mathbf{s}\begin{pmatrix} \varphi^0 \\ 1 \end{pmatrix}^T \theta = 0, \qquad (17)$$

where the parameters are $\theta = (\theta_1 \quad \theta_2 \quad \theta_3)^T$ with the constraint

$$g(\theta) = \theta_1^2 + \theta_2^2 + 1 = 0 \qquad (18)$$

to guarantee a unique solution. The covariance matrix of $(\varphi_m^T \quad 1)^T$ is:

$$S = Cov\begin{pmatrix} \varphi_m \\ 1 \end{pmatrix} = \begin{pmatrix} R & 0 \\ 0 & 0 \end{pmatrix} \qquad (19)$$

The (total) model error can now be defined as

$$\varepsilon = \left((\varphi_m - \varphi^0)^T \quad 1 \right)\theta \qquad (20)$$

The errors in the parameter estimate have minimum variance when the error covariance matrix is proportional to the identity matrix, i.e., R ~ I. If this is not the case, as in this example, the error covariance matrix R must be scaled, see Huffel[75].

The Cramer-Rao lower bound of the ME model

It is always desirable to understand how a particular estimation scheme performs under a certain model. If we assume some distribution of the perturbations, a lower bound on the error covariance of the estimated parameters can be calculated by the Cramer-Rao lower bound (CRLB). Consider the measurement error model above and assume that e_ξ and e_z are independent and Gaussian distributed with zero mean and variance $\sigma_{e_\xi}^2$ and $\sigma_{e_z}^2$, respectively. The CRLB states that the quality of any estimator in terms of its mean-square error (MSE) is bounded from below as

$$E\left((\hat{\theta} - \theta^0)(\hat{\theta} - \theta^0)^T \right) \geq J^{-1} \qquad (21)$$

where $E()$ is the expectation value, $\hat{\theta}$ is the estimate of θ and θ^0 contains the true, unknown values and finally, J is the Fisher information matrix. Following the calculations by Subhasis [76] et.al. for J the CRLB of this system can be expressed as:

$$Var\left(\hat{\theta}_1 - \theta_1^0\right) = \frac{1}{ND}$$

$$Var\left(\hat{\theta}_3 - \theta_3^0\right) = \frac{1}{N} \frac{\overline{E}\left(\xi - \frac{\theta_1}{\sqrt{1-\theta_1^2}}z\right)^2}{D}$$ (22)

$$D = \overline{Var}\left(\xi - \frac{\theta_1}{\sqrt{1-\theta_1^2}}z\right),$$

where N is the number of samples, $\overline{Var}(x)$ is the approximated variance, $\overline{Var}(x) = \overline{E}(x^2) - \overline{E}(x)^2$, where $\overline{E}(x^2) = 1/N \sum_{i=1}^{N} x_i^2$ and $\overline{E}(x) = 1/N \sum_{i=1}^{N} x_i$. Note that θ_2 is a function of θ_1, and not included in the CRLB expression.

Example: CRLB as a function of scan angle

Steinvall[77] gives a simplified model of the geometry for a pulse response is described. In the model the η axis is ignored, see Figure Y, and α corresponds to the scan angle. This model is simplified, but it can give us a sense of the problem. Using this model we can express the estimated slant range to the object, $\hat{r}$ (an estimate of r^0), as

$$\hat{r} = \frac{\hat{\xi}}{\sin\hat{\alpha}} = \frac{\hat{z}}{\cos\hat{\alpha}}$$ (23)

Using a first order Taylor expansion the measurement uncertainties in ξ and z can be expressed as,

$$\sigma_{e_\xi}^2 = \sigma_{e_r}^2 \sin^2\hat{\alpha} + \hat{r}^2 \sigma_{e_\alpha}^2 \cos^2\hat{\alpha}$$

$$\sigma_{e_z}^2 = \sigma_{e_r}^2 \cos^2\hat{\alpha} + \hat{r}^2 \sigma_{e_\alpha}^2 \sin^2\hat{\alpha}$$ (24)

where $\sigma_{e_r}^2$ is the variance of the error in $\hat{r}$ and $\sigma_{e_\alpha}^2$ is the variance of the error in α. Setting $\hat{\xi} = \hat{r}\sin\hat{\alpha}$ and $\hat{z} = \hat{r}\cos\hat{\alpha}$ in the CRLB expression above, we receive a CRLB expression that is a function of the number of samples, the slope of the surface, slant range and angle measures. A numerical illustration is shown in Figure Y+1. In this case we have no bias, i.e., $\overline{E}\left(\xi - \frac{\theta_1}{\sqrt{1-\theta_1^2}}z\right) = 0$ and $Var\left(\hat{\theta}_1 - \theta_1^0\right)$ is constant.

Design and atmospheric design parameters

Design parameters in the laser radar system that will a.ect the CRLB expression are:

- The scan angle
- The forward-looking angle
- The speed of the platform (if applicable)
- The PRF (pulse repetition frequency)
- The uncertainty in the laser range finder
- The size of the footprint
- The geometry of the object
- The GPS system
- The inertia system of the laser radar system
- Noise in amplifier and receiver
- The type of detection algorithm in the receiver of the laser radar system

In Steinvall[78] and Carlsson[79] et. al. models of how atmospheric properties affect the laser beam is described. It would be interesting to also connect those models with the CRLB expression. Some additional parameters that will affect the CRLB expression are:

- Specular and diffuse reflection
- Turbulence
- Beam divergence
- Intensity variations

Our goal is to connect the system parameters in such a way that we can say how they can be modified to get a parametric description of the object, with the smallest error variance. For example, what is the maximum scan angle if only a certain estimation error is allowed? Another interesting approach is to study how the atmosphere will affect the estimate. A future laser radar system may be designed to automatically adapt when atmospheric conditions change during a measurement session.
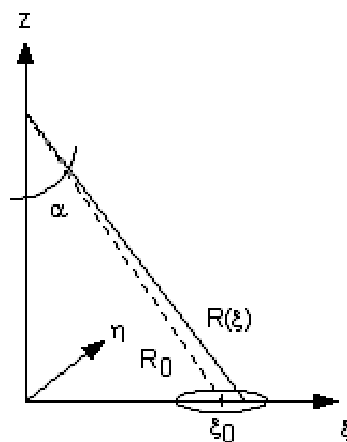
Figure 78: *The geometry of a pulse response when η is ignored. α corresponds to the scan angle. The slant range is denoted R (r in text). This is a simplified model.*
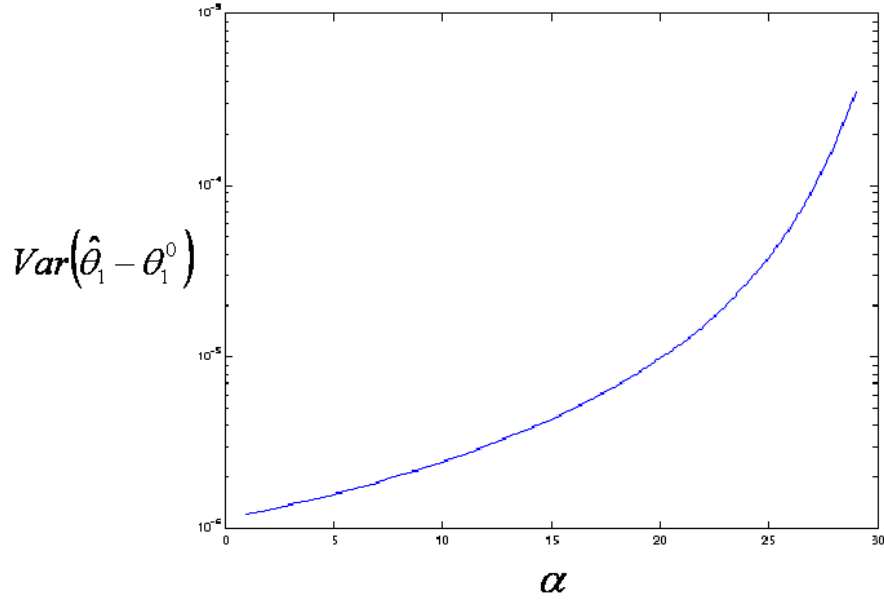
Figure 79: *The CRLB for a parameter used in target estimation (θ_1), as a function of scan angle (α) of the measurement system. α in degrees. The variance in the estimate of θ_1 increases when α increases. In this case we have no bias, and $Var\left(\hat{\theta}_1 - \theta_1^0\right)$ is constant (and not shown).*

Ex. of systems and their expected radiometric performance

We will give example of four system applications and their expected hardware parameters and performance from a radiometric point of view:

- Long range flash laser radar for target ID
- UAV system for terrain mapping and targeting
- Terminal seeker for target ID and aim point selection
- "Pathfinder", laser radar for autonomous navigation and targeting.

Basic radiometric formulas

The received power P_r for a monostatic laser radar looking at a target at a range R can be written:

$$P_r = P_t \cdot \eta_r \cdot \eta_t \cdot G \cdot A_r \cdot T_{atm}^2(R) / R^2 \qquad (25)$$

where P_t is the transmitted power, η_r and η_t the receiver and transmitter efficiency and $T_{atm}^2(R)$ the two-way atmospheric transmission loss. The receiver area is A_r and G is the normalized reflected intensity (sr^{-1}) from the target. For a Gaussian beam and a diffuse target with reflectivity ρ the target factor G can be written

75

$G = \rho/\pi \ [1\text{-}\exp(\text{-}A_{\text{target}}/A(R))]$ where A_{target} is the target cross sectional area and $A(R)$ is the beam area. We can rewrite eq. 12 to give the number of photons per pixel as:

$$N_{ph\_pix} = E_p \cdot \frac{\rho}{\pi} \cdot \frac{\pi D^2}{4R^2} \cdot \frac{1}{N_{pix}} \cdot \frac{1}{h\nu} \cdot T_{atm}^2 \qquad \textbf{(26)}$$

where E_p is the laser pulse energy, N_{pix} is the number of pixels in the array and D is the receiver diameter. In order to calculate performance we have to estimate the signal to noise ratio. The signal to noise ratio (SNR) (optical power which translates to a current SNR electrically) is given by :

$$SNR = \frac{P_r}{NEP} \qquad \textbf{(27)}$$

The threshold SNR_T for a 90 % detection probability and a 10^{-5} false alarm probability is about 5.7 for pulse detection in Gaussian noise. The turbulence influence for direct detection is not as large as for coherent systems. The laser spot at the target is often larger than the lateral coherence length leading to spatial averaging. Spatial averaging across the receiver will also reduce scintillation effects.

.

For *direct* detection the noise equivalent power NEP is given by[80]:

$$NEP = \frac{[(\overline{I_{BN}^2} + \overline{I_{DN}^2})M^2 F + \overline{I_{PN}^2}]^{1/2}}{R_D M} \qquad \textbf{(28)}$$

where I_{BN} is the background shot noise current, I_{DN} the shot noise dark current and I_{PN} the preamplifier noise current. M is the detector gain, F the excess noise factor and R_D the responsivity. The total shot noise due to background and signal is given by:

$$\overline{I_{BN}^2} = 2eB(P_b + P_r) * R_D \qquad \textbf{(29)}$$

where e is the electronic charge, B the bandwidth, P_r the received laser power and P_b the background power from the daylight given by:

$$P_b = N_\lambda \cdot \rho_b \cdot (\pi \cdot D^2 / 4) \cdot \theta_{pix}^2 \cdot \Delta\lambda \cdot \eta_r \cdot T_{atm} \qquad \textbf{(30)}$$

where N_λ is the background spectral radiance ($Wm^{-2}sr^{-1}\mu m^{-1}$), ρ_b the target reflectivity (sr^{-1}), θ_{pix} angular pixel resolution, $\Delta\lambda$ the receiver optical filter bandwidth, η_r the receiver optical efficiency and T_{atm} the one-way atmospheric transmission at the laser wavelength (filter centre wavelength).

The dark current shot noise current is given by:

$$\overline{I_{DN}^2} = 2eB \cdot i_D \qquad \textbf{(31)}$$

where i_D is the unity gain detector dark current.

1/ Long range flash laser radar for target ID

Suppose that we want to recognize a 2.5*5 m^2 target at 20 km range during non turbulent limiting conditions (like high altitudes or slant path air to ground or vice versa). For an operator recognition we need about 6-7 pixels across the smallest critical target dimension meaning about 0.4 m cross range and for automatic target recognition we need about 200 pixels cross the target or a pixel size at the target of about 0.25 m together with a range resolution of 0.15 meters.

The system is thought to be based on existing or upgraded EO pods containing FLIR, laser range finder and/or laser target designators.

Tentative data

Receiver:
   Detector: CMT APD array
   Responsivity R_D at 1.55 μm = 0.8
   Unity gain dark current: i_D
   Excess noise factor Fe: 2
   Gain M: 10
   Bandwidth B: 300 MHz
   Preamplifier noise I_{PN}: 0.1 pA/Hz $^{0.5}$
   Pitch : 25 μm
   Size: 128*128 alt. 256*256
   Optical efficiency: η=0.6
   $\Delta\lambda$ = 0.01 μm
   Optics: f = 2500 mm
   Diameter: D = 0.2 m

Laser:
   Wavelength, λ : 1550 nm
   Pulse energy E_p: 0.1-1 J
   Pulse length t_p: 3-5 ns
   Prf   : 1-20 Hz
Environment:
   N_λ is the background spectral radiance: 30 W/m^{2}srμm
   Visibility V km, Varies.
   Background reflectivity: 30 % (diffuse)
Target:
   Target reflectivity: 10 % (diffuse)
   Resolved target

Range resolution: 15 cm

SNR$_{pix}$ threshold for imaging: 3

Size and weight: 20 liters, 25-30 kg

Figure 80 shows the range performance vs. visibility and vs. laser pulse energy with the assumed data found above. The calculated NEP=0.58 nW/pixel is close to the shot noise limit which is 0.4 nW. Scaling the range performance to a ten times higher NEP (5,8 nW) is easily done by looking at the curve for a 10 times lower pulse energy.
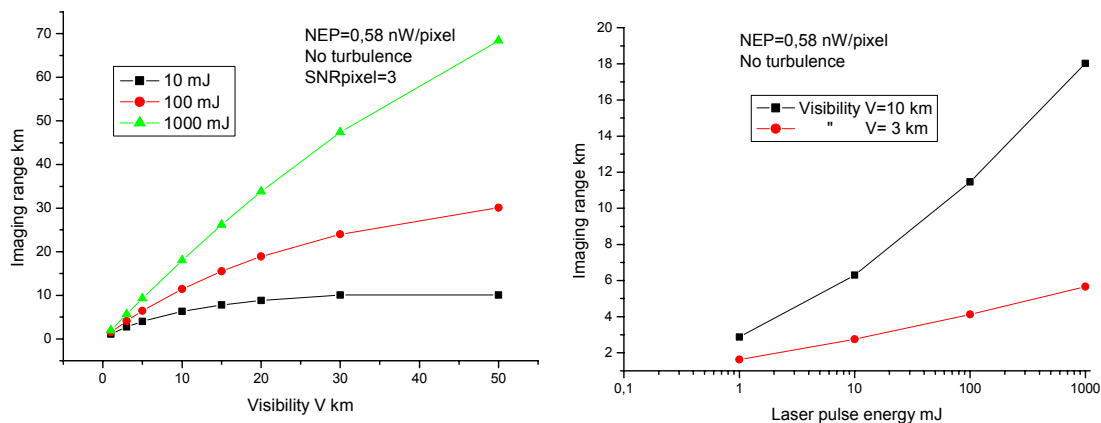
Figure 80: *Left shows the maximum range for a pixel SNR=3. The NEP= 0.58 nW is close to the shot noise limited value. Right shows the maximum range vs. laser pulse energy for a visibility V= 10 km and V=3 km.*

For vehicle sized targets recognition by an operator approximately 25 cm in target pixel size is needed (from the Johnson criteria). Let us take the attack pod of type Litening III (see figure below) as an illustrative example.

Figure 81: *An Israel Air Force/Lockheed Martin F-16D equipped with a Rafael Litening I targeting pod. The pod contains a gen. III (3-5micron) FLIR, with a 640x480 digital detectors array. This system is also equipped with a target marker, which improves the coordination of ground and air forces, by designation of targets by day or night. Litening III system is also equipped with a dual-wavelength diode-pumped laser for ranging and designation.*

The FLIR, with a 640x480 digital detectors array, has a narrow filed of view equal to 1*1 degrees. The instrument resolution is then 27*36 µrad or 27*36 cm^2 target pixels at 10 km range. The diffraction limit for a 20 cm optics (a guess) given by ca $\lambda/D=$ 20 µrad for $\lambda=4$ µm. We can thus estimate the recognition range for a vehicle target to be around 10 km under the following circumstances:

- The target contrast against background is high enough for the operator to recognise the target, something which might be difficult to achieve especially during wintertime.

- The target is separated from the background, meaning that it is not too obscured by vegetation or camouflage or in sunlit terrain clutter.
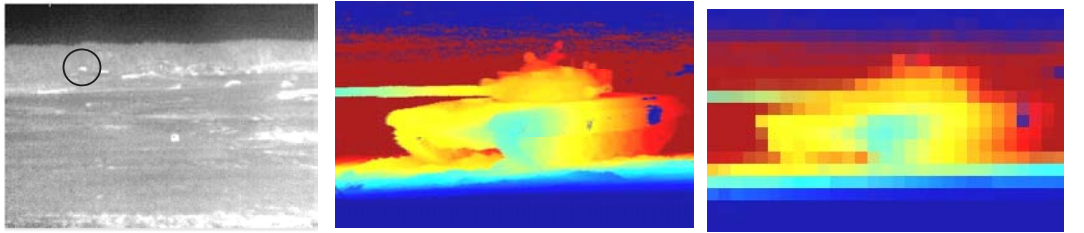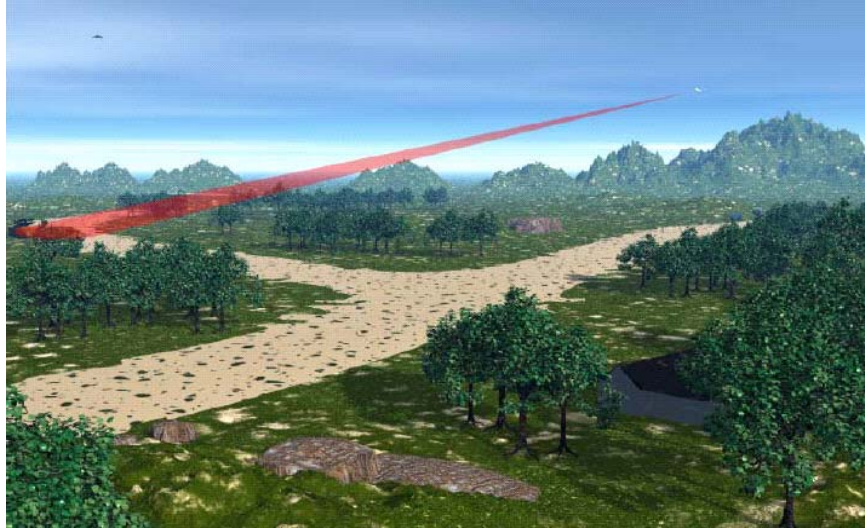
Figure 82: *Illustration above, targeting at long ranges from an airborne platform (image DARPA). Below an illustration on how it might look in the FLIR in a WFOV mode and at the laser radar display in a narrow FOV. The middle image is a high resolution 3 D image and the right is a down sampled version to about 20 cm pixels.*

A 3 D FPA receiver will improve the recognition capabilities by extending the range for recognition (out to 20 km or more) and by offering a much better target to background separation. The same designator/rangefinding laser (for Litening III running at approximately 20 Hz and 100 mJ pulses at 1.06 and 1.5 µm) can be used as an illuminator for the 3 D FPA.

2/ UAV system for terrain mapping and targeting

Operational needs

- Capability to destroy time critical targets (AA artillery, tanks etc.)
- Cost effective autonomous weapon system with good area coverage
- Autonomous search at low altitude to reduce the likelihood of detection by enemy
- Target discrimination, aim point selection and optimised and graduated effects with low collateral damage against various targets.
- Multi-target capability in each mission
- High capability in bad weather
- Terrain mapping capability for use in a rapid terrain visualization system for on line or laser mission planning etc.

The given operational needs can be solved by a small turbojet-driven UAV which can deliver submunitions in a similar way as the LOCAAS system. There is probably a great advantage if the different mini-UAV:s can communicate with each other for target detection, localization and an optimal weapon effect with damage assessment. Low operational altitudes (50-300 m) ensures operation below clouds, low probability of interception and good weather capability. An advanced sensor combination of laser/IR and or RF like mm waves and or an RF signal warning give good automatic target recognition capability in a compact system. A high 3 D spatial resolution from the laser radar give optimized aim point selection with a good weapon effect using a small submunition.

System performance

Laser/IR system:

Mission time in target area:	0.5-1 hour
Maximum transport range:	150-300 km
Area coverage rate:	36-430 km^2/h
Flight velocity:	200 m/s
Altitude:	50-600 m
Swath:	approx. equal to altitude
Search mode	about 1 km in front of UAV or just below
Target detection	IR camera and laser in combination alt. RF emission, reflection
ATR=Aut. Target recognition	Using laser radar (3 D) plus IR
Signal processing ATR:	Segmentation, position, attitude, feature extraction, finger printing, 3 D correlation against target templates
Storage of terrain data	3 D data at 10 cm level plus reflectivity and IR imagery stored for immediate or laser use in

synthetic environments. Linked in real time to ground station, to a ship or to other aircraft.

Battle damage assessment (BDA):   Based on laser radar and IR from one or several UAV:s

Communication:

Between UAV:s

Laser link
Cooperation :   2-10 UAV:s
Max. comm. distance   5-700 meter
Communicated information   ID for each UAV, position, detected target types, target positions, Battle Damage Assessment (BDA) info, terrain data

From central UAV to
ground station   Terrain data, BDA info.

Probability of kill:

Target area 4*6 km^2, 10 targets
48 submunitions

Without communication link   20 %
With a 700 meter link between UAV s: 90 %
<u>Technical data</u>

Laser radar
Laser type   Diode pumped YAG or fiber-based laser
Wavelength   1.06 alt.1.5 μm
Laser power (mean)   10-25 W
Pulse length   1-3 ns
Pulse energy   50-125 μJ

Scanning   Parallell scan+capability to get multiple target views
                              Pointing capability to increase target ID (zoom mode)
Scanner   Galvo driven mirrors + gimbal for pointing

Scanner frequency mirror   < = 80 Hz

Zoom mode   10*10 m^2 with 10 Hz update rate
Laser receiver optics   5 cm
Laser detectors   10-element array plus 128*128 array for better ID at longer ranges.

NEP   < 1 nW per pixel

IR/CCD sensor

FOV TV/CCD (color)	1*0.75°-14*10°
FOV IR:	2*1.5°-20*15°
Angular resolution:	0.1 mrad
Detector IR	Uncooled bolometer, camera weight 1-2 kg
Temperature resolution	< 100 mK

Positioning

GPS , alt. Terrnav

Communication

Main alternative	Laser link (balanced system as sensors are optical)
Reserve alternative	RF link
Laser power	1-10 W
Laser type	Laser diode array
Laser lobe	160*30 degrees
Laser receiver	
Optics	Hemispherical, 3 cm in diameter
Detector	Photo diode

Note. All UAV have full duplex communication capability. Certain UAVs can also be equipped with a retro-modulator to be tapped of information from a ground based illuminating laser source.

This page illustrates some capabilities of laser radars relevant to UAV, namely detection and identification of targets hidden in vegetation and at the same time collect and update high resolution terrain data.
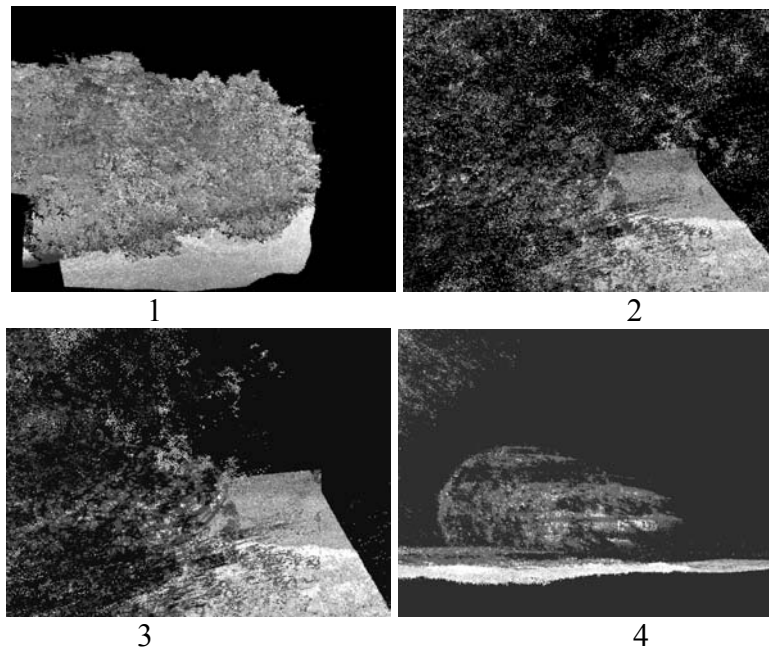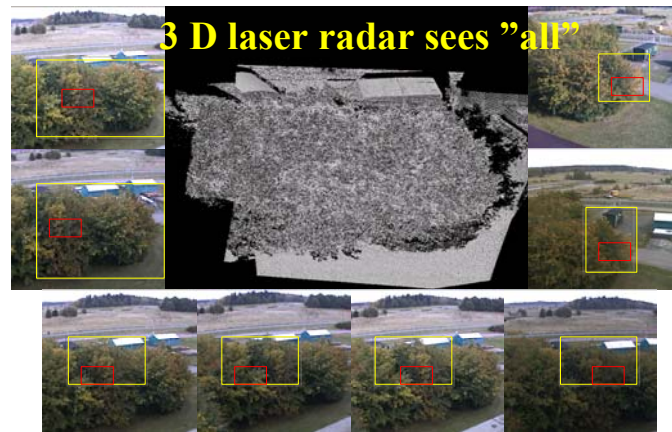
Figure 83: *Top image a clump of trees and a hidden target. Also shown is a series of views scanned by a high resolution laser radar. Below a sequence of 3 D laser radar images that can be combined to give a well-resolved 3 D target image (frame nr 4). Images FOI.*
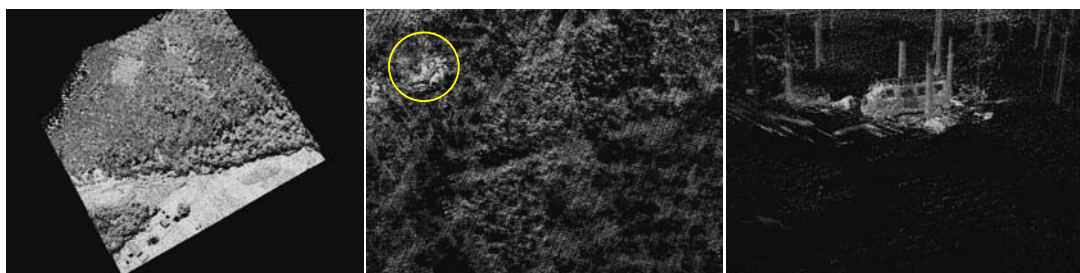

Figure 84: *Example of 3 D images from Top Eye and the ILRIS 3 D scanner illustrating how a future UAV equipped with a scanning/staring laser radar can perform mapping and targeting. Data FOI.*

3/ Terminal seeker for target ID and aim point selection

In today's net-centric warfare we can expect radar and other sensor to communicate and detect and position targets with high accuracy. If a targets position is known to an uncertainty of 10 or 50 meters, the seeker can have a relatively simple design and low resolution mode. The 3 D capability facilitates target recognition and aim point selection. The target can be decomposed into subparts, which can be identified and positioned with high accuracy for the final steering of the missile. This is illustrated in Figure 85, which also shows simulated laser range images of different resolution.

Suppose that the uncertainty volume is a $25*25*25$ m^3 cube and that the seeker is updated on this position until the missile is 1 km away. If the aim point is to be selected with an accuracy of 0.1 m and we assume that this selection is done within the last 1-200 meters the pixel FOV has to be less than 1-2 mrad. If the target has to be recognized by the missile we can assume that this has to be done at a range of at least 1-2 km giving a demand of about 200 pixels cross range. For a target cross section of 10 m^2 this means about 25 cm pixels at the target or 0,13-0,25 mrad. A receiver lens diameter of 5 cm and a focal length of 10 cm may be reasonable. This means a pixel size of between 13-25 μm and array size of 100*100 pixels to cover 25*25 meter at 1 km range. We will use this assumption as a guide for a system performance estimate.
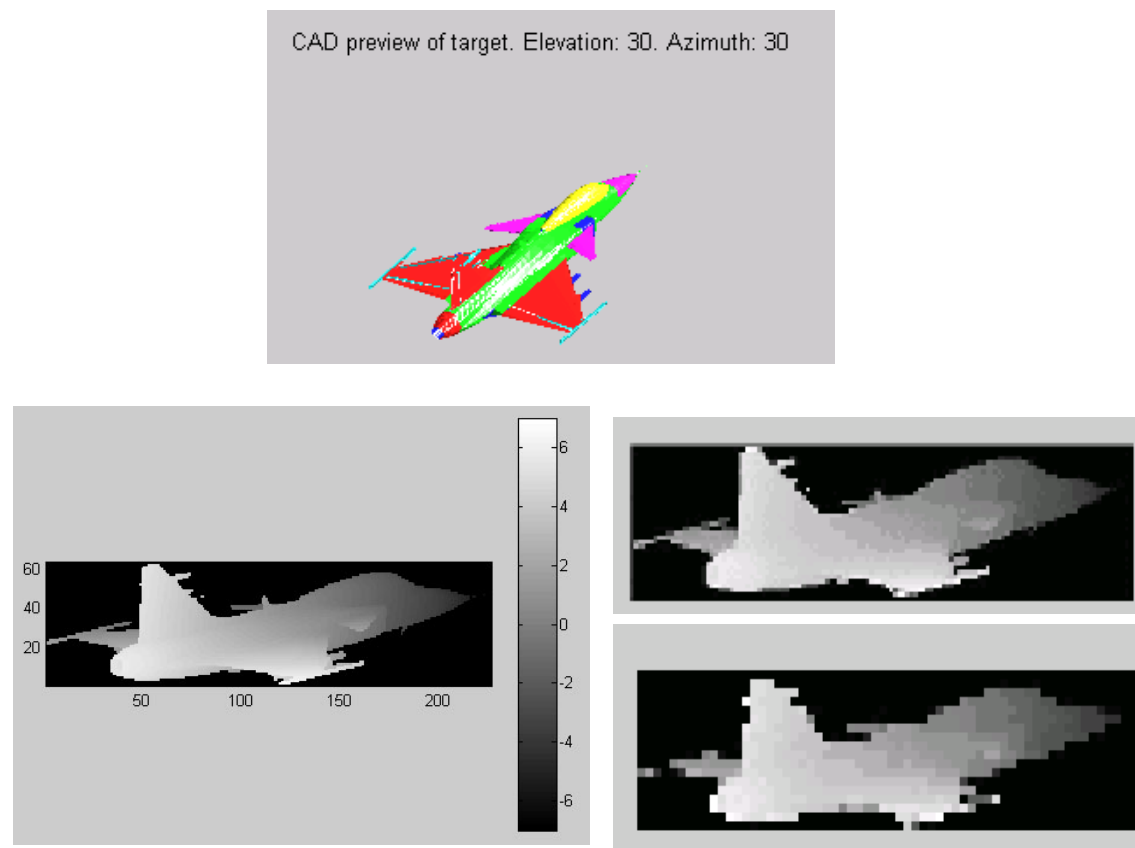

Figure 85: *Above shows an aircraft CAD model composed of different parts suitable for 3 D identification and aim point selection. Below shows a range image (vertical scale in meters) with a pixel corresponding to 256*256, 128*128 and 64*64 pixels (note the images are cropped in the vertical direction).*

Tentative data for an air-to-air or air-to-ground missile seeker

System performance and technology aspects

We will have a missile for an air target in mind. The missile is released towards a target whose position is known with high accuracy, less then 25 m in a cube. For long shooting ranges this position may be updated during the missile flight. The missile seeker is a scanning or stare/scan laser radar seeker giving a high target recognition probability from about 1 km, discriminating decoys. The target recognition might have been done before launch and information transferred to the missile computer. The seeker will use the 3 D data, which at 1 km correspond to about 0.25 meter in cross range and 15 cm in depth, to select a proper impact point, critical to the target function and hit that with a small war head. The staring seeker has a FOV corresponding to the target position uncertainty (25 meter cube) given at 1 km distance from the target. A seeker might also have a small scanning capabilty to increase the field of regard for allowing relocking on a highly moving target. The seeker id updated at 400 Hz PRF and is very countermeasure resistant due to the 3 D data capability and the time gating of the receiver. Figure 86 shows the pulse energy needed at 1 and 0,5 km range vs. visibility. A laser pulse energy of about 3 mJ is needed for single pulse detection. An attractive alternative from a laser technology point of view is to use a high PRF and low pulse energy laser. A microchip laser giving 50 µJ at 500 kHz PRF has been developed for car radar applications (Figure 87). Integration of 1000 pulses at 500 Hz update rate correspond approximately to a single pulse energy of 1.5 mJ. The same type of data is also available from fiber lasers.
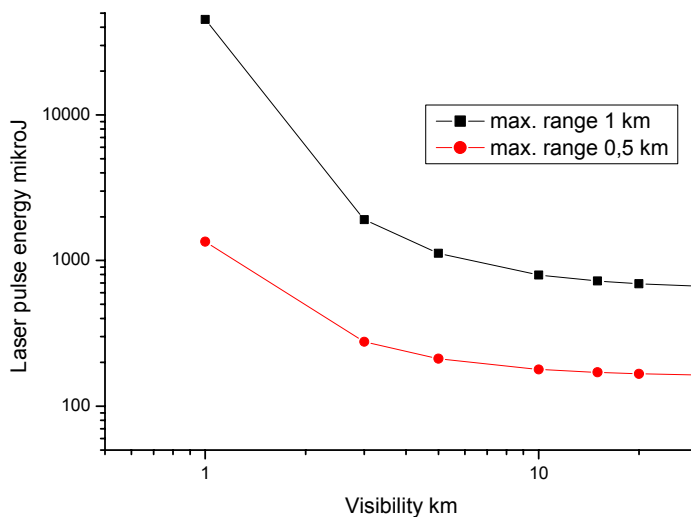
Figure 86: *Laser pulse energy for single pulse detection at maximum 1 and 0.5 km range.*

Figure 87: *Compact laser radar for car applications developed by Leti in France.*

In Figure 88 we show an example of a compact non-expensive single pulse range finder which can be updated to 400 Hz operation by adding cooling and more electrical power. The range finder is developed at US Army's Night Vision and Sensors Directorate. The weight is only 0.7 kg and the size $6.3*10*4.4$ cm^3.
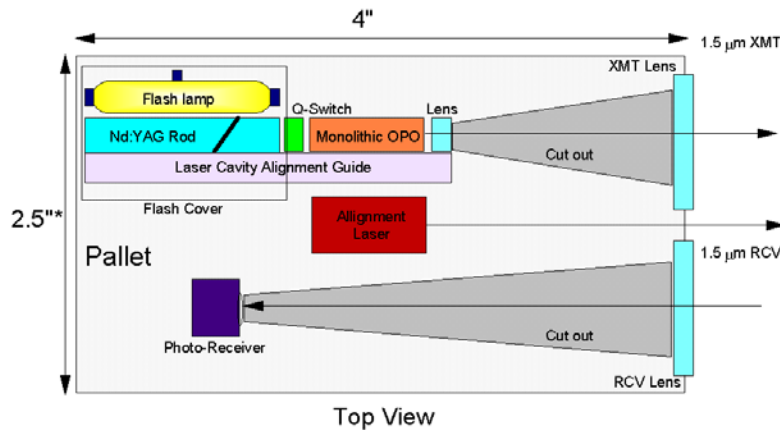
Figure 88: *Example of a simple non-expensive eye-safe laser range finder developed for US Army. http://www.repairfaq.org/sam/lr/.*

Figure 89 shows the principle for the staring and staring/scanning concept. The scanning speed will be low due to the extended detector array and the low scanning demands for search. Several new technologies, beside conventional galvo- and gimbal solution, for compact scanning are being developed. Some examples are given by Figure 90 and Figure 91. Non-mechanical beam steering and beam forming[81] is of special interest.
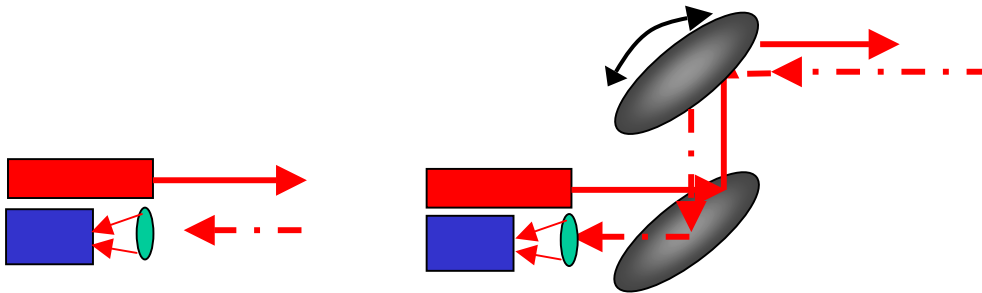
Figure 89: *Concept for staring and scanning configurations.*

In Figure 92, some laser radar seeker concepts are shown together with a Locaas seeker head. Laser radar seekers will bring new precision and capability to future missile systems.
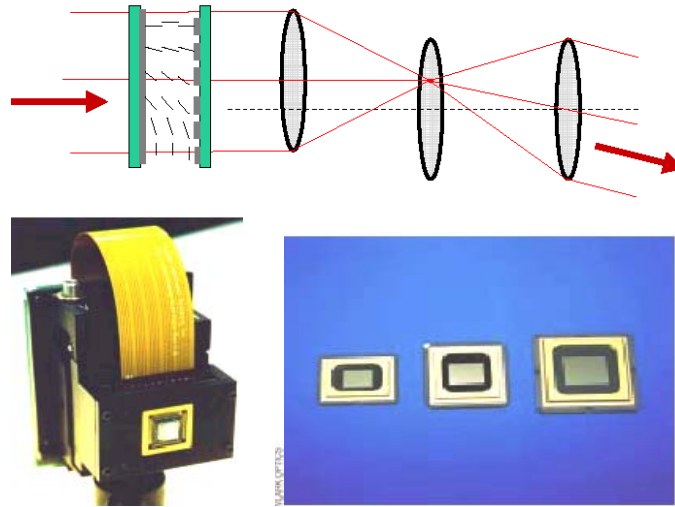
Figure 90: *Above example of a compact scanner solution combining fine steering by an optical phased array and below example of a commercial liquid crystal steerer and a micro mirror devices.*

Figure 91: *Lightweight, low power and low cost scanner based on optical MEMS technology dev. By Lockheed Martin.*
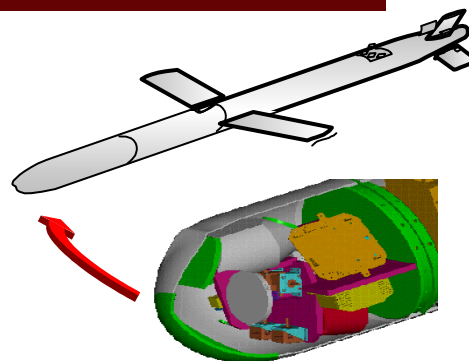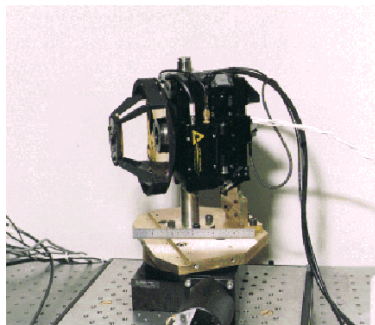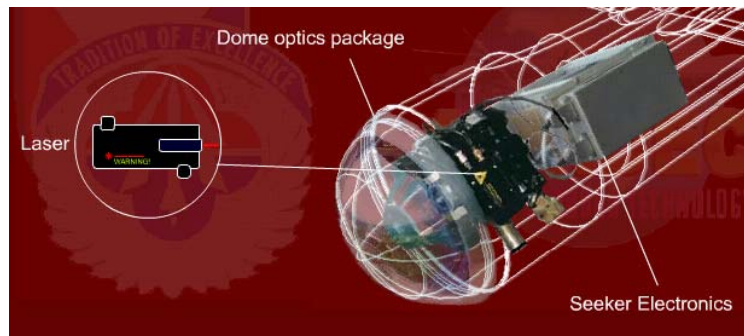
Figure 92: *Above laser radar seeker concept for an air to ground seeker , below a Locaas seeker head (US Air Force) and a laser radar seeker for a cruise missile (US Navy).*

Technical data

These data have been used for Figure 86 and similar performance estimates.

Receiver:
      Detector: CMT APD array
      Responsivity R_D at 1.55 μm = 0.8
      Unity gain dark current: i_D
      Excess noise factor Fe: 2
      Gain M: 10
      Bandwidth B: 300 MHz
      Preamplifierf noise I_{PN}: 0.1 pA/Hz $^{0.5}$
      Pitch : 25 μm
      Size: 100*100 elements
      Optical efficiency: η=0.6
      $\Delta\lambda$ = 0.01 μm
      Optics: f = 100 mm
      Diameter: D = 0.05 m
Laser:
      Wavelength, λ : 1550 nm
      Pulse energy E_p: < 3 mJ (single pulse detection, lower for pulse integration)
      Pulse length t_p: 3-5 ns
      Prf   : 400 Hz ?
      Average laser power: 1-5 W
Environment:
      N_λ is the background spectral radiance: 30 W/m^{2}srμm
      Visibility V km . Varies.
      Background reflectivity: 30 % (diffuse)
Target:
      Target reflectivity: 10 % (diffuse)
      Resolved target

Range resolution: 15 cm
SNR_pix threshold for imaging: 3
Size and weight: 1-2 liters, 3-4 kg

4/ "Pathfinder", ladar for autonomous navigation and targeting.

Future unmanned vehicles should be able to navigate and observe in various forms of terrain and in urban areas along the streets. The 3 D direct sensing and the 3 D data of the environment will be crucial for this precision navigation, obstacle avoidance and intelligent route planning to provide cover. The 3 D sensor will of course also collect data and store these for updating existing terrain data and urban data-bases. The same 3 D sensor can also be used for targeting and with a small addition have the capability to communicate with the same or a collinear laser enabling high bandwidth, secure transmission of data.
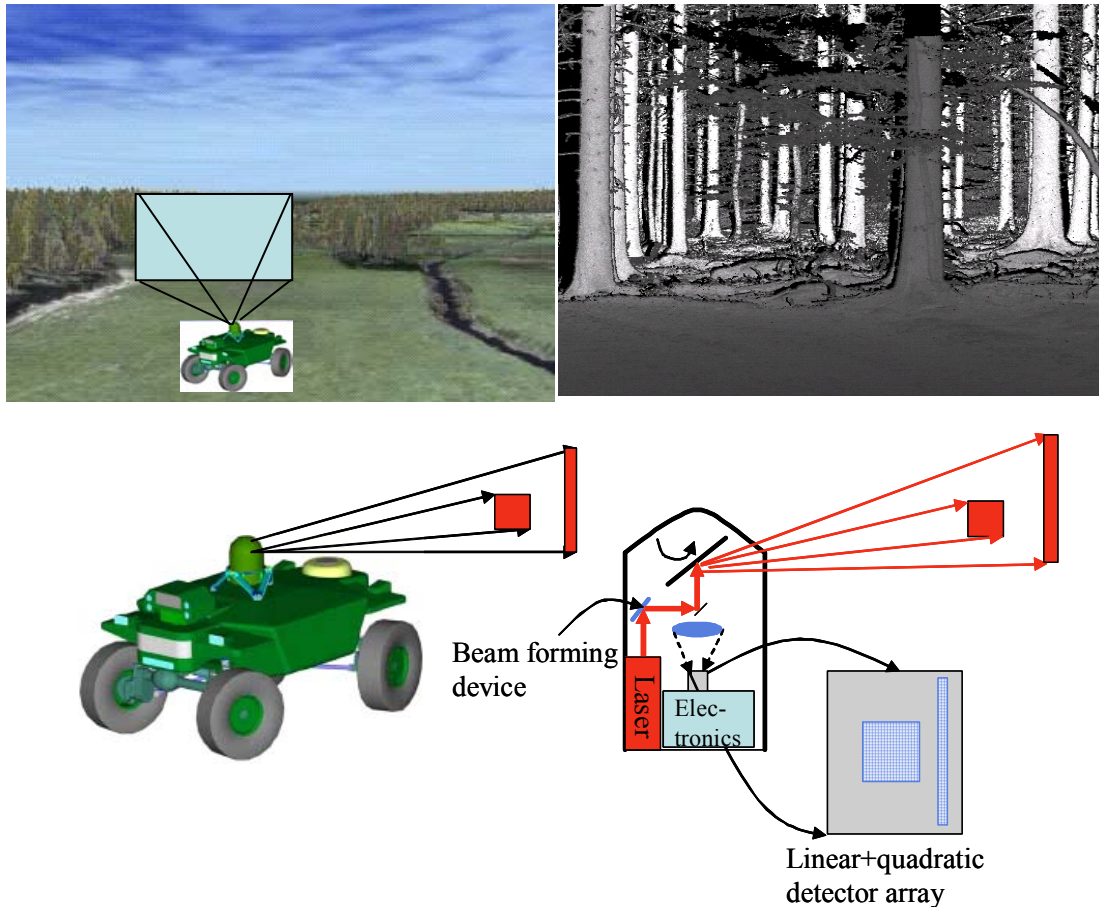
Figure 93: *Concept for a UGV capable of terrain mapping, pathfinding and targeting using a combination of scanning and staring 3 D FPA s and a optical phased array for beam forming to the detector of choice.*

Figure 93 illustrates an UGV operating in terrain looking up strategic positions for surveillance, targeting etc. This type of vehicle may very well communicate with a UAV system obtaining or transferring data. The laser system can have a number of functions, for example supporting navigation/obstacle avoidance as well as long range target detection, positioning, recognition and designation and 3 D mapping. The acquisition and pointing head should combine full circular coverage with accurate pointing. In this way a communication laser might also be incorporated.

The target search, for example by detecting optical glints, the 3 D mapping and target recognition and the navigation will need different laser pulse energies and beam

forms. The search/3 D mapping mode will have a slit formed beam and the target recognition mode a quadratic beam. Assume a 10 W average laser and a maximum range of 1 km for mapping. For an angular pixel size of 0.3 mrad formed in linear array of 200 pixels, we will have a search height of 60 mrad or 3.5 degrees. Let us also assume that we want a scanning rate of 5 turns/second allowing 3 D mapping "on the move". All this together means a pulse repletion rate of about 100 kHz or 100 µJ per laser pulse. For 15 cm optics and a NEP of 1 nW, we are talking about maximum ranges out to 1 km for visibilities down to 1 km and out to more than 2 km for clear weather. For the navigation mode only we want the vehicle to be covert and not easily detected by laser warning devices when laser active. Laser warning devices typically have sensitivities on the order of 1 W/m^2. For the navigation mode the maximum range can be turned down to about 50 meters meaning a laser pulse power around 200 W or so. Assuming a 10 % diffuse ground reflection, this means that the reflected irradiance should be below the threshold 1 W/m^2 at ranges larger than a few 10's of meters. For long range target identification other optics have to be switched in to enable pixel angular resolutions of about 10-20 µrad to enable target recognition up to 10 km if wanted. For integration during for example 10 ms at 100 kHz prf about 1000 pulses with an integrated pulse energy of 100 mJ should be obtained supporting the long range capability.

For urban warfare one UGV mission might be to do "window clearing" that is locate potential enemies in dark room of behind Venetian blinds. While passive IR and passive EO sensors have difficulty here the 3 D laser radar sensor is ideal looking for 3 D manlike "objects" in the room or detecting rifle optics etc. This is illustrated in the figure below.
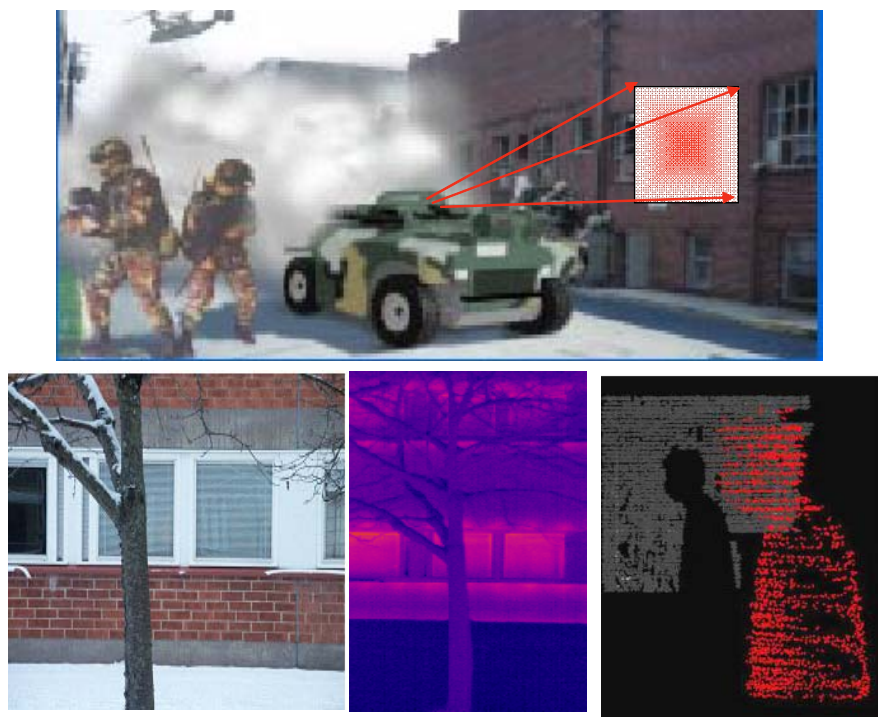
Figure 94: *Upper image show an artist conception of "window clearing" mission. Below is illustrated how a laser radar, but not the visual and IR sensors, reveals person behind the venetian blind. Lower Images (FOI), upper image modified after original found at www.arl.army.mil/wmrd.*
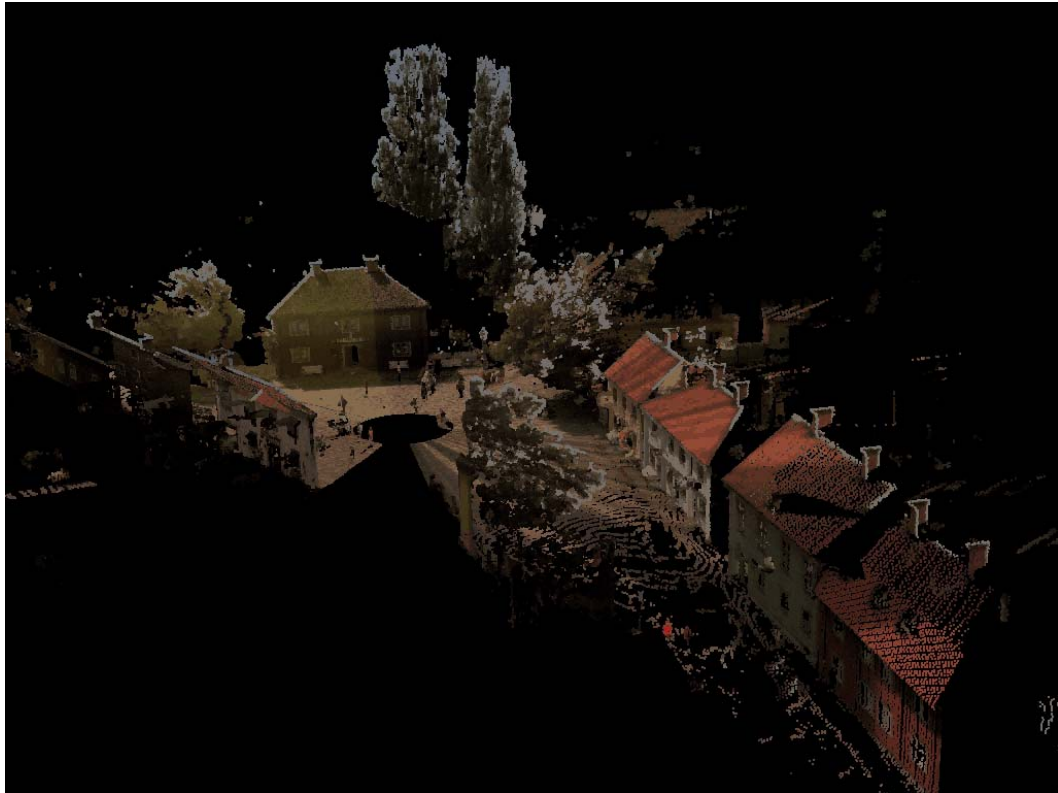
Figure 95*: Example of what information one revolution of the 3 D laser scanner for the "Pathfinder" could provide. Image FOI (using the RIEGL 3 D scanner). The scene is from "old Linköping".*

Technical data Pathfinder

These data are typical but must be further evaluated for a specific system configuration

Receiver:

Detector: CMT APD array
Linar 200*1 elements for search
128*128 for target recognition at long ranges.
Responsivity R_D at 1.55 μm = 0.8
Unity gain dark current: i_D
Excess noise factor Fe: 2
Gain M: 10
Bandwidth B: 300 MHz
Preamplifierf noise I_{PN}: 0.1 pA/Hz $^{0.5}$
Pitch : 25 μm
Size: 200*1 elements+128^2 elements
Optical efficiency: η=0.6
Δλ = 0.01 μm
Optics: f = 100 mm for the array
f = 1500 mm for the long range ID mode.
Diameter: D = 0.05 m

Laser:

Wavelength, λ : 1550 nm

Pulse energy E_p: 100 μJ (single pulse detection, lower for pulse integration)

For the search and mapping and ID modes.

For navigation: < 1μJ per pulse 50-100 range only.

Pulse length t_p: < 3 ns

Prf   : 100 kHz

Average laser power: 10 W

Environment:

N_λ is the background spectral radiance: 30 W/m^{2}srμm

Visibility V km . Varies.

Background reflectivity: 30 % (diffuse)

Target:

Target reflectivity: 10 % (diffuse)

Resolved target

Range resolution: 15 cm.

Range performance: 3 D mapping 5*360 degrees revolution per second.

Fan beam 0.3 mrad*60 mrad (3.5 degrees).

Range 1 km down to 1 km visibility, > 2 km for clear weather.

Target ID after 10-100 ms integration > 10 km.

Size and weight: 5-10 liters, 5-10 kg ?

Active and passive EO systems in combination

So far we have concentrated on laser imaging techniques, especially those for 3 D imaging. In this section we will comment on the potential of combining passive and active EO sensors creating truly N dimensional imaging using N larger than 3 to extract and recognize targets of different kinds.

As pointed out by Steinvall and Letalick[82], passive and active sensors are complementary in many ways. Passive electro-optical sensors have been used for a long time in military applications. Starting from low-resolution hot spot sensors, thermal cameras are now providing fairly high-resolution imagery with good quality.

Passive thermal sensors do however often have a high clutter problem and are very sensitive to diurnal and ambient effects. Night capability is offered by FLIR's and image intensifiers but the recognition capability for long ranges > 3 km is limited due to high demands on optical size (8-12 μm) and focal plane spatial resolution. Passive sensors can be precisely located and jammed by lasers or obscurants. Laser sensors might also give away their position but this risk can be reduced by a controlled emission. Laser sensors are harder to jam and have some obscurant and camouflage penetration capability.

The laser sensor, being an active device, has the general advantage of adapting to a lot of signature features which are hardly possible with a passive sensor, at least not during night-time. On the other hand the narrow beam makes laser systems less suitable for reconnaissance and the cost and complexity of laser systems might be higher than for passive sensors. In table 8 we have made an attempt to list measurable signatures and capabilities for passive and active EO sensors.

Table 8. *Overview of EO/Laser sensor signatures and capabilities. From ref. 71.*

Sensor	Signatures							Capabilities				
	Shape	*Reflec-tion*	*Tempe-rature*	*Trans-mission / absorp-tion*	*Polariza-tion*	*Range/ Doppler*	*Others: Fluorescence, Raman-scattering*	*Search*	*Tracking, Fire control, guidance*	*Recog-nition*	*Multi-function**	*Com-plexity cost*
TV 0.4-1 μm	+	+	0	0	0	0	0	++	+	+	0	++
Image intensifiers	+	+	0	0	0	0	0	+	0	0	0	+
Passive 1-5 μm	+	+	+	+	+	0	0	++	0	+	+	+
Passive 8-12 μm	0	0	++	+	+	0	0	++	+	0	+	0, +
Laser sensors	++	++	0(+)	++	++	++	+	(+)	+	++	++	0 ?

Key to the table: ++ very favorable, + favorable, 0 less favorable

Table 9. *Examples of improvements by adding a laser channel to a passive EO-sensor. From ref.55.*

Improved functionality	Comments
Target reconnaissance	Better performance. Higher false alarm rate, for one or two sensors, more signatures, support of passive sensor by range / Doppler info, atmospheric data etc. ensures high probability of detection
Target recognition	Increased range and recognition performance using range imaging, Doppler information, polarisation, fluorescence etc.
Target tracking, weapon guidance	Target geolocation, improved weapon guidance, intelligent aim point selection gives smaller and smarter munitions.
Autonomous systems	Navigation, steering by combining passive and range imagery
Battle damage assessment	Difference detection in range + passive imagery enables automatic and efficient damage assessment.
Search and rescue (SAR), landing aids, special operations	Beacons for night vision devices, dye detection, retro-detection
Rapid terrain visualisation, synthetic environments	3-D laser radar, IR and radar enable realistic synthetic environments for planning and improved mission execution.
Countermeasure resistance	Improved by noting that a laser system is more difficult to jam than a passive sensor.
Platform protection	Adding a laser radar/jammer to the passive missile warner, smoke system etc. heavily improves survivability
Communication, IFF	Covert communication for real time transfer of image and other sensor data. Coded laser emission before weapon delivery and radio transponder reduces risk of shooting at own troops.

New capabilities for active/passive sensing

Sensor networks will certainly imply new ways of using sensors in reconnaissance and targeting systems as well as in guided weapons. By wireless communication the 3 D imaging capability will improve using both passive and active EO sensors. Multiple views for laser radars will enable a "shadow free" imaging in 3 D. The absolute positioning of the point cloud from the laser enables reconstruction in 3 D (cf. the JIG SAW approach).

There are several new components and technologies[83,84] beside focal plane arrays which support the development of future active/passive sensors. Among these we can mention:

SLM- Spatial Light Modulators based on micro-mirror or liquid crystal technologies will have impact on adaptive optics and non-mechanical beam steering and beam control. It will be possible to compensate for atmospheric turbulence and to do optical phased arrays allowing multiple beam generation, for tracking and positioning and for scanning. The SLM wave front control may improve coherent system by dynamic matching of the local oscillator wave front to that of the incoming signal.

SLM:s can also be used for dynamic spectral and spatial adaption of a sensor selecting regions of interest and reducing electrical bandwidth.

Multi- and hyperspectral sensing may be done passively but with limitation on full night capability. An active laser sensor relying on tunable or multiple line emission will overcome this limitation and add new features like 3 D to the scene.

Miniature lasers like fiber, μ-chip and diode lasers will be well suited for compact 3 D imaging applications.

Artificial and augmented vision are important areas for research with a number of applications in autonomous systems, sensors, operator support and others. By artificial vision we mean systems that mimic the human vision and perception system. Combining passive sensing for overview and large FOV and active sensing using 3 D information seem to be one way to realize an artificial vision system.

Augmented vision refers to overlaying the human vision with relevant and processed data from other sensors and data bases. One way of doing this is by scanning a low power laser into the retina. If we use other displays and other means (audio, smell etc.) to present the data we are talking of augmented reality. The 3 D laser sensor has a great capability to generate such artificial vision and artificial realities. Example of application include driving and flying in low visibility conditions, seeing in smoke, seeing trough fires etc. The position sensors like TN and GPS systems enable this to be done in real time.

Advanced concepts include combined active/passive EO sensors using the full potential of both active and passive sensing in a system where data are fused and individual sensor modes are activated by the overall autonomous sensor management. On the active side we will see combined coherent /direct detection systems for optimal range and Doppler imaging enabling GMTI (Ground Moving Target Indicator) and vibration sensing.

The development of Synthetic Aperture Laser Radar (SAL) will give higher resolution with much smaller apertures than the present SAR-systems. It will also shorten the time needed to record an image. On the another hand, the problem of isolation of the platform movements in optical phase measurements is surely non-trivial. When the observation range is 100 km or more, there are no other methods of centimetre-class resolution with reasonable aperture sizes (< 1 m)[85]. The 3 D FPA array detector is important in this kind of systems as the transverse resolution in a SAL system (pixel size) is $D_T/(2Nsc)$ where D_T is the transmitter optics diameter and N_{sc} is the number of successive scans over the area of interest. Normally for SAR N_{sc}=1. The receiver optics might however be M times larger and thereby collecting M^2 times more light from each ground pixel but the receiver footprint is M times smaller, meaning that a heterodyne array has to be used for an efficient long-range system.

The objective of the DARPA/AFRL SALTI (Synthetic Aperture Lidar for Tactical Imaging) program is to conduct a proof-of-concept airborne demonstration of a sensor and associated ground data processing which generates high-resolution 2D and 3D imagery combining the interpretability of electro-optics, the long-range day/night access of high-altitude X-band synthetic aperture radar, and the exploitability of 3-dimensional lidar. The proposed sensor system is anticipated to have a multi-channel multicolor coherent laser transceiver capable of day/night operation and operation in

partially degraded weather, which would collect coherent optical phase history data and range-Doppler data. This data would be processed into synthetic aperture optical imagery.

Figure 96: <u>DARPA/AFRL SALTI (</u>Synthetic Aperture Lidar for Tactical Imaging) program, see **www.darpa.mil**.

R&D issues relevant for laser 3 D sensors

Below we have tried to list some examples of issues for research and development within the area of laser sensors, with emphasis on 3 D imaging.

Surveillance and target recognition

<u>Hardware</u>:   Active/passive integrated EO sensors, single aperture sharing, multifunctional systems radar/EO. Tunable/multicolor lasers with variable emission formats. Multicolor 3 D FPA. Chip integrated processing of pixel waveforms.
For synthetic aperture lidars (SAL): Long coherence time (1-10 ms), fast chirp rate and high pulse rep rate lasers.

<u>Software</u>: Active passive EO fusion algorithms and sensor management. Fast vegetation and camouflage removal algorithms. Robust ATR (Automated Target Recognition) algorithms.
For SAL: SAR processing methods extended to the optical frequency domain. Vibration correction by measuring and compensation for platform induced phase errors.

<u>System issues</u>. Net centric warfare concepts and sensor management.

Battle damage assessment

Hardware: High resolution flash imaging 3 D FPA systems. Combine range/Doppler capabilities. Combine laser radar with passive EO sensing.

Software. Difference detection, vibration signatures, physical damage estimation. Detailed target information.

System issues: Data fusion using data from a single or physically separated sensors, multiple views etc.

Target tracking, weapon guidance

Hardware: Compact μchip lasers and 3 D FPA for combined proximity fuses and seeker applications. 3 D FPA enables excellent tracking by combining intensity and range information. Target segmentation from the background is another key feature important for tracking performance which is rather straightforward in 3 D sensing.

Software: Algorithms for high accuracy tracking and aim point selection.

System issues: How to implement and use non-expensive 3 D imaging laser seekers in a network centric concept.

Automous systems

Hardware: Combined active/passive sensor suite. Laser sensor for 3 D mapping, navigation and targeting- separate or combined sensor.

Software: Data fusion, route planning, steering, ATR, use of existing high resolution 3 D environment data bases.

System issues: Passive active modes, communication, operator assistance, tactical use etc.

Rapid terrain visualization

Hardware: Small compact high resolution and high area coverage laser radars to be operated from UAV:s, UGV:s, AUV;s or manned platforms.

Software: Fast generation of synthetic environment from laser radar, SAR, video and IR imagery. Object/terrain classification procedures.

System issues: Update rates, collection and fusion from many types of sensors and missions.

Discussions and conclusions

We are living in a three-dimensional world. The potential to image this world with cm resolution at full video rate and at both close and very long ranges will revolutionize many military and civilian applications. Many applications are found for example in robotics, rapid terrain visualization, augmented vision, reconnaissance and target recognition, weapon guidance including aim point selection and many others. The net-centric warfare[86] will demand high resolution geo-data for a common description of the environment, for mission planning, for sensor management and sensor fusion, electronic warfare and communication and many others functions related to the network concept.

This report has described the technology as found in open sources and has given examples of 3 D imaging and related activities at FOI. Hopefully we have convinced the reader about the importance of the area. For the future we recommend:

- Providing means of building demonstrators to evaluate the 3 D imaging capability for different applications. These demonstrators should involve both hardware and software development.

- Increasing the effort of combining 3 D sensor data from lasers and other sensors to build rapid terrain visualization capabilities. Special efforts should include surveillance and target recognition.

- Providing means of establishing a national competence and capability in the three-dimensional FPA hardware area.

- Looking for technology transfer and cooperation between the civilian and military efforts in this area. There are many common needs and applications of 3 D imaging from robotics, geo-info to search and rescue etc.

- International cooperation should have high priority to get insight into primarily the hardware development.

- Signal processing of 3 D data should be a high priority area for Sweden.

References

[1] J.M. Vaughan, K.O. Steinvall, C. Werner and P.H. Flamant, "Coherent Laser Radar in Europe", Proc. IEEE,Vol. 84,No. 2, pp. 205-226, February 1996.

[2] M. Xing, Z. Bao, B. Pei, "Properties of high-resolution profiles", Opt. Eng. Vol. 41, No. 2, pp. 493-504, 2002.

[3] O. Steinvall, H. Olsson, G. Bolander, C. Carlsson, and D. Letalick "Gated viewing for target detection and target recognition", Proc. SPIE Vol. 3707, *Laser Radar Technology and Applications IV*, Orlando, 6-9 April, 1999.

[4] Qinfen Zheng, Sandor Z. Der and Hesham Ibrahim Mahmoud, "Model-Based Target Recognition in Pulsed Ladar Imagery", IEEE Transactions on image processing, Vol. 10, No. 4, April 2001.

[5] ARMDEC US Army research and development and engineering centre.

[6] R. Axelsson, O. Steinvall, and P. Sundberg, "Programmable scanner for laser bathymetry", International Hydrographic Rev., Vol. 67, No.1, pp. 161-170, January 1990.

[7] O. Steinvall, U. Söderman, S. Ahlberg, M. Sandberg, D. Letalick, and E. Jungert, "Airborne laser radar: Systems and methods for reconnaissance and terrain modeling", Proc. SPIE Vol. 3707, pp. 12-26 (1999).

[8] O. Steinvall, D. Letalick, U.Söderman, L.Ulander, A.Gustavsson, "Laser radar for terrain and vegetation mapping", FOI-R--0232—SE, October 2001.

[9] Taken from ref. 8

[10] O. Steinvall, M. Tulldahl, M. Andersson "FLASH G2, A study of international laser- and electrooptical systems for underwater detection", FOI RH –report.

[11] http://www.toposys.com/toposys_e.htm

[12] J. Andrew Hutchinson et.al. "Multifunction laser radar III", Proc. SPIE on Laser radar Technology and Applications VI, SPIE Aerosense Orlando, 16-20 April 2001.

[13] http://www.missilesandfirecontrol.com/our_products/strikeweapons/LOCAAS/product-locaas.html

[14] K.R.Schulz, S. Scherbarth, U. Fabry," Hellas: Obstacle warning system for helicopters", Proc. SPIE on Laser radar Technology and Applications VII, SPIE Aerosense Orlando, Vol. 4723, 1-5 April 2002.

[15] C. Rasmussen, "Combining Laser Range, Color, and Texture Cues for Autonomous Road Following", Proceedings of the 2002 IEEE International Conference on Robotics & Automation ,Washington, DC ,May 2002

[16] B. Stann, A. Abou-Auf, S. Frankel, M. Giza, W. Potter, W. Ruff, P. Shen, D.Simon, M. Stead, Z. Sztankay, L. Lester," Research progess on scannerless ladar systems using a laser diode transmitter and FM/cw radar principles, Proc. SPIE on Laser radar Technology and Applications VI, SPIE Aerosense Orlando, 16-20 April 2001.

[17] B.L. Stann, A.Abou-Auf, K.Aliberti, M.Giza, G.Ovrebo, W.Ruff, Debbie Simon, M.Stead, "Research progress on a focal plane array ladar system using a laser diode transmitter and FM/cw radar principles", Proc. SPIE on Laser radar Technology and Applications VII, SPIE Aerosense Orlando, Vol. 4723, 1-5 April 2002.

[18] W. Ruff, K. Aliberti, M.Giza, P. Shen, B. Stann, M. Stead,"Characterization of a 32-element linear self-mixing detector array for an FM/cw ladar", Proc. SPIE on Laser radar Technology and Applications VII, SPIE Aerosense Orlando, Vol. 4723, 1-5 April 2002.

[19] C. J. Karlsson, F. Å. A. Olsson, D. Letalick, and M. Harris, "All-fiber multifunction continuous-wave coherent laser radar at 1.55μm for range, speed, vibration, and wind measurements," Appl. Opt. Vol. 39, No. 21, pp. 3716–3726 (July 2000).

[20] Colin L. Smithpeter, Robert 0. Nellums, Steve M. Lebien, George Studor, "A Miniature, High-Resolution Laser Radar Operating at Video Rates", Proc. of SPIE Vol. 4035, Laser Radar Technology and Applications V, 2000.

[21] J. T Sackos, R. O. Nellums, S. M. Lebien, C. F. Diegert, J. W. Grantham and T. Monsson, "A Low cost, high resolution, video-rate imaging optical radar", Proc SPIE. Vol. 3380, Laser Radar Technology and Applications III, Orlando, 14-16 April, 1998.

[22] Colin L. Smithpeter, Robert O. Nellums, Steve M. Lebien, George Studor, George James, "LADAR Measurements of the International Space Station", Proc. of SPIE Vol. 4377, Laser Radar Technology and Applications VI, 2001.

[23] T. Monson, J.W. Grantham, S.W. Childress, J.T: Sackros, R.O. Nellums and S.M Lebien, " Characterizatin of a scannerless LADAR", Proc. of SPIE Vol. 3707, Laser Radar Technology and Applications IV, April 1999

[24] A.V. Jelalian, " Laser Radar Systems", Artech House, 1991.

[25] J. W. McLean, J. M Murray, "Streak tube lidar allows ocean surveillance", Laser Focus World, pp. 171-176, Jan. 1998.

[26] Anthony D. Gleckler, "Multiple-Slit Streak Tube Imaging Lidar (MS-STIL) Applications", Proc. of SPIE Vol. 4035, Laser Radar Technology and Applications V, 2000.

[27] A. D. Gleckler, A. Gelbart, J.M. Bowden, " Multispectral and hyperspectral 3D imaging lidar based upon the multiple slit streak tube imaging lidar", Proc. of SPIE Vol. 4377, Laser Radar Technology and Applications VI, 2001.

[28] Asher Gelbart., Brian C. Redman, Robert S. Light, Coreen A. Schwartzlow, and Andrew J. Griffis, "Flash lidar based on multiple-slit streak tube imaging lidar", Proc. of SPIE Vol. 4423, Laser Radar Technology and Applications VI, 2002.

[29] M.J. Halmos, M. Jack, J. Asbrock, C Anderson, S. Bailey, G. Chapman, E. Gordon, P. Herning, M.Kalisher, L. Klaras, K. Kosai, V. Liquori, M. Pines V. Randall, R. Reeder, J. Rosbeck, S. Sen, P. Trotta, P. Wetzel, A. Hunter, J. Jensen, T W. Trussell , A. Hutchinson, R. Balcerak ,"3-D FLASH LADAR AT RAYTHEON, ", Proc. of SPIE Vol. 4377, Laser Radar Technology and Applications VI, 2001.

[30] Ralph Burnham, "Three-dimensional laser radar for long-range applications", Proc. of SPIE Vol. 4377, Laser Radar Technology and Applications VI, 2001.

[31] R. Stettner, H. Bailey, R. Richmond, "Eye-safe laser radar 3-D imaging", Proc. of SPIE Vol. 4377, Laser Radar Technology and Applications VI, 2001.

[32] R. Stettner and H. Bailey,"Staring underwater laser radar (SULAR) 3-D Imaging", Proc. of SPIE Vol. 4377, Laser Radar Technology and Applications VI, 2001.

[33] J.D. Beck, C.F. Wan, M-A. Kinch, J.E. Robinson, "MWIR HgCdTe avalanche photodiodes", Proc. SPIE on Materials for Infrared detectors", Vol. 4454, 2001.

[34] K. Johnson, M.Vaidyanathan, Song Xue, W. Tennant, L. Kozlowski, G. Hughes and D. Smith, "Adaptive LADAR Receiver for Multispectral Imaging", Proc. of SPIE Vol. 4377, Laser Radar Technology and Applications VI, 2001.

[35] See ref 33.

[36] M. Browder, B.Evans, J.Beck, M.Blessinger, W.Blattner, R. LeBlanc and B. Miles, "Three Dimensional Imaging Sensors Program", Proc. of SPIE Vol. 4377, Laser Radar Technology and Applications VI, 2001.

[37] Se ref. 29.

[38] R.M. Heinrichs, B.F. Aull, R.M. Marino, D.G. Fouche, A.K. McIntosh, J.J. Zayhowski, T.Stephens, M.E. O'Brien, M.A. Albota, R.M. Heinrichs, B.F. Aull, R.M. Marino, D.G. Fouche, Three-Dimensional Laser Radar with APD Arrays, Proc. of SPIE Vol. 4377, Laser Radar Technology and Applications VI, 2001.

[39] M.A. Albota, R.M. Heinrichs, D.G. Kocher, D.G. Fouche, B.E. player, M.E. O'Brien, B.F. Hull, J.J. Zayhowski, J. Mooney, B.C:, Willard and R.R. Carlson, " Three- dimensional imkaging laser radar with a photon-counting avalanche photodiode array and microchip laser" Appl. Optics, Vil. 41, No. 346, pp. 7671-7678, Dec. 2002.

[40] K. Johnson, M. Vaidyanathan, S. Xue, W.Tennant, L. Kozlowski, G.Hughes and D.Smith, Adaptive LADAR Receiver for Multispectral Imaging, Proc. of SPIE Vol. 4377, Laser Radar Technology and Applications VI, 2001.

[41] R. Lange, "3D Time-of-flight distance measurement with custom solid-state image sensors in CMOS/CCD-technology", Ph.D Dissertation, Univ. of Siegen, GE

[42] O. Steinvall, "Effects of target shape and reflection on laser radar cross sections" Applied Optics, Vol. 39, no.24, pp.4381-91,Aug. 2000.

[43] O. Steinvall, T.Carlsson,"Three-dimensional laser radar modelling", SPIE, *Laser Radar Technology and Applications VI*, Orlando April 2001.

[44] O. Steinvall, H. Olsson, G. Bolander, C. Carlsson, and D. Letalick "Gated viewing for target detection and target recognition", Proc. SPIE Vol. 3707, *Laser Radar Technology and Applications IV*, Orlando, 6-9 April, 1999.

[45] L. Klasén, O. Steinvall, G. Bolander, M. Elmqvist, "Gated Viewing - Initial test at long ranges", FOI-R— 0302--SE, Dec., 2001

[46] N. Kopeika, A System Engineering Approach to Imaging, SPIE Press, Bellingham, USA, 1998.

[47] L.C. Andrews, R.L. Philips and C.Y. Hopen, "Laser Beam Scintillation with Applications ", SPIE Press, Bellingham, USA, 2001.

[48] Pierre Andersson, "Automatic Target Recognition from Laser Radar Data- Applications to Gated Viewing and Airborne 3 D laser Radar", FOI-R—report in manuscript May 3002.

[49] Q. Zheng, S.Z. Der and H. I. Mahmoud, "Model-Based Target Recognition in Pulsed Ladar Imagery", *IEEE Trans. on image processing*, Vol. 10, No. 4, April 2001.

[50] R. Bolle and D. Cooper, "On optimally combining pieces of information,with application to estimating 3-D complex-object position from range data," *IEEE Trans. Pattern Anal. Machine Intell.*, vol. PAMI-8, pp. 619–638, May 1986.

[51] R. Hoffman and A. Jain, "Segmentation and classification of range images," *IEEE Trans. Pattern Anal. Machine Intell.*, vol. PAMI-9, pp.608–620, May 1987.

[52] R. Rimey and F. Cohen, "A maximum likelihood approach to segmenting range data," *IEEE J. Robot. Automat.*, vol. 4, no. 3, pp.277–286, 1988.

[53] F. Solina and R. Bajcsy, "Recovery of parametric models from range images: The case for superquadrics with global deformations," *IEEE Trans. Pattern Anal. Machine Intell.*, vol. 12, pp. 131–147, Feb. 1990.

[54] J. Verly, R. Delanoy, and D. Dudgeon, "Model-based system for automatic target recognition from forward-looking laser-radar imagery," *Opt. Eng.*, vol. 31, no. 12, pp. 2540–2552, 1992.

[55] T. Green and J. Shapiro, "Detecting objects in three-dimensional laser radar range images," *Opt. Eng.*, vol. 33, p. 865, 1994.

[56] S. Der, B. Redman, and R. Chellappa, "Simulation of error in optical radar range measurements," *Appl. Opt.*, vol. 36, no. 27, pp. 6869–6874,1997.

[57] Q. Zheng, S.Z. Der and H. I. Mahmoud, "Model-Based Target Recognition in Pulsed Ladar Imagery", *IEEE Trans. on image processing*, Vol. 10, No. 4, April 2001.

[46] See ref . 48

[59] See ref. 48.

[60] M. Wellfare, T.Holmes, S. Pohlman, Duane Gec, K. Norris-Zachery, R. Patton, Identification of vehicle targets from low-cost ladar seeker imagery, Proc. SPIE Vol. 2748, *Laser Radar Technology and Applications IV*, Orlando, April, 1996 .

[61] See for example www.darapa.mil/SPO/Solicitations/BAA01-15/briefing,ppt

[62] M. Elmqvist, "Automatic Ground Modelling using Laser radar Data", Master's Thesis, Linköping University, LiTH-ISY-EX-3061.

[63] B.W. Scilling, D.N. Barr, G.C. templeton, L.J. Mizerka and C.W. Trussell, " Multiple-return laser radar for three-dimensional imaging through obscurations", Appl. Optics Vol. 41, No. 15, pp. 2791-2799, May 2002.

[64] Christina Carlsson, "Vehicle Size and Orientation Estimation using Geometric Fitting", 2000, Thesis no. 840, LiU-TEK-LIC-2000:36, Dept. of Electrical Engineering, Linköping University, Linköping, Sweden.

[65] Lena Klasén, "Image Sequence analysis of Complex Objects – Law Enforcement and Defence Applications", Linköping Studies in Science and Technology, Dissertion No. 762, 2002, Dept. of Electrical Engineering, Linköping University, Linköping, Sweden.

[66] J. Svensson, "Matching vehicles from laser radar images in the target recognition process", Linköping, FOA 2000, FOA-R--00-01606-408—SE, Sci. Report.

[67] O. Steinvall,"Theory for laser systems performance modelling", FOA-R--97-00599-612--SE, Oct 1997

[68] O. Steinvall,"Waveform simulation for 3-D sensing laser radar", FOA-R--00-01530-612, 408--SE, May 2000.

[69] T. Carlsson, O. Steinvall, D. Letalick, "Signature simulation and signal analysis for 3-D laser radar", FOI-R--0163--SE, July 2001.

[70] S. Der, B. Redman, and R. Chellappa. Simulation of error in optical radar range measurements. *Applied Optics,* 36(27):6869-6874, September 1997.

[71] O. Steinvall, T.Carlsson,"Three-dimensional laser radar modelling", SPIE, *Laser Radar Technology and Applications VI*, Orlando April 2001.

[72] O. Steinvall, "Effects of target shape and reflection on laser radar cross sections" Applied Optics, Vol. 39, no.24, pp.4381-91, Aug 2000.

[73] C.Grönwall and F. Gustafsson, "A Cramer-Rao Lower Bound Expression for a Scanning Laser Radar System", unpublished from workshop, 30-31 May, 2002, Linköping University, Linköping.

[74] C. Grönwall, T. Carlsson and F. Gustafsson,:"Performance analysis of measurement error regression in direct-detection laser radar imaging", To be presented at ICASSP, Hong Kong, China, 06 -10 April, 2003.

[75] S. Van Huffel and J. Vandewalle. The Total Least Squares Problem. Computational Aspects and Analysis. SIAM, Philadelphia, 1991.

[76] C. Subhasis and S. Chatterjee, "Performance analysis of total least squares methods in three-dimensional motion estimation", IEEE Transactions on Robotics and Automation, Vol. 7, No. 5, pp. 707—713, 1991.

[77] See ref. 68.

[78] See ref. 72.

[79] See ref. 69.

[80] The Infrared and Electro-Optical Systems Handbook, vol. 6, ch. 2, Soc. of Photo-Optical Eng. 1993.

[81] S. Hård, S. Jacobsson, B. Löfving, U. Olikn, P. Rudquist, L. Sjöqvist, O. Steinvall ohc S. Walles, " Laser beam steering – an introductory study", FOI-R—99-00000-314—SE.

[82] O. Steinvall, D. Letalick, "The potential of combined active and passive electro-optical sensors" FOA-R--00-01605-408—SE, September 2000.

[83] Lars Sjöqvist, "Adaptive Optics in Laser Countermeasures-An Introduction", FOA report, FOA-R--00-01736-612--SE, 2000.

[84] Ingemar Renhorn, "Integrated Computional Imaging Systems", FOI report, FOI-R--0455--SE, 2002.

[85] R.L. Ucke, L.R. Richard, "Photon-limited synthetic aperture imaging for planet surface studies", Appl. Optics, Vol. 41, No. 24, 20 August, 2002.

[86] O. Steinvall, L. Klasen, C, Grönwall, U. Söderman, S.Ahlberg, M, Elmqvist, H. Larsson, D. Letalick, " High resolution three dimensional laser imaging
- new capabilities for the net centric warfare", paper at CIMI, 20-22 May, 2003, Enköping, Sweden.